Advances in spectral techniques for fruit quality evaluation: case of ULF-NMR and NIRS

by

Jean Frederic ISINGIZWE NTURAMBIRWE

Thesis presented in partial fulfilment of the requirements for the degree of Doctorate of Philosophy in Engineering in the Faculty of Engineering at Stellenbosch University

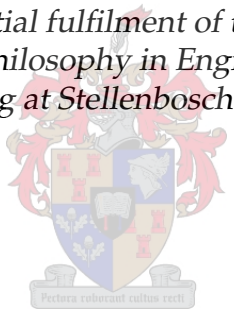

Department of Electrical and Electronic Engineering
University of Stellenbosch
Private Bag X1, 7602 Matieland, South Africa

Supervisors:

Prof. W.J. Perold Prof. U.L. Opara

March 2017

The financial assistance of the National Research Foundation (NRF) towards this research is hereby acknowledged. Opinions expressed and conclusions arrived at are however those of the author and are not necessarily to be attributed to the NRF.

Declaration

By submitting this thesis electronically, I declare that the entirety of the work contained therein is my own, original work, that I am the sole author thereof (save to the extent explicitly otherwise stated), that reproduction and publication thereof by Stellenbosch University will not infringe any third party rights and that I have not previously in its entirety or in part submitted it for obtaining any qualification.

Date: March 2017

Abstract

Industrial application of non-destructive analytical techniques still faces a challenge of lack of general and specialty models for quality evaluation. Current developments strive to alleviate this problem by the development of new cost effective equipment. In the food industry, and especially the horticultural industry, two spectroscopic methods seem to lead the way in terms of analytical variety, advancement in software for data handling and analysis, and relevance. The techniques in question are nuclear magnetic resonance (NMR) and near-infrared (NIR) spectroscopy. This project used practical experimental studies of fruit quality, using both techniques, to further research towards their non-destructive and online application, especially for horticultural products. A SQUID-NMR (B_m = 1Gauss) system was used to study the ripening of banana and predict its ripening index. Measurements of the NMR spin-lattice (T_1) and the spin-spin (T_2) relaxation times were acquired prior to destructive measurements. Various physico-chemical attributes were monitored for changes during the ripening process. Four out of six measurements, taken over a period of 10 days of storage (at 15 ^oC and 85%RH), were significantly different. Average T_2 gave less promising results than average T_1, that was highly correlated to attributes that changed during ripening, namely, lightness, L* (r=0.61), chromaticity coefficient, b* (r=0.65), totoal soluble solids, TSS (r= 0.72), sugar:acid ratio, TSS/TA (r=0.82), chromaticity coefficient, a* (r=0.84) and hue angle, h (r=-0.85). Correlations with T_2 were found for TSS (r=-0.53), TSS/TA (-0.54) b* (-0.58) and pH (r=0.70), all significant at $p<0.05$. The ripening index was defined subjectively, based on the visual standards of the ripening index in banana. Average T_1 distinctively explained the variance in ripening index, together with TSS, TSS/TA color parameters a* and h and total color difference. Calculation of the multicomponent distribution of T_1 resulted in two components, one slow and another fast. Improvements in consistency of the transform is still required before it can be used for further analysis and accurate peak assignment. The results above show that there are opportunities of using SQUID detected NMR spectral data in the T_1 domain for further studies of banana quality, and very likely other fruits as well. It is apparent that issues of temperature dependence of T_1 should be taken

into account in building more robust models. Fourier transform NIR (FT-NIR) was used in studying internal quality and mechanical damage in apples. Using three cultivars from two sources and three spectrometer modes from two FT-NIR spectrometers, we were able to account for the need of variability in building robust models. Different levels of predictability for each attribute were obtained for different cultivars, using PLS regression methods. The predictive ability was different between distinct spectral acquisition modes as well, but also depended on attributes. It was noticed that, in all scenarios considered (single exclusive and all inclusive cultivar or source), the emission head (EH) of the Matrix-F spectrometer led to similar model performances as for the integrating sphere (IS) of the multipurpose analyzer (MPA) FT-NIR spectrometer, in models predicting TSS. Model optimization was done successfully using both pre-processing methods and genetic algorithms applied on PLS of non-processed spectra. The influence of either cultivar or instrument on models predicting TA was different than that obtained for TSS and for TSS/TA, and overall, with lower model performance. Results revealed aspects that are likely to favor calibration transfers between the EH and IS acquisition modes. Bruising in apples is very common and quite intricate to detect if it is internal or not showing on the outside yet. NIR, mostly multispectral, hyperspectral imaging and visible spectrum (VIS) combined with NIR (VIS/NIR), have been used frequently to distinguish between bruised and sound tissue of apple fruits. It has been customary, as seen from many reports, that bruise studies by NIR calls for variable selection. The study carried out on bruise damage in this project involved variable selection by genetic algorithm, influenced by cultivar, and validated by a variable importance in projection (VIP) method, that used a different approach to the filter method. Favored wavebands were brought to light. Both methods were compared to the literature. This may serve as a good basis for further development towards online applications in the horticulture industry.

Overall, advanced prospects in applications of the two most highly developed spectroscopic techniques to non-destructive fruit quality evaluation were identified and recommendations were given in light of possibilities for future industrial application.

Opsomming

Industriële toepassings van nie-destruktiewe analitiese tegnieke is tans skaars a.g.v. 'n gebrek aan spesialiteitsmodelle vir kwaliteitevaluering. Huidige ontwikkelinge op hierdie gebied streef daarna om hierdie probleem op te los deur die ontwikkeling van koste effektiewe nuwe toerusting. In die kosbedryf, en spesifiek die vrugtebedryf, is daar twee spektroskopiese tegnieke wat tans die voortou neem t.o.v. analitiese verskeidenheid, die vooruitgang in programmatuur vir dataverwerking, en relevansie.Hierdie tegnieke is kern magnetiese resonasie (KMR) en naby-infrarooi (NIR) spektroskopie. In hierdie projek is praktiese eksperimentele studies op vrugte gedoen deur beide tegnieke te gebruik om hul toepaslikeid vir nie-destruktiewe toetsing en aanlyn toepassings op vrugte te bepaal. 'n SQUID-KMR (B_m=1Gauss) stelsel is gebruik om die rypwordingsproses van piesangs te bestudeer en om die rypwordingsindeks te bepaal. 'n Verskeidenheid van fisio-chemiese eienskappe is waargeneem gedurende die rypwordingsproses. Vier uit ses metings oor 'n tydperk van 10 dae van berging (15°C, 85%RH) was beduidend verskillend. Metings van die KMR uitsterftyd T_1 (spin-latwerk) en T_2 (spin-spin) is geneem voordat destruktiewe metings gedoen is. Gemiddelde T_2-metings het minder belowende resultate gegee as T_1-metings, wat hoogs gekorreleerd was t.o.v. eienskappe wat verander gedurende die rypwordingsproses, soos TA (r=-0.52), L* (r=0.61), b* (r=0.65), TSS (r= 0.72), TSS/TA (r=0.82), a* (r=0.84) and h (r=-0.85). Korrelasie met T_2 is gevind vir TSS (r=-0.53), TSS/TA (-0.54) b* (-0.58) en pH (r=0.70), almal beduidend met $p<0.05$. Die rypwordingsindeks is subjektief bepaal, gebaseer op visuele standaarde van die rypwordingsineks van piesangs. Gemiddelde T_1-metings kon die variansie in die rypwordingsindeks, saam met TSS, TSS/TA, kleurparameters a* en h en die totale kleurverskil, verklaar. Die bepaling van die multikomponent verspreiding van T_1 het twee komponente tot gevolg gehad, een stadig en die die ander vinnig. Verbeteringe in die herhaalbaarhied van die transform is egter nodig voordat verdere analise en die betroubare indentifisering van pieke gedoen kan word. Die verkreë resultate wys egter dat daat geleenthede is vir die gebruik van SQUID-gemete KMR spektrale data in die T_1-gebied vir verdere studies van die gehalte van piesangs, en waarskynlik ook ander vrugte. Dit is egter belangrik dat

die temperatuurafhanklikheid van T_1 in berekening gebring moet word wanneer meer robuuste modelle ontwikkel moet word.

Fourier transform NIR metings is gebruik om die interne gehalte en meganiese skade in appels te bestudeer. Drie kultivars van twee verskillende bronne, en drie spektrometer modusse van twee FT-NIR spektrometers is gebruik om robuuste modelle te bou. Verskillende vlakke van voorspelbaarheid vir elke eienskap is verkry vir verskillende kultivars, deur van PLS regressiemetodes gebruik te maak. Die voorspelbaarheid was ook verskillend tussen die spesifieke verkrygingsmetodes, en was ook afhanklik van die eienskappe. Dit is waargeneem in al die scenario's (enkel-inklusief en alles-inklusief, asook bron) dat die emissie kop (EK) van die Matrix-F spektrometer tot dieselfde model gedrag gelei het as vir die integrerende sfeer (IS) van die veeldoelige analiseerder (VDA) FT-NIR spektrometer, in alle modelle wat TSS voorspel het. Modeloptimisering is suksesvol gedoen deur beide voorafprosseringsmetodes en genetiese algoritmes toe te pas op PLS van niegeprosesseerde spektra. Die invloed van kultivar of die tipe instrument op modelle wat TA voorspel, was verkillend van modelle wat TSS en TSS/TA voorpspel, en in die geheel met slegter modelprestasie. Die resultate het getoon dat sekere aspekte waarskynlik voorkeur sal toon vir kalibrasie oordrag tussen EK en IS verkrygingsmodusse.

Kneusing in appels kom dikwels voor en is moeilik om waar te neem, veral as die skade nog nie ekstern sigbaar is nie. NIR, meestal multispektraal, hiperspektraal en VIS/NIR, word dikwels gebruik om tussen beskadigde en nie-beskadigde weefsel in appels te onderskei. Dit blyk uit talle navorsingsverslae dat dit gebruiklik is om veranderlike seleksie te doen met NIR. In hierdie studie op kneusingskade is veranderlike seleksie deur genetiese algoritmes, soos beïnvloed deur kultivar, gedoen en gevalideer deur die veranderlike belangrikheid in projeksie (VBP) metode, wat 'n ander benadering is as die filtermetode. Voorkeur golflengtebande is hieruit geïdentifiseer. Beide metodes is met die literatuur vergelyk. Die navorsing is 'n goeie basis vir toekomstige ontwikkelinge in aanlyntoepassings in die vrugtebedryf.

Addisionele gevorderde toepassings van twee hoogsontwikkelde spektroskopiese tegnieke om nie-destruktiewe evaluasie van vrugtegehalte te doen, is geïdentifiseer. Aanbevelings vir toekomstige industrietoepassings is gemaak aan die hand van die belowende nuwe toepassings.

Acknowldgements

Firstly, I would like to thank my supervisor, Prof Willem J Perold for all his help, the opportunities for learning and self growth and for the encouragement throughout the project. His guidance and support are acknowledged and greatly appreciated.

Also thanks to my co-supervisor, Prof Umezuruike L Opara, for his support and feedback on my work. Your inputs were highly valuable and are acknowledged.

I would like to thank Dr Helene Nieuwoudt from wine biothechnology for her help with the laboratories and for providing and introducing me to softwares I needed.

Also, thanks to Prof Martin Kidd and Prof Daan Nel for helping with some data analysis and arrangement, and Ricardo Leardi for providing the genetic algorithm used in this project.

I would also like to thank all the administrative personnel. To Mr Johan Booysen, Mr Larry Morkel and Ms Nazneen Ebrahim, thank you all for all the hard work behind the scenes that you did for me.

To all my colleagues in office E210, past and present, all colleagues in postharvest technology, thanks for all the good times. The last four years would not have been the same without all of you.

To all my friends, thanks for the support, for checking on me from time to time. Thanks for listening to me when things did not go according to plan. I would not have made it if it were not for your support.

Special thanks go to my family. My mother and father regularly encouraged me throughout my studies, as well as my uncle and my sister who always called and for their moral support. I love you all. Lastly, a special thanks to Zinash A Belay, thanks for all your love and support. You played an invaluable role throughout this project.

Contents

Nomenclature

Abbreviations

1der	:	First derivative
2D	:	Two-dimension
ANN	:	Artificial neural networks
BD	:	Bruise diameter
Cal	:	Calibration
Ch	:	Checkers groceries store
CH	:	Hydridocarbon
CH_2	:	Dihydridocarbon
COE	:	Constant offset elimination
CPMG	:	Car-Purcell-Meiboom Gill
EH	:	Emission head
E_i	:	Energy of impact
FID	:	Free induction decay
FLM	:	Food Lovers' Market
FTIR	:	Fourier transform infrared
FT-NIR	:	Fourier transform near-infrared
GA	:	Genetic algorithm
GD	:	*Golden Delicious* apple cultivar
GS	:	*Granny Smith* apple cultivar
HPLC	:	High-performance liquid chromatography
ILT	:	Inverse Laplace transform
IS	:	Integrating sphere
LF	:	Low field
LIFS	:	Laser-induced fluorescence spectroscopy
Loc	:	localised waveband
LV	:	Latent variable
MIT	:	Massachussetts Institute of Technology
M-Mnorm	:	Min-Max normalization
MPA	:	Multi-purpose analyzer
MRI	:	Magnetic resonance imaging
MSC	:	Multiplicative scattering correction

NIR	:	Near-infrared radiation
NIRS	:	Near infrared spectroscopy
NMR	:	Nuclear magnetic resonance
OH	:	Hydroxyde
OPLS-DA	:	Orthogonal partial least squares discriminant analysis
PCA	:	Principal component analysis
PLS	:	Partial least squares
PLS-DA	:	Partial least squares-Discriminant analysis
PLSR	:	Partial least squares regression
PSO	:	Partical swarm optimization
PTR-MS	:	Proton transfer reaction mass spectroscopy
R^2	:	Coefficient of determination
RG	:	*Royal Gala* apple cultivar
RH	:	Relative humidity
Ri	:	Ripening index
RMSEC	:	Root mean square error of calibration
RMSECV	:	Root mean square error of cross validation
RMSEP	:	Root mean square error of prediction
RPD	:	Ratio of performance to deviation
SD	:	Standard deviation
SLS	:	Straight line subtraction
SNV	:	Standard normal variate
SSC	:	Soluble solids content
SQUID	:	Superconducting quantum interference device
SQUID-NMR	:	SQUID-detected NMR
TA	:	Titratable acids
TCD	:	Total color difference
TSS	:	Total soluble solids
TSS/TA	:	Sugar:acid ratio
ULF	:	Ultra-low field
UPEN	:	Uniform penalty
Val	:	Validation

List of Figures

List of Tables

Chapter 1

Introduction

1.1 Motivation and problem statement

Fruits and vegetables account for an integral part of food consumption. They are consumed as fresh produce and used in juice and wine making, and in cooked foods. Fresh fruit constituted an important part of up to (50%) of the total exportation of agricultural products in South Africa, valued to R26 billion ($ 2.4 billion) in 2014 [1]. The demand for high quality delivery require the availability of better technologies for quality control.

Quality testing and control of agricultural products are of key importance to ensure good quality of the products sold to consumers. It is also useful in determining appropriate time to harvest of the crops that are still in the field, and it provides a good way of grading the products before packaging for delivery. Knowledge of the appropriate harvest times is very important to ensure long storage periods for fruits and optimal ripening after harvest [2, 3]. Quality testing is best achieved by non-destructive methods, as they prevent postharvest losses, which is seen as one of the ways of reducing food shortages in the world [2]. The existing non-destructive technologies for internal quality are expensive, require a high level of expertise, or are time consuming. To improve effectiveness in quality control one should prioritize simple non-destructive techniques, requiring minimum expertise, and affordable for both large and small scale farmers or industrial companies. Nuclear magnetic resonance (NMR) and Near infrared spectroscopy (NIRS) are among the most versatile analytical tools for non-destructive quality evaluation applicable in the food industry [4].

The NMR is used to elucidate the properties of studied materials by exploiting the relaxation processes of nuclear spin magnetization. It has demonstrated a lot of potential for quality testing, particularly for portable and ex-situ systems [5], and further exploitation of the technique is thought to be best achievable through col-

laborative research [6]. The interest in this technique is based on, amongst others, its simplicity of operation [7], its ability to probe internal quality, its non-destructive nature, it being non-laborious and its cost and time effectiveness.

Most of the latest technological developments of this technique have been focusing on developing systems working at low-field, which is best achieved by utilizing a superconducting quantum interference device (SQUID) as the sensor and proving its potential in various applications [8, 9, 10]. The extent to which it can be used is not completely known, and the interpretation of the results of measurements is not fully understood. Full protocols for quality detection of most fruit types already studied are nonexistent.

Dedicated investigation of the applicability of the technique to agricultural products would revolutionize the technology in the food industry, especially for probing internal quality on automated sorting lines or portable devices, which has been a challenge to implement so far. These hurdles are associated to many things, as explained in [6], and to implement such a full prototype, one needs to start from a focused specific application (specific type of fruit or attribute). There is still plenty of room to further the progress of implementing SQUID-NMR for routine measurements, and it is understood that extensive studies of the specific application precedes the inclusion of all its features that are needed in the measurement system.

To implement the SQUID-NMR technique for such industrial applications, it is required to establish models usable for routine measurements. Such models are expected to be at the simplest, based on attributes that are highly correlated to measurable NMR parameters, the relaxation times in this case [11].

The establishment of models usable for routine measurements would be a key requirement for developing SQUID-NMR systems that meet the required degree of user-friendliness, and thus improve competitiveness of growers on the local and international market. This would improve the quality of produce supplied to the market and the nutritional value for fruit consumers, and help prevent or reduce losses emanating from defects developed in products stored during export.

NIR/IR spectroscopy is also arguably the most advanced analytical technology in quality testing of food stuff, especially in terms of adaptability of design, possible and actual applications, data analytical tools there associated, etc. Some of its limitations may lie in the issue of the radiation's penetration depth which depends on the nature of the material under study. As an example, the thick rind of citrus fruits makes it difficult to probe internal quality of whole, unpeeled fruits. In some cases where the NIRS can't provide enough information as desired, mid-infrared spectroscopy, mass or Raman spectroscopic techniques may be used conjointly to

complement or shine more light to the subject matter. Handheld NIR devices and online NIR systems have had the main attention in the application to horticultural industry [12, 13]. Even though NIR hyperspectral imaging made it possible for online sorting [14], it's still an expensive equipment and faces challenges related to high speeds used on conveyor belt in real industrial application. Also, every application (type of product, features to be studied, etc.) requires its own model(s) and calibration transfers from one spectrometer to another requires expert's hand and may require modifications or extended studies [15]. In South Africa, and likely allover Africa, such advanced systems and calibrations appropriate for locally produced agricultural products are scarce and non-existent in some countries. Substantial evidence to this can be drawn from research reports summarized in Table 2.1. There is not only a need to introduce low-cost non-destructive techniques, but also to study the feasibility of their implementation (e.g. adaptability to small scale farmers' needs) and build calibrations that are appropriate for local produce. The emission head of the 'Bruker' Matrix-F FT-NIR system is one typical design intended for process monitoring that allows for large sample sizes and a tool towards online applications.

The two high-end analytical technologies mentioned above constituted the focus this research.

1.2 Aims and objectives

A study that investigates the usability of low-field NMR to predict quality of different fruit types was conducted, and a model for predicting maturity of fruit based on monitoring changes in ripening banana was proposed.

Also evaluated, was the usability of the Matrix-F FT-NIR in non-destructive quality testing of fruit in reference with laboratory standard FT-NIR spectrometers.

The objectives were to:

* Explore the untapped potentials of the SQUID-detected NMR for its applications to agricultural products.
* Characterize fruit quality (both internal and external) using averaged frequency domain and time domain relaxation time and propose answers to some issues related to peak assignment.
* Further studies of internal quality of fruits using FT-NIR techniques in different scenarios implying the inclusion of biological variability.
* Explore genetic algorithm based model optimization at predicting some internal quality attributes.

* Study the performance of the Matrix-F FT-NIR spectrometer in light of online applications and calibration transfer issues.

* Study the feasibility of detecting external damage in fruit (differentiation between bruised and healthy tissue in apple fruit cultivars and predicting bruise severity)

* Investigate variable selection and model optimization as applied to the study of bruising damage.

* Provide insight on the performance of the online use-oriented FT-NIR system (Matrix-F) in reference to the standard laboratory use FT-NIR system (multipurpose analyzer - MPA).

1.3 Structure of the dissertation

The next chapter gives an overview of the background literature on the recent developments related to the aspects addressed in this project.

In Chapter 3, a detailed account of the methodology used in this study, including experimental design and execution, and data analysis is provided. Dedicated sections were used to present methodologies for individual chapters.

Chapter 4 focused on aspects of fruit quality studies using SQUID-NMR by probing different quality attributes, both external and internal, in banana fruit during ripening. Both the average and multicomponent NMR relaxation times were used as parameters for non-destructive method.

NIRS-based studies of internal fruit quality were reported in Chapter 5. Apple fruit soluble solids content, titratable acids and their ratio were used to build prediction model using NIR spectra as predictor. Models optimization was performed in different scenarios involving apple cultivars and spectrometer variability by using pre-processing and genetic algorithms.

In Chapter 6, bruise damage in apple fruit was investigated using different NIR spectrometers, techniques of model optimization and variable selection were used to specify regions of the spectra that best describe the aspects of bruising in apples.

A summary of the findings is discussed in Chapter 7 and concluding remarks and future research prospects are given.

Chapter 2

Literature Study

2.1 Fruit quality: concept and evaluation

Quality is understood as all those characteristics of a fruit (including sensory and perception related characteristics) that lead to a consumer's satisfaction. Convenience and health remain key motives for consumers selecting items of fruit, and changes in consumer awareness and response to health issues has an impact on fruit sales [16]. Diverse science disciplines such as psychology, marketing, economics, postharvest, and sensory science have studied consumer responses to fruit, so the context of consumer preferences can be viewed in different perspectives, and can thus be complementary. Quality control and evaluation can take place at many stages of the value chain and is essential for deciding fruit market value. Methods for quality evaluation can be either subjective (human senses are used) or objective (more precise, use instrumentation). During quality evaluation, fruit may be destroyed (entirely or partially) and the method used is destructive. Non-destructive methods leave the fruit samples intact. More on quality attributes diversification, classification and evaluation methods can be found in [17, 18, 19].

2.1.1 Non-destructive methods

Non-destructive methods are useful, not only because they don't waste the sample, but also because it can be used in the field before and after harvesting. They provide a possibility for measuring multiple attributes simultaneously and may allow for rapid online use for sorting and grading of products [17]. Non-destructive methods make it possible to detect both external quality, such as shape, size and defects, and internal quality which include internal defects, rots, internal breakdown, granulation, dehydration, etc. Cameras are commonly used for fruit sorting based on color, and are applicable even on commercial packing lines. On the other hand,

magnetic resonance imaging (MRI) is considered the most successful technique in detecting internal defects, relative to its competitors (optical, X-rays and acoustic wave based techniques) [20, 21, 22, 23]. However, it is too expensive and needs advanced technical expertise. It is thus not yet fit for industrial use. Online sorting based on sugars (total soluble solids) or similar attributes, and mobile devices usable in the orchard, has been achieved using NIR spectroscopy and hyperspectral imaging [14, 4]. Nevertheless, the number of attributes that are currently used for online sorting is limited and could be increased by building specific models that are appropriate to the attributes to be used.

2.2 Nuclear magnetic resonance

2.2.1 Definition and history

It is in 1943 that Stern discovered the magnetic moment of a proton. A year later, Rabi developed a resonance method to record such a property. The radar technology developed during World War II influenced many of the electronic aspects of the NMR spectrometer and made it possible for the first development of the related spectroscopy by teams at Stanford and Massachusetts Institute of Technology (MIT) in 1946 [24]. The first measurements of Nuclear magnetic resonance (NMR) were realized by Bloch and Purcell, winning them a Nobel price for Physics in 1952. Soon after, NMR emerged as a triumphant spectroscopic tool for exploring the composition and chemical environment of molecules in the liquid state [25], leading to high resolution NMR techniques in 1991, by Ernst Wuthrich. Applications have spread from chemistry [26] to medicine, food industry and many more. Figure 2.1 summarizes the evolution of NMR technology, from inception to present and future.

2.2.2 Magnetic resonance domains

NMR spectrometry is alluded to in terms of resolution or field strength. Usually, the higher the magnetic field used the higher the resolution. The field strength increases with homogeneity, complexity and of course, with cost. Low-field regimes are usually used in time-domain instead of frequency domain, and are appropriate for quality control using relaxation and diffusion studies (relaxometry and diffusometry). They are also the way to go for industrial applications. A summary of NMR regimes is given in Figure 2.2.

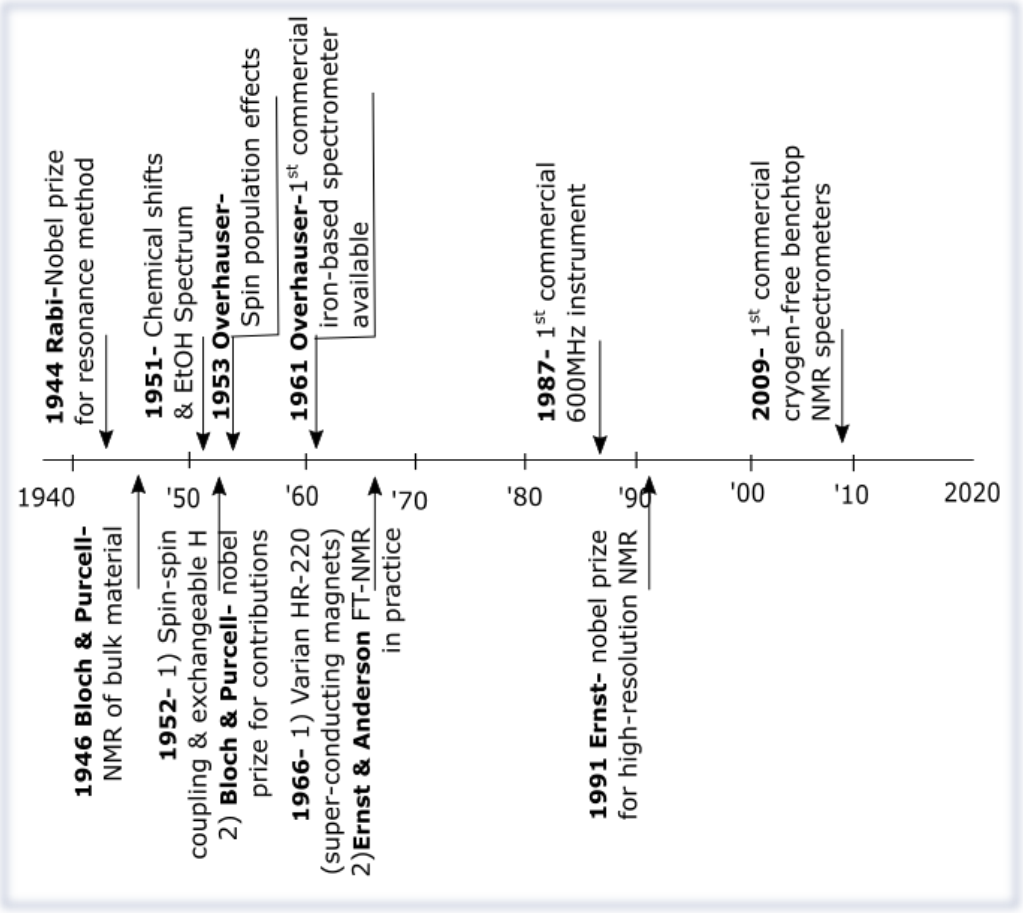

Figure 2.1: The evolution of NMR technology: from inception to present and future [27]

2.3 Nuclear Magnetic Resonance at low fields

The term low-field is commonly used in NMR systems that work in the kilohertz regime and below, while the megahertz regime is called high-field [28]. The detection of the decaying NMR signal (FID) and the methods used in spectral transforms present different levels of challenge from one NMR regimes to the other, and thus are mostly different. Detection of the NMR signal at low fields is best done by using superconducting quantum interference devices (SQUIDs), while Faraday detectors are most popular for high-field NMR detection [18]. In extremely complex multicomponent, multiphase systems with high heterogeneity from molecular to macroscopic scales, such as real food (mostly soft solid) items, low-field (LF) NMR has real proven potential in probing food functionality in real time changing situations (storage, processing, etc.) [29]. LF NMR relaxation and diffusion studies have mostly been one-dimensional and are essentially single nucleus measurements at

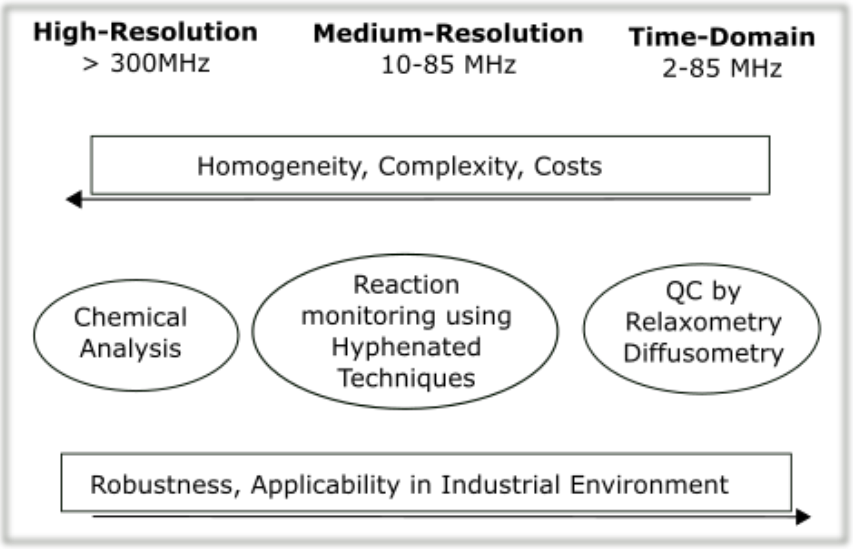

Figure 2.2: The trend of NMR technology field- and application-wise [10]

a fixed frequency, which in some cases may not allow to exploit the huge amount of information potentially available in the NMR signal. Multidimension relaxometry and diffusometry have opened doors for more possibilities for NMR based research in foodstuff [29]. It has also been reported that at LF, open access, one sided, and most generally low cost NMR systems that allow for non-destructive measurements can be developed [30, 31]. Imaging of some materials that normally couple with applied magnetic fields causing susceptibility artifacts broadens resonance lines at high fields. It becomes easy at LF and ultraULF where these artifacts become significantly reduced [32].

2.4 Using SQUIDs to detect Low-field NMR signal

Detecting NMR signal at low-fields and ultra low-fields requires the use of a superconducting magnetometer (SQUID), a magnetic flux-to-voltage converter of very high sensitivity with a response that is independent of frequency [32]. This solves the problem that Faraday detection, usually employed in conventional systems, is difficult to measure at LF and ULF, since in conventional detectors, the induced voltage signal scales with the Larmor frequency. Progress in improving the quality of ULF NMR detection and exploiting its full potential is continuously being made in different areas of application, including food contaminant detection [33, 34]. Matlashov and coworkers reported on the first MRI system that uses a SQUID gradiometer in the microtesla range (1 Gauss). It was tested in Albuquerque airport for non-invasive detection of liquids in 2008 [9]. SQUIDs have allowed for simul-

taneous measurements of biomagnetic signals (magnetocardiography and magnetomyography) by NMR, which is a capability that conventional rivals cannot offer. This offers a way of increasing efficacy and decreasing errors in current techniques of neuroimaging [35]. Michelle Espy, in her review, reported that the achieved performance in SQUID-based ULF systems is not without challenges and critical advances are to be made over the next few years if it is to move past the work of a few research groups [36]. More about designs and applications of SQUID detected LF and ULF NMR can be found in [8, 37, 38].

2.5 The nature of NMR relaxation and relaxometry

Applications of low-field NMR in the industry are commonly based on relaxation time analysis. NMR spectroscopy is part of a wide range of physical methods that are represented by a sum of exponential decays. Some other related methods are fluorescence spectroscopy and chemical relaxation. In chemically or physically heterogeneous systems such as vegetal tissue, relaxation decays are of a multiexponential nature [39]. Information about processes like exchange and diffusion, and compartmentalization, can result from the analysis of these decays. Multiexponential decay analysis is done by various mathematical methods, and they are based on either a discrete number of exponential terms (e.g. Marquardt algorithm)or continuous distribution of relaxation terms (inverse Laplace transform with Padé approximation, linear prediction, etc. [40]).

2.5.1 Multiexponential relaxation curve fitting

In the course of developments of NMR imaging Bakker and Vriend proposed a 'simplified' bi-exponential model for implementation in quantitative MRI. All biological tissues tested, were found to be best bi-exponentially characterized with mostly two components of T_1 (T_{11}<20ms and T_{12}>300ms), except for fat [41]. Musse and coworkers in their study of postharvest ripening of tomato fruit based on T_1 and T_2 relaxometry used both the maximum entropy method [39] and the Levenberg-Marquardt algorithm [42] to obtain multicomponent relaxation distributions. Changes in both characteristic times were found to depend on the tissue type and matched fairly well between fruit [43]. Pedersen et al. devised a method, named SLICING, for two-dimensional and noniterative T_2 decomposition of low-field NMR data, similar to other algorithms like DECRA [44] and MATRIXFIT [45]. Relaxation times distributions are used to characterize fluid content, type and pore size in porous media [46, 47, 48]. Various other methods have been used in various instances for the determination of the multicomponent distribution of relaxation times and for

solving the issues related to the inversion problem. Related details, including the method's limitations and/or practical uses, can be found in [49, 50, 51, 52, 53, 43].

2.5.2 Inverse Laplace Transform

The Fourier transformed NMR shows resolved signals from a nuclear magnetization that depends on more than one resonance frequency, in the frequency space. However, there are several systems where heterogeneity of the sample is not reflected on anisochronicity in the NMR frequency spectrum, which becomes a hindrance in conducting a detailed study. This heterogeneity is reflected in the spin relaxation times T_1 and T_2 [54] and achievable only at low fields where chemical shifts are not resolved [55].

Relaxation experiments give indirect measurements that are linear integral transforms (2.5.4) of quantities to be estimated [56]. Different proton pools within a sample are each characterized by different relaxation times, so the data is best represented as a normalized continuous distribution of relaxation times. Within this framework, the observed signal, $M(t)$, is now given by

$$M(t) = M_\infty \int dT_1 P(T_1)[1 - 2e^{-t/T_2}] \tag{2.5.1}$$

or

$$M(t) = M(0) \int dT_2 P(T_2) e^{-t/T_2}. \tag{2.5.2}$$

The expressions (2.5.1) and (2.5.2) are Laplace transforms of the probability $P(T_1)$ and $P(T_2)$ respectively. These can be called relaxation time spectra and are obtained by inversion of the Laplace transformation of the signal $M(t)$. In the 2D relaxation spectra, protons with the same T_2, but different T_1 values, can be resolved. This is achieved by combining both parts so that the observed signal becomes a 2D matrix $M(t_1, t_2)$, such that

$$M(t_1, t_2) = M_\infty \int dT_1 \int dT_2 P(T_1, T_2) \times [1 - 2e^{-t/T_1}] e^{-t/T_2}. \tag{2.5.3}$$

The Inverse Laplace Transform, as it is generally understood, can be represented by a function $f(t) = \mathbf{L}(g(R))$, such that

$$f(t) = \int_0^\infty g(R) e^{-Rt} dR, \tag{2.5.4}$$

where $R = 1/T$ is the relaxation rate, $g(R) = \mathbf{L}^{-1}(f(t))$ a certain function of R to be estimated. $\mathbf{L}$ is the Laplace operator. To elucidate the sample heterogeneity based on relaxation processes, one has to deal with inverting linear operator

equations and these are generally ill-posed problems (there exists many possible solutions which fit to the data within experimental error). Hence, the inversion is not straightforward, and statistical regularization methods are required. Some methods include maximum entropy and non-negative least squares [56, 54].

The first algorithm with capabilities to perform ILT of NMR data was introduced in 1982 by S W Provencher, and given a name 'CONTIN' [57]. Lee and co-workers introduced a pulse sequence that enabled detection of exchange between species with different transverse relaxation rate constants, for 2D ILT NMR [54]. Nowadays two algorithms ('WINDXP' and 'UPENWIN') are available, that are capable to perform the transform, and represent data in a flexible graphical form [58, 59, 55, 60, 61]. The advent of a new algorithm for 2D Laplace inversion in 2002 by Song et al., have revolutionized the use of low-field NMR. The algorithm performs a constrained non-negative least squares fit on 2D data [62]. Venturi and Hills proposed new protocols of acquiring 1D and 2D relaxation time spectra, emphasizing their implementation on low-field benchtop systems that have no pulse-shaping capabilities and equipped with constant non-switched gradient [55]. Resolved peaks arise from intra- and extra-cellular proton pools, from metabolites and cell biopolymers, which are especially evident in 2D $T_1 - T_2$ relaxation spectra. It is therefore evident that relaxation time spectra have far greater diagnostic potential than single effective T_1 or T_2 spectra.

The uniform-penalty inversion (UPEN) algorithm is basically a least square minimization routine involving some added penalty factors to the square error of fit and curvature. Ghosh et al. use simulated CPMG data to study the accuracy of the UPEN algorithm [63]. Since such an inverse problem is of ill-conditioned nature, a small noise results in enormous change in the model estimate. Data synthesized from a known T_2 distribution helped estimate the accuracy of the algorithm. They came up with some reliability measures of the computed models, which are dependent to the SNR of the data.

Nonetheless, the progress made thus far promoting the use of low-field NMR, and the interpretation of relaxation spectra of heterogeneous materials are not fully understood, especially in agricultural products. Extensive studies need to be conducted in the context of these proven new capabilities of the technique.

2.6 Applications of low-field NMR in horticultural products

Low-field NMR has been vastly applied to study quality of horticultural products, both fresh and processed. Table 2.1 summarizes some reported studies and their

main findings. The regions (country) where the research was conducted, the NMR field regime, the fruit characteristic studied and NMR parameter used in the study are also indicated. More studies were reported on greek grape [64] and class greek wine [65], almonds [66], apple fruit [67], potato [68], tomato (cell water distribution) [69], lignin [70], orange juice [71] and more [72, 73].

Product	Quality	Finding-summary	MR-parameter	Location	NMR regime	Reference
Apple	Mealiness	Increasing mealiness caused an increase in T_2	MRI & NMR water ^1H T_2	Belgium	HF(100MHz)	[74]
Corn (sweet)	Maturity	A possibility for T_2 based models for the prediction of sweet corn maturity to determine harvest time	T_2	USA	HF(4,7T)	[75]
Potato (cooked)	Texture	LF-NMR (CPMG) relaxation on raw potatoes can be an alternative rapid method for detecting sensory texture of cooked potatoes.	Bi-exp T_2	Denmark	LF (0,47T)	[76]
"	Dry matter	T_1, the CPMG relaxation curves and the amplitudes of T_{21} and T_{22} were highly correlated with the dry matter content	T_1, T_{21} and T_{22}, CPMG curve	"	LF(0,47T) & HF(7T)	[77]
Potato (raw)	Texture	Quality templates for calibration of the MRI instrument can be developed, enabling sorting for desired quality attributes	T_1 weighted spin-echo images	"	HF(7T)	[78]

Product	Quality	Finding-summary	MR-parameter	Location	NMR regime	Reference
Potato (processed)	Starch	T_1-T_2 reveals differences in types A and B starches under the same treatment and in A type starch under two distinct processes.	2D T_1-T_2 correlation	Norwich, UK	LF(23.4MHz) HF(300MHz)	[79]
Latex	Stability	According to T_2, the latex continuously had significant degradation after 6 months of storage at ambient conditions, when no chemical or physical treatment is used	1H-T_1,T_2	RJ, Brazil	LF (23MHz)	[80]
Egg, cellular tissue, hydrocolloids		Results illustrate the considerable potential of 2-D T_1-T_2 spectroscopy for quality control in the agro-food sector	2D T_1-T_2 correlation	Norwich, UK		[81]

Product	Quality	Finding-summary	MR-parameter	Location	NMR regime	Reference
Tomato	Ripening	A demonstration of macroscopic structural changes as well as the changes in the T_2 and T_1 with fruit maturity provided knowledge on the ripening process and important information for further studies of tomatoes and other fruit	T_1, T_2	Rennes Cedex, France	LF(0,2T) & HF(0,47T)	[43]
	Firmness	Correlation between T_2 and fruit firmness in two seasons was poor. Experimental results didn't support continued development of an NMR sensor based on T_2 differences for in-line sorting of processing tomatoes.	T_2	Davis CA, USA	LF(0,1T)	[82]

Product	Quality	Finding-summary	MR-parameter	Location	NMR regime	Reference
Banana	Ripening	By analysis of T_2 and D: description of sub-cellular water distribution, changes of water dynamics and possibility to measure translational mobility of water molecules in cellular compartments	T_2, D	Roma, Italy	LF(20MHz), HF(11,7T)	[83]
	"	The novel interpretation for the increase in T_{2vac} based on reduction of Fe+3 and O2 concentration is an alternative mechanism to that based on the hydrolysis of starch in amyloplasts	T_2, D, T_1-T_2	Sao Paulo, Brazil	HF(2,1T), LF(2MHz)	[49]

Table 2.1: A summary of NMR spectroscopy and relaxometry applied to agricultural products, fresh and processed.

2.7 Near-infrared spectroscopy

The technology of near-infrared spectroscopy is based on the interaction between matter (molecular bonds) with the electromagnetic radiation in the near-infrared range (780 - 2500nm). While mid-infrared induces vibrational changes in the molecular bonds that can be exploited to characterize the material interacting with the radiation, near-infrared allows for analyzing matter by exploiting the overtones of the fundamental vibrational energy of the mid-infrared and combinations [84].

There exist a wide variety of NIR spectrometers with different capabilities based on their specific design and application flexibilities. Hand-held NIR spectrometers can be used 'on-field' where temperature changes [85, 86], which normally affect NIR measurements, can be regulated or taken into account automatically. Other devices are fit for lab use only, whereas some, appropriate for online use, may accept different terminals for radiation channeling, like fibre optics to access difficultly reachable areas, such as pipeline or other processing systems.

It can be seen from Figure 2 that specific chemical bonds undergo certain effects that depend on wavelength regions. In such an amalgamation of information it is often necessary to use mathematical and/or statistical methods to extract relevant information from the spectra.

2.8 NIR and Chemometrics

Chemometrics is the application of mathematical and statistical methods to improve chemical measurements for the optimal obtention of relevant information from chemical and physical measurements on material systems [87, 88]. Chemometrics goes toe to toe with analytical methods, one of which is NIR spectroscopy. Partial least squares (PLS) is one of the most common methods used to elucidate the embedded information from NIR spectra. In horticultural products, various PLS algorithms are used to build calibrations to elucidate various quality attributes and is the basis of many wavelength selection techniques [89]. Guidetti et al. [90] conducted non-destructive measurements with NIR on red grapes for quick prediction of ripening parameters of fresh berries in the range of $450 - 980$nm. They developed a handheld NIR device and used it to develop chemometric models for Nebbiolo grapes (Italy). TSS, TA and phenolic content (by the Glories method) were also measured using PLS-discriminant analysis (PLS-DA), principal component analysis (PCA), coefficient of determination (R^2) and root mean square errors for calibration (RMSEC) and prediction (RMSEP) as modeling parameters. In a study of browning (internal and external) of two white seedless grapes (Thomson and Regal), Daniels [91] distinguished healthy from browned berries after storage

by using PCA (test of accuracy on training and test datasets). No variable selection was done and all the different browning types were also used together. The study of browning before harvesting is also possible. As per author's recommendation [91], further analysis of the data could be based on using variable selection techniques like particle swarm optimization (PSO) to select certain wavelengths strongly associated with the browning phenomenon and only on the main types of browning (netlike on Regal Seedless and internal browning on Thompson Seedless) [91]. These examples and uncountably many other studies [92, 93, 94, 95, 96, 86, 97, 98, 15, 99, 100, 101, 102, 103, 104] have shown the effectiveness of mathematical and statistical tools in extracting relevant information from the NIR spectral data and adding to the board of knowledge of material properties, especially in horticultural and food materials.

2.9 Spectral pre-processing techniques

NIR spectral data may carry effects of physical phenomena that are unwanted in multivariate statistical analysis. Techniques for pre-processing of NIR spectra have become an important part of chemometrics and are so often used to remove these, allowing for the improvement of statistical models. These pre-processing techniques are usually either spectral derivatives or scatter-correction methods [105], as explained in the list below.

- Constant offset elimination: It is used to shift the spectra and set the y-minimum to zero.
- Vector Normalization: In order to normalize a spectrum, it calculates the average intensity value and subtracts this value from the spectrum. Then the spectrum is divided by the square root of the sum of the squared intensities, subsequent to its calculation. As a typical example, this method can be used to account for different samples thicknesses.
- Straight Line Subtraction: This fits a straight line to the spectrum and subtracts it to account for a tilt in the spectrum, if any.
- Min-max Normalization: It will subtract a linear offset and then set the y-maximum to a value of 2 by multiplication with a constant. The use is similar to that of vector normalization.
- First Derivative: It calculates the first derivative of the spectrum, allowing to emphasize steep edges of a pronounced peak, but with small features over a broad background, as well as spectral noise enhancement.

- Multiplicative Scatter Correction: Each spectrum undergoes a linear transformation in order to be best matched to the mean spectrum of the whole set. This method is often used for spectra measured in diffuse reflection.
- Second Derivative: It gives a more drastic result, but is similar to the first derivative.

2.10 Variable selection methods in PLS

NIR spectroscopy has proven usefulness in many areas of science and gains extensive uses as an analytical tool. Variable selection for the reduction of high dimensionality of the NMR data is important for improved interpretability. PLS regression being among the main modelling approaches associated with NIRS, is linked to a number of variable selection methods. Mehmood and coworkers classify them in three categories, namely filter, wrapper and embedded methods, based on how they operate PLSR [106].

According to Mehmood, the so-called filter methods use the output from the PLSR-algorithm to 'identify' a subset of important variables under certain threshold conditions of importance. 'Wrapper' methods are essentially based on iterating procedures between model fitting and variable selection. They can re-fit the PLSR-model using variables identified by the filter methods, yielding reduced models. The methods are mainly distinguished by the choice of the underlying filter method and how the wrapping is implemented. Embedded methods do the variable selection at component level. They operate as an integrated part of a modified PLSR-algorithm. Even though up to fifteen methods are mentioned, in their remarks it is noted that it is difficult to find a method that always works better than others. However, combined methods are likely to improve on individual methods. Some methods do present advantages. Genetic algorithms, for instance, do not need defining thresholds, since it can be set to perform independent random runs. It is thus unlikely to get stuck at local minima. Methods to prevent over-fitting are also established [107] and allows for not only effectively simplifying the model through variable selection, but also optimizing it.

2.11 Genetic algorithms with PLS

Genetic algorithms are used in various search and optimization problems and are based on principles of natural evolution. They use operators such as selection, crossover and mutation, similarly to those happening naturally in chromosomes. These operators direct the initial population towards convergence at the global op-

timum, through time steps called generations [108]. Variables that yield fitted models showing higher performance (or fitness) have higher probability to survive the selection and are included in variable sets in subsequent model refits [106]. Figure 2.3 is a flowchart showcasing the general view of a typical genetic algorithm.

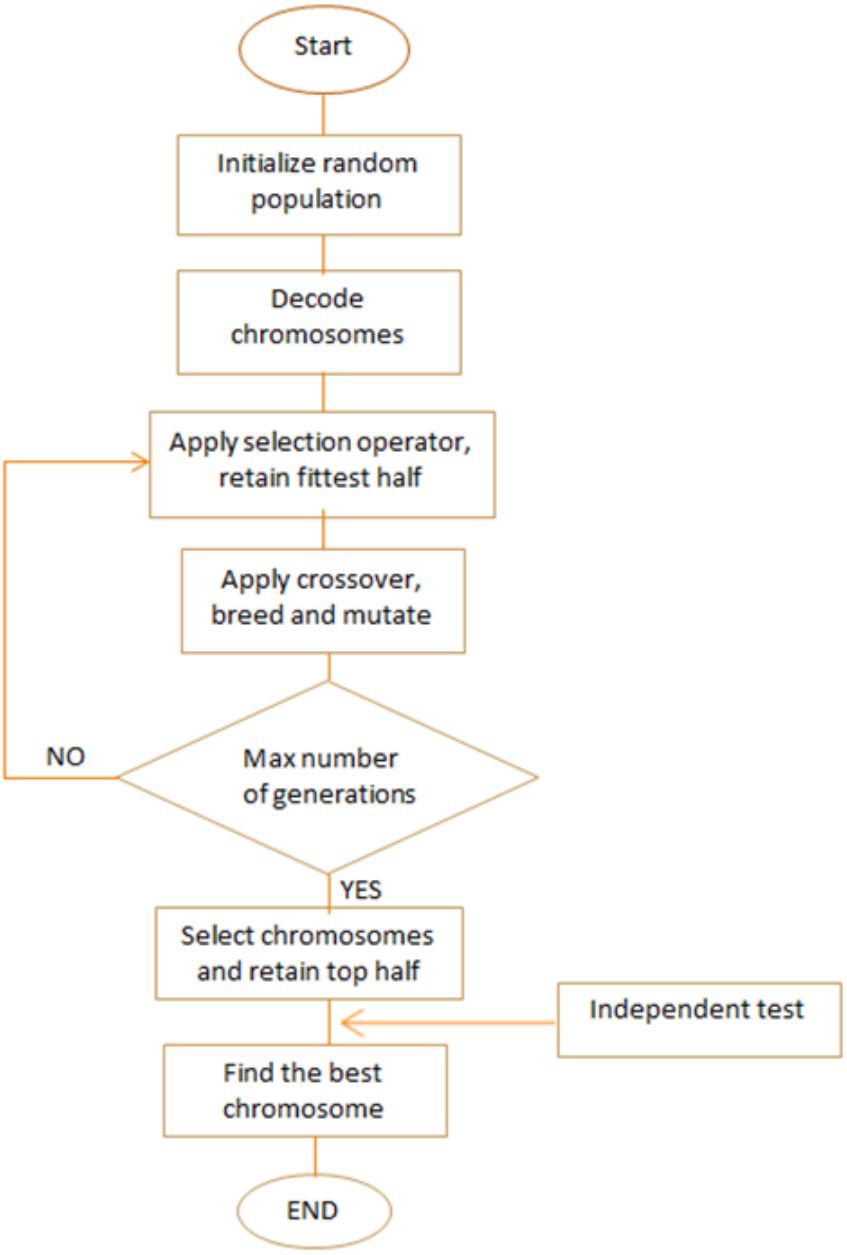

Figure 2.3: A flowchart for a typical genetic algorithm

A typical genetic algorithm follows the following steps [109, 110]:

1. Initialize population of variable sets by setting bits for each variable randomly, where bit 1 represents inclusion of a corresponding variable and 0 represents exclusion. The approximate size of the variable sets must be set in advance.

2. Fit a PLS model to each variable set and compute the performance (usually error of prediction) by, for example, a preferred cross-validation method.

3. Select 50% of variable sets with highest performance to participate in the next generation (run).

4. Perform crossover to generate offspring and then apply mutation on new generation (both surviving set and their offsprings) to form a new population. Both crossover and mutation are attached to certain probabilities.

5. Check for stopping criteria (usually a certain number of runs or an acceptable error achieved).

6. Repeat steps 2 to 5 until stopping criteria are met.

2.12 Application of genetic algorithms to NIR spectroscopy

Genetic algorithms (GAs) have been used often to optimize PLS regression models (GA-PLS regression), and they were found capable of improving PLSR models. Tewari and coworkers used genetic algorithms in combination with artificial neural networks to develop a method for quantifying sugars and to classify citrus fruits by origin using FT-NIR. PLS with HPLC reference data gave high correlation coefficient ($R^2 > 0.99$). Correspondence analysis successfully classified citrus according to variety and origin [95, 111, 112]. An example of applications of GA in combination with PLS [113, 114] on NIR data is given in Table 2.2.

2.13 Conclusion

In this chapter, the principles of low-field NMR were introduced. Principles of relaxometry and methods for inversion were discussed. NIR spectroscopy and variable selection strategies were also briefly explained. The choice in the methods used in this project was motivated.

Table 2.2: Application of genetic algorithm to NIR studies

Product	Attribute	Reference
Apple (Fuji)	SSC SSC	[115] [116]
Citrus		[95]
Pear		[117]
Mango	Firmness	[118]
Wheat		[114]
Durum wheat	classification	[119]
Egg	freshness	[120]
Beer	aging	[121]
Cow's milk	Fatty acid	[122]
Foodstuff		[114]
Gasoline		[114]
Resorcinol		[114]
Al Oil additives		[123]
Papers	Gelatin	[112]
Polymer film		[124]
Diesel fuel		[125]
Fescue grass		[125]
Pharm. tablet		[125]
soil		[126]
cafelexin		[127]

Chapter 3

Methodology

In this chapter, details on the methodology used in every chapter of this project are presented in corresponding sections.

3.1 Chapter 4: Study of banana ripening by SQUID-NMR

3.1.1 Materials and sampling

Banana samples were purchased from the *Fruit Lovers Market* in Stellenbosch and were visually classified into three distinct stages of ripeness, based on peel color (green with some yellow peel, more yellow than green, and yellow flecked peel with brown patches). Based on the classification these ripening stages would correspond to stages 2, 4 and 7 respectively, according to [128]. Figure 3.1 (A) shows ripening stages of banana fruit and was used as reference for subjective classification on day one of experiments. A ultra-low field SQUID-NMR system was used for NMR relaxation measurements. The NMR system utilizes a high-T_c dc SQUID as the sensor and provides a possibility of studying the relaxation processes of the water proton in samples containing water. The system used in this study has a cylindrical sample holder, which allows for a sample size equal to $4cm$ in diameter and $5cm$ in height. Such a sample size enabled conducting non-destructive (as far as the sample size allowed) measurements on banana fruit samples. The high-T_c SQUID-NMR was purchased from *MagQu* in Taiwan. The constant magnetic field is around 100μT (Bm = 1 Gauss) with a prepolarization field of about $60mT$ generated by a water-cooled copper-made coil. The high-T_c dc SQUID used in this system is from *Star Cryoelectronics*, and is operated in a separate magnetically shielded cryogenic unit, filled with liquid nitrogen (see Figure 3.1 (B)).

Other devices that were used are a digital refractometer (*Atago*, Japan) for TSS

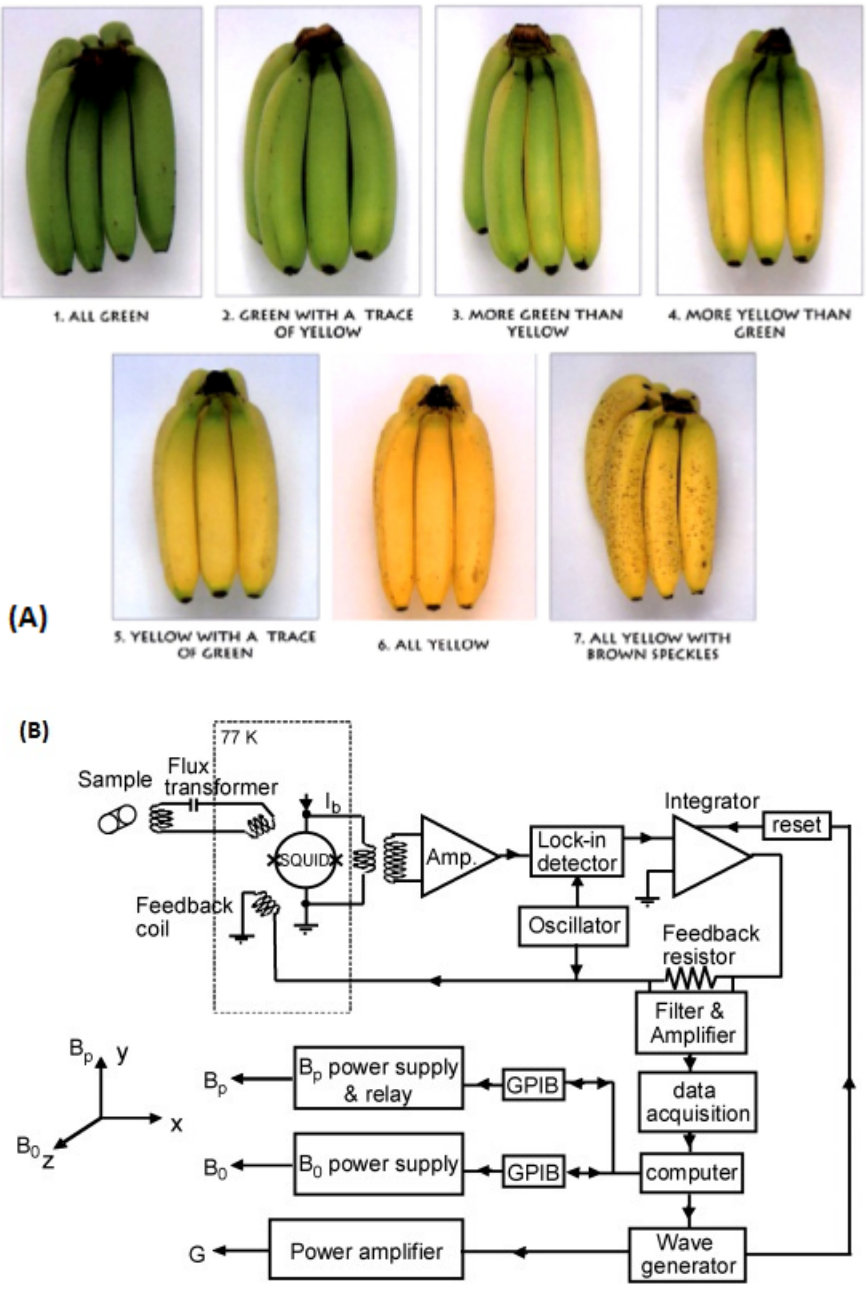

Figure 3.1: The ripening stages of banana fruit as commonly established based on peel color (A) and a schematic diagram of a high-T_c SQUID-based NMR detection system used for experiments (B) [128], [129]

measurements, and an automatic titrosampler (Metrohm) for titratable acidity measurements. A texture profile analyzer was used to measure firmness (TA.XT Plus, *Stable Microsystems*, England), and a Chroma Meter CR-400 (*Minolta Corp*, Osaka, Japan) was used to measure changes in color of the peel.

3.1.2 Experimental and analytical methods

3.1.2.1 Postharvest ripening

Fruits were stored for 10 days under conditions that favor their optimal ripening process (15 ^oC, at 80% RH). Measurements were taken every other day over 10 days of storage, i.e. six instances of measurements from day zero to storage day 10. Measurements of firmness and color index were taken first, followed by NMR measurements and then, destructive measurements at last. The measurements followed two approaches. On the first day measurements were carried out on fruits subjectively classified in three different ripening stages, based on their peel color. Secondly, fruits at the earliest ripening stage were monitored during their ripening process.

3.1.2.2 NMR relaxometry

Fruit samples were placed into the sample holder up to the maximum capacity, loaded into the instrument (SQNMR, from *MagQu*, Taiwan), followed by measurement of the T_1 and T_2 relaxation times. Each measurement was performed twice per sample, and recorded using the SQNMR software. Measurements of spin-lattice relaxation time, T_1, and spin-spin relaxation time, T_2, were conducted on fruit samples on an every other day basis to monitor their ripening process. An inverse recovery pulse sequence was used to measure T_1, and two values per unit sample (fruit) were taken. Unpeeled bananas were sized down to a length of $6cm$ by cutting through transversely and loaded longitudinally into the sample holder in such a way that the center of the sample was placed in the center of the constant magnetic field. The part closest to the pedicel, about a third of the banana in length, was left unused for the NMR measurements. The choice of which end to cut off was non-objective, but should not impair the outcome of the results. The T_1 relaxation time was measured from the reconstruction of the longitudinal magnetization M_z. The prepolarization time t_p was varied in a sequence of 0.5, 1, 1.5, 2, 2.5, 3, 3.5, 4, 5 and 7 *sec*. From a logarithmic fitting of the measured peak intensities (from the Fourier transformed spectra) with the corresponding times t_p, the T_1 values were calculated directly in the SQNMR software upon spectrum acquisition. Every single spectrum was averaged over three measurements, and only a 90^o rf pulse was used, as is shown in the pulse sequence that was used (see Figure 3.2). The time t_d was about 20 *ms* and the SQUID was triggered 5 *ms* after the rf pulse.

T_2 time measurements were acquired by spin-echo pulse sequences with 8 echoes per spectrum. The pulse sequence is shown in Figure 3.2. The envelope of the decreasing amplitudes of the echoes characterizes the T_2 decay. The echo time t_e,

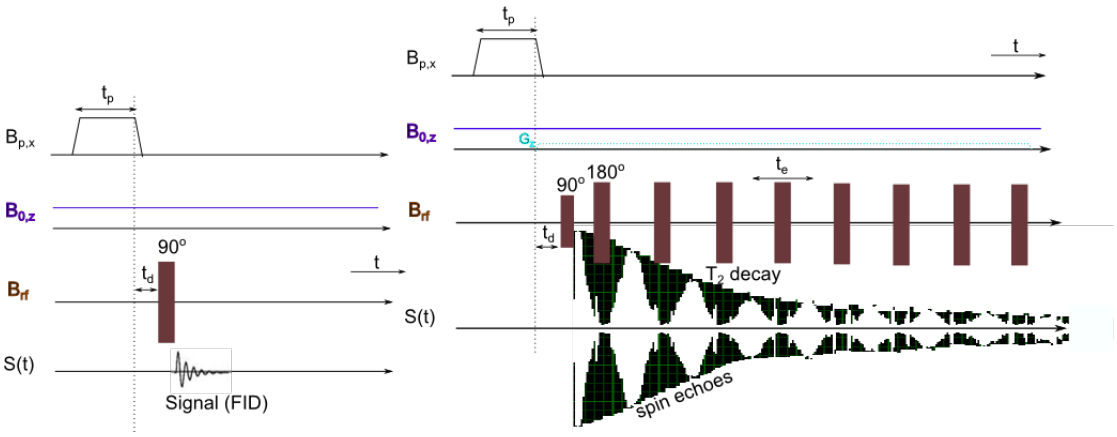

Figure 3.2: A schematic diagram of the pulse sequences used to measure T_1 (left) and T_2 (right) with the high-T_c SQNMR system

which is also the time interval between two 180^o pulses, was 35 ms. During the T_2 measurement, a gradient field G_z was used to optimize the spin echo NMR signals. The echo amplitudes or the peak intensities from the frequency domain spectrum were fitted with their corresponding elapsed times, by an exponentially decaying function to generate the value of T_2. This exponential relationship is of the form

$$S(t) = S_0 exp(-t/T_2), \tag{3.1.1}$$

where S_0 is the maximum signal intensity. Three values per unit sample were taken. These values were used later on for data analysis.

A quasi-continuous distribution of relaxation times with density $f(T_{1,2})$ was obtained by inverting the experimental multi-exponential relaxation curves with the inversion algorithm UPEN (Uniform PENalty) of the UpenWin software [47, 130]. This implements an iterative feedback procedure to compute the Inverse Laplace Transform of the NMR signal given by the expression (3.1.1), in the presence of the random noise. Mathematically speaking,

$$S(t) = \int f(T_{1,2}) \exp(-t/T_{1,2}) dT_{1,2} + \epsilon, \tag{3.1.2}$$

where $T_{1,2}$ applies for both components of T_1 or T_2 and ϵ is the error term. The distributions show features, usually peaks and/or shoulders, which can be assigned to components and/or water compartments. The area under each feature, obtained by integrating $f(T_{1,2})dT_{1,2}$ over that feature, is proportional to the number of protons contributing to its signal. The ratio between this area and the total area under the whole distribution gives the fraction of signal contributing to that component, also called "weight". In our case the signal is related to ^{1}H of water and, thus, the

weight is the fraction of water of each component.

3.1.2.3 Physicochemical quality attributes

Experiments were conducted on fruit samples to determine some of their physical properties, such as color and firmness.

The texture profile analyzer was calibrated for force with a weight of 10,000 g and to a fixed height of 4 cm. Two values were taken on banana samples at about a 1/4 of the length of the banana from both extremities. Firmness measure was considered to be the force of compression of the fruit down to 7 mm, expressed in N (Newton).

Color components were measured in the XYZ color space using a colorimeter (Chroma Meter CR-400, *Konica Minolta Sensing Inc.*, Japan) after calibration. Two values per sample were taken for color measurements, in two opposite spots at points about a 1/4 of the length of the banana from the extremities. The Chromameter was first calibrated on a standard white calibration tile (CR-A43; Y = 93.1, x = 0.3138; y = 0.3203), wiped for spotlessness. The measured values were loaded on a computer in an MS Excel spreadsheet and converted from the XYZ coordinates into the CIELAB system. A pretreatment of measured data was done on color components and data were converted to the L*a*b*(CIELAB) and L*C*h color spaces. Values of the parameters L*, a*, b*, C* and h were used in the analysis of experimental results. The CIELAB is widely used in almost all fields to measure object color and is known to produce improved results compared to the XYZ color space. The coordinates of chromaticity are a*, which varies from -60 (green) to 60 (red), and b* from -60 (blue) to 60 (yellow), as indicated in [131]. L* is an indicator of lightness and varies from 0 (very dark) to 100 (very pale). C* is the value of Chroma and varies from 0 upwards, according to the value from the center. On a full circle, the hue angle is expressed as h in degrees, starting from 0 degrees at the +a* axis.

Total color difference is used to showcase the variation of color, relative to control samples, during storage or fruit development [131]. Here we have set samples at maturity level 2 on day 1 as our control samples. We, therefore, discuss color difference in fruit samples during their ripening process. Total color difference (TCD) [132] is denoted as ΔE, and given by (3.1.3).

$$\Delta E = \sqrt{(L^* - L_c^*)^2 + (a^* - a_c^*)^2 + (b^* - b_c^*)^2} \tag{3.1.3}$$

where, the subscript c designates the control measurements.

The total soluble solids were measured using a digital refractometer (*Atago*, Japan) on juice blended from banana flesh. Three drops of juice per banana were measured and two values were averaged for every drop. The pH was measured

using a pH meter, and a titrosampler (Metrohm) was used to measure titratable acids.

All the experimental data were grouped in 12 variables corresponding to measured quality parameters, namely T_1, T_2, TSS, TA, pH, firmness, color parameters (L*, a*, b*, h and C*), and TSS/TA. Multivariate analysis methods were used to elucidate relationships between the variables. The ripening index of banana was based on visual appearance in peel color changes that occured during ripening. Regression analysis was used to determine the relationship between ripening index (Ri) and other attributes, and most specifically the NMR parameter T_1.

All statistical analyses were done using STATISTICA 11 software. Replicated measurements were averaged, and a mean value per sample unit was used for the analysis. The statistical methods involved correlation, multiple regression and Principal Component analysis. Data analysis was also done following both measurement approaches (subjective and objective), to examine whether the initial classification could be reproduced. Results from the objective classification are reported in 4.2.

3.2 Chapter 5: Measurement of internal quality of apple by NIR

3.2.1 Sampling

Apples were purchased in two installments (in two consecutive months) from two different retail shops in Stellenbosch, South Africa. A batch of 100 apples were sources from *Checkers* retail shop (Ch) and, a month later, 114 apples from *Food Lover's Market* (FLM), both in Stellenbosch. Three cultivars of apple, namely *Golden Delicious*, *Granny Smith* and *Royal Gala*, were acquired in both instances, in nearly equal proportions (see Table 6.1). Fruits were kept in cold storage (5 ^oC) pending destructive and FT-NIR measurements. They were left at room temperature for three hours to equilibrate, before being used for experiments.

Figure 3.3 summarizes the experimental design from sampling to targeted data analysis methods.

3.2.2 Destructive measurements

Both destructive and non-destructive measurements were carried out on whole fruit samples. Destructive measurements consisted of the measurement of total soluble solids (soluble solids content) and titratable acidity. The soluble solids contents were measured by slicing a small portion of apple tissue from both sides of

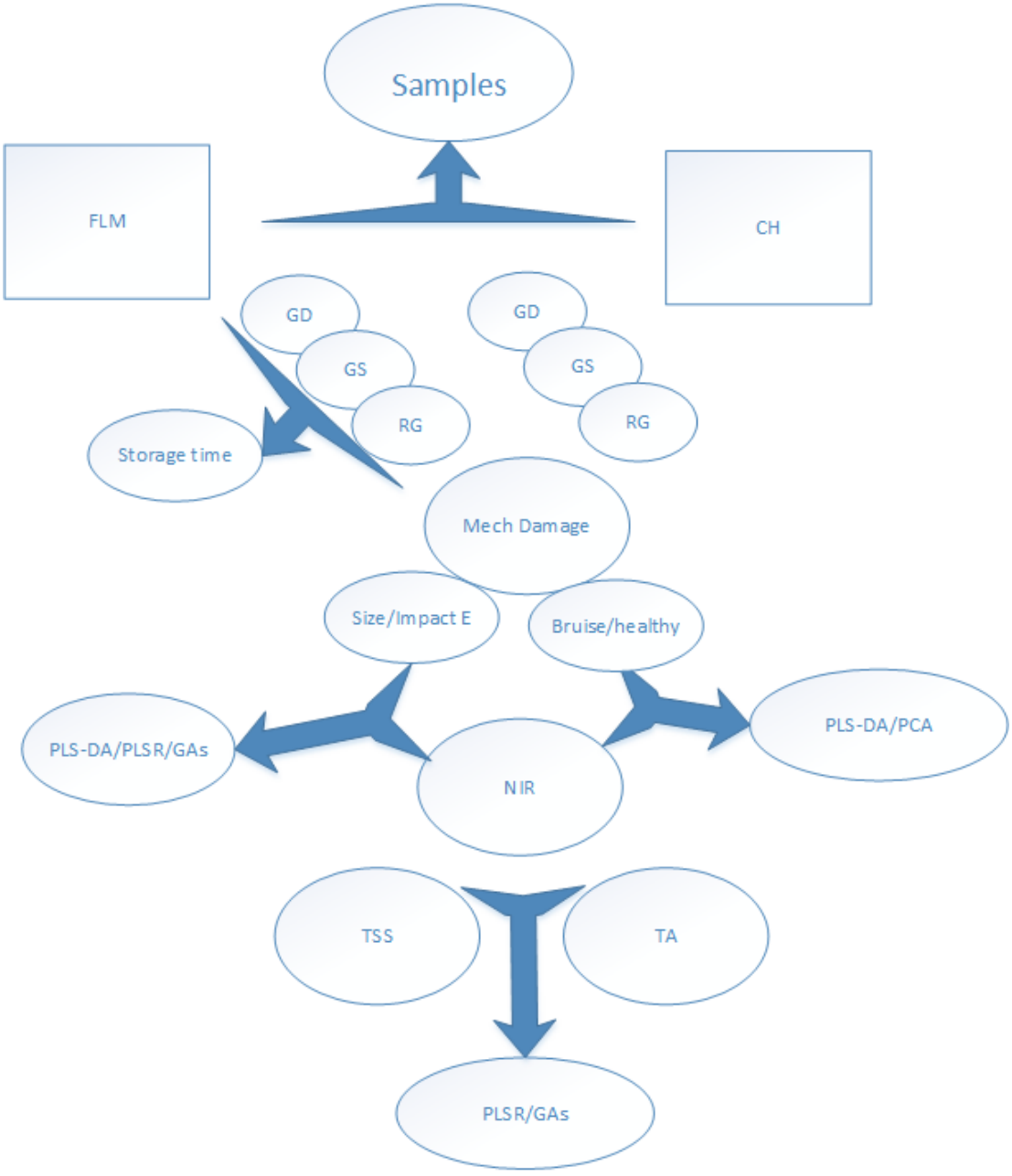

Figure 3.3: Experimental setup for NIR measurements on apples

the apple where the NIR spectra were acquired, and squeezing out the sliced tissue's juice on the lens of a hand-held digital refractometer (Palette, PR-32 α, Brix 0.0-32.0, *Atago Co. Ltd.*, Japan) for measurement. A refractometer calibration with distilled water was required before commencing the actual data acquisition. Titratable acidity (TA) on the other hand was measured on apple juice from blended fruits, whereby individual samples were prepared from single apple juice separately. TA values were acquired by titrating 2 mL of juice against 0.1 N NaOH to an end point of pH=8.2 using a compact titrosampler (862 Compact Titrosampler®, *Metrohm*, Switzerland) and the '2 mL' juice method. The values for total tiratable acids were used for the calculation of a third, derived attribute, that represents the sugar-acid ratio (TSS/TA).

3.2.3 NIR measurements

Non-destructive measurements were performed by means of near infrared spectroscopic techniques. Two opposite points around the equatorial plane of every apple were scanned on two different spectrometers under three different acquisition modes, namely the solid probe and integrating sphere mode of the multipurpose analyzer (MPA), and the open non-contact Matrix-F spectrometer. Descriptive details on these acquisition systems were given in section 3.3.1 Every spectrum was averaged over 64 scans with a spacing of 0.25 nm in all the acquisition methods. The NIR scanning range was 800 - 2780 nm on the MPA and 833 - 2500 nm on the Matrix-F. A brief overview of the data acquisition in relation to the quality attributes targeted in the data analysis is given by the chart in Figure 3.4.

3.2.4 Data analysis

A number of multivariate data analysis were used to achieve the goals in this chapter. They included but not limited to principal component analysis, partial least squares, etc.

Principal component analysis (PCA) is a technique for reducing the amount of data when there is correlation present. It is worth stressing that it is not a useful technique if the variables are uncorrelated [133]. It approximates a data matrix, X (N objects $\times$ K variables), by the product of two matrices T and P' that capture the essential data patterns of X. By so doing, a new set of variables, the principal components (PCs), which are uncorrelated, and which are ordered so that the first few retain most of the variation present in all of the original variables [134]. Many goals can be achieved through PCA including simplification, data reduction, modeling, outlier detection, classification, variable selection, etc. [135]. PCA was used in this work mainly to to detect outliers, to explore the validity of data and classification.

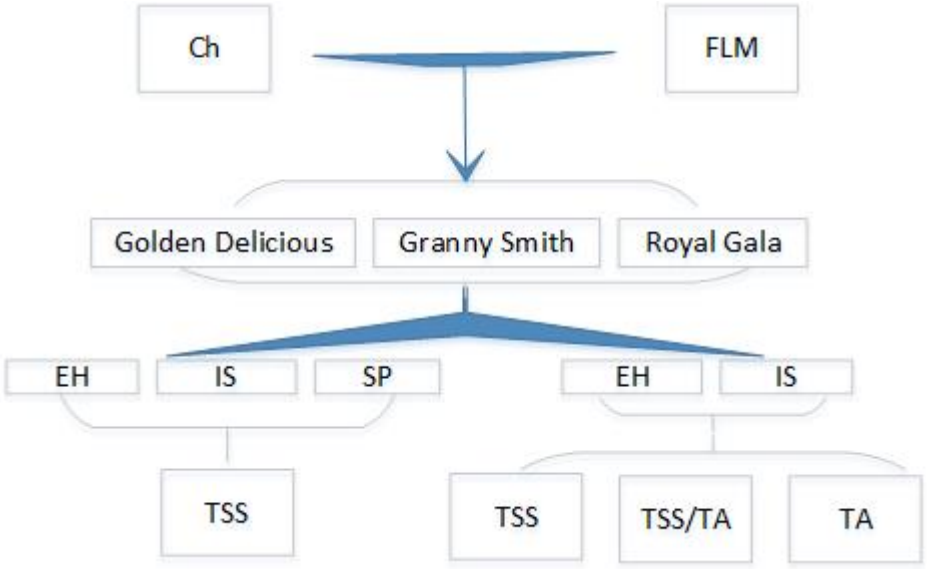

Figure 3.4: A summary of data acquisition modes and respective targeted attributes for the analysis.

PLSR is a method for relating two data matrices, X (predictors) and Y (response), by a linear multivariate model, but goes beyond traditional regression in that it models also the structure of X and Y [133]. Its ability to analyze data with many, noisy, collinear, and even incomplete variables in both X and Y makes it very useful. PLSR has the desirable property that the precision of the model parameters improves with the increasing number of relevant variables and observations [136]. Many PLS algorithms have been developed, including the orthogonal score PLS, on which most variable selection methods are based [106]. PLS regression methods were used to establish models for predicting internal quality of apples.

Spectral data were averaged per fruit (two spectra per sample) and mean-centered. Prediction models were built using 20% (22 samples) of the samples set as validation set. For every Y variable (TSS, TA, and TSS/TA) an individual model was established and results were summarized in 5.2. Furthermore, genetic algorithms described in 3.3.3 were applied to the dataset in order to try and improve prediction model performance.

Prediction models were built in different scenarios. The effect of cultivar on model performance was investigated by following the descriptive chart in Figure 3.5.

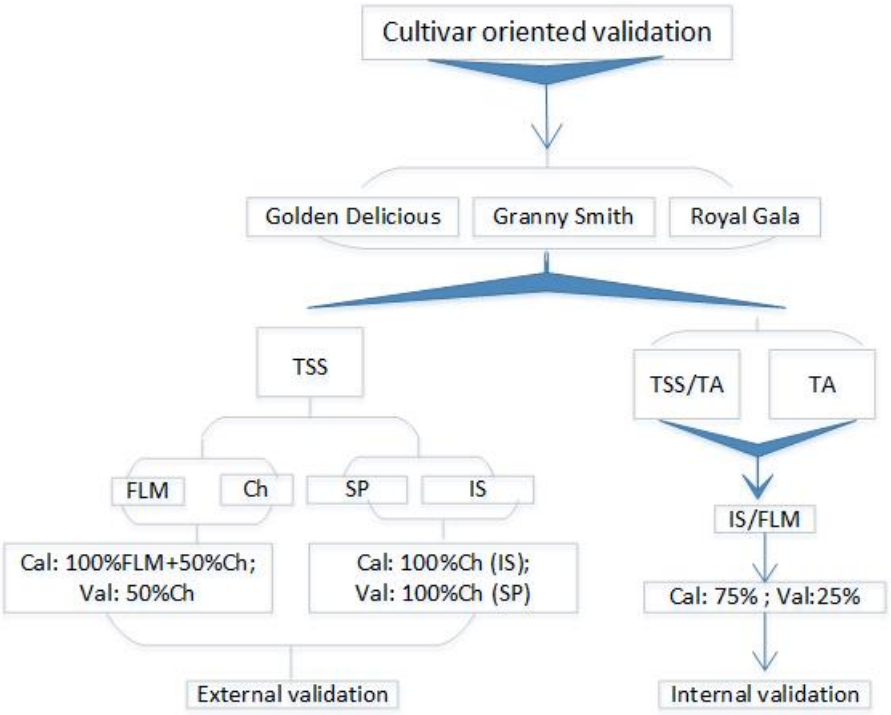

Figure 3.5: Model validation summarty applied to all cultivars individually.

3.3 Chapter 6: A study of bruise damage in apple using NIRS

3.3.1 Instrumentation and measurements

The study was carried out on three apple cultivars, namely *Golden Delicious*, *Granny Smith* and *Red Globe*. The apples were subjected to external forces by vertically dropping a steel ball (116 g, 25.34 mm in diameter) on opposite sides of the apple in their equatorial plane, one side at a time [137, 138]. A double layer of fruit tray was placed under the fruit to ensure that the bruise is produced only on the side exposed to the impact. The spots on the fruits, where these forces were exerted, resulted in bruises. The steel ball in free fall was guided in a plastic tube, 1 m long and graduated in height distances from 20 to 80cm, in steps of 15 cm. Each drop height corresponded to a specific value of impact energy (in Newton) exchanged at the time of impact between the falling ball and the fruit, assuming that virtually all of the energy of the ball was absorbed on the first impact [139]. The impact energy was calculated by the physical law of free fall, expressed as Eq. (3.3.1).

$$E = mgh, \tag{3.3.1}$$

where E is the energy of the ball as it touches the fruit (impact energy in Joule), m the mass of the ball in kilogram and h the drop height of the ball in meter. The plastic tube was perforated on both sides longitudinally, to reduce air resistance. The fall is estimated to be near 'free'. Bruise sizes were obtained by vertically slicing the fruit at a perpendicular axis through the center of the bruise, and measuring the bruised tissue sizes [138], using a pair of digital Vernier callipers (± 0.01mm). Table 6.1 shows the calculated values of impact energy relative to drop heights, and the energy levels that were used to establish bruise severity.

Fruits were placed on fruit trays, put in boxes and stored in a ventilated cold room at 5 ^oC and 85 % Rh, for two weeks. Fruits would be taken out of storage and left for four hours for their temperature to level up with room temperature before NIR spectroscopy measurements were taken.

NIR absorbance spectra were acquired on apples on the bruised spots. Three NIR modes were used, namely the Bruker MPA (Multipurpose Analyser) spectrometer (*Bruker Optics*, Germany) using the fiber optic solid sample probe (5 *mm* in diameter) and the rotating integrated sphere mode, on one hand, and the Bruker Matrix (Matrix-F duplex from *Bruker Optics*, Germany) system on the other hand.

The probe uses a permanently aligned and highly stable Rock Solid^{TM} interferometer and a 20 W Tungsten halogen lamp as NIR source. The interferometer is equipped with a high reflective surface and inert, gold coated mirrors and has a wavenumber accuracy and reproducibility better than 0.1 cm^{-1} and 0.04 cm^{-1}, respectively. The beam splitter is made of a quartz substrate with proprietary coating. The position and velocity of the movable mirror is accurately calculated using a He-Ne class 1 laser. The fiber optic probe contains both, in a bifurcated optical configuration, the source fibers that guide the light to the sample (in direct contact with the optic probe) and the detector fibers that receive the reflected light.

The integrated sphere mode is used to measure diffuse reflectance of highly scattering solid media. It has a 50 mm width sample cup holder for measurements of heterogenous samples, on which apples were placed, bruised spot facing the light source. Diffuse reflectance measurements are simplified by using an integrating, gold coated sphere. The NIR beam is directed into the sphere and travels directly through the center of the sphere and the optical window into the fruit sample. The beam scatters off the sample and the reflected light beams re-enter the sphere. Due to the gold coating, all light beams are collected and directed towards the detector. The integrating sphere uses the same spectroscopic elements as for the fiber optic probe, except for the detector. The integrating sphere makes use of a high sensitivity PbS detector with non-linearity correction. The resolution, the scanning region and the number of scans are the same as for the fiber optic probe.

An internal gold reference spectrum was obtained by mechanically closing the optical window with a gold reference plate.

The MATRIX-F FT-NIR spectrometer is equipped with a fiber optic NIR illumination and detection head (185 mm height and 230 mm diameter) and allowed for measurement on almost half of the fruit surface in a single exposure (see Figure 3.6). The fiber optic illumination head contains 4 air cooled tungsten NIR light sources (tungsten halogen, 12 V, 20 W). The diffusely reflected light from the sample is collected and guided via a fiber optic cable to the spectrometer detector (a highly sensitive, thermoelectric cooled and temperature controlled InGaAs diode detector).

Figure 3.6: Apple fruit exposed under the Matrix-F NIR spectrometer

The wavelength region scanned was from 4000 cm^{-1} to 12000 cm^{-1} with a resolution of 4 cm^{-1}. For each single measurement, each spectrum was an average of 64 scans. Two measurements were taken per fruit, each on a bruised spot at two opposite sides of the fruit.

3.3.2 Spectral pre-processing

Additional to mean centering and exclusion of the noisy extremities of the spectra, different pre-processing methods were applied to NIR spectral data and the best was selected and used for analysis. Pre-processing methods that were used included the first and second derivatives, vector normalization (SNV), straight line

subtraction, multiplicative scattering correction (MSC), constant offset elimination (COE), min-max normalization and double combinations of some of the above. The performance of a method was evaluated in terms of the RMSECV value generated with Opus software.

3.3.3 Data Analysis

NIR spectral data were used to segregate apple bruised tissues from healthy ones using the orthogonal PLS-DA (OPLS-DA) tool of SIMCA (CAMO chemometrics software). The OPLS model is an extension of the PLS model. It separates the systematic variation in X (predictors set) into two parts, one that is linearly related (and therefore predictive) to Y (response variables) and one that is orthogonal to Y. The X/Y predictive variation is modeled by the predictive components. The variation in X which is orthogonal to Y is modeled by the orthogonal components. The interpretation of scores and loadings and other OPLS model parameters is analogous to that of a PLS model (see section 3.2.4). The classification accuracy was calculated using Eq. 3.3.2.

$$\text{Classification accuracy} = (TP + TN)/(TP + TN + FP + FN), \tag{3.3.2}$$

where four possible outcomes of the classification are denoted as follows: Normal samples correctly classified as positive (true positive; TP), normal samples erroneously classified as negative (false negative; FN), bruised samples correctly classified as negative (true negative; TN) and bruised samples erroneously classified as positive (false positive; FP) [140].

Statistical analyses (PLS regression) were performed on NIR spectra using the 'Quant 2' method of OPUS software (*Bruker Optik GmbH* 2012). Spectral data taken on bruised spots of apples were combined with measures of bruise severity (bruise diameter) to establish calibration models. The bruise sizes used here had resulted from bruising apples with three different impact energies (0.228, 0.398 and 0.739J), see Table 6.1. Individual apples were exposed to a single value of impact energy. Raw spectra were pre-processed in order to minimize unwanted information in the data. The noisy parts at the beginning and at the end of the spectra were cut off before regression analysis was carried out.

A genetic algorithm [114] was applied to the same spectral data to investigate its applicability in improving PLS regression models. Spectral data were captured in a spreadsheet, side by side with the reference data (bruise size) and sorted with respect to the column of reference values. The sorted data from the spreadsheet

were imported into Matlab software (Version 7.11.0) and a Matlab code (by Ricardo Leardi, Genova Italy) that implements a genetic algorithm combined with a PLS regression analysis (PLS-GA), which was used to establish the performance of the cross-validated models from the data. The PLS-GA models were evaluated according to the values of the RMSECV and the coefficient of determination.

Each GA iteration starts by creating a new population of subsets by applying crossover and mutation operators to the current population of subsets. First, the subsets in the current population are randomly divided into pairs of subsets and crossover is applied to each of the pairs of subsets with a given probability (we used pc = 0.6 in all experiments). The crossover first randomly reorders one solution. Then it iterates through the elements in the two subsets and, with probability 50%, it exchanges elements in any position of the two subsets unless the exchange would make any of the two subsets invalid due to repeated occurrence of some elements. After applying the crossover, each subset undergoes mutation. Mutation iterates through the subset and modifies each element of the subset with probability 1%.

3.3.4 Wavelength selection strategy

Since not all wavelengths have the same effect on scanned objects, it is of interest to find only vital wavelengths that are the most influential on quality, from complete spectra. Numerous variable selection methods are used for PLSR, using different approaches. Mehmood et al., in their recent review on variable selection methods in PLSR, classified the variable selection methods in three categories, based on the properties, namely filter methods, wrapper methods and embedded methods [106]. Filter methods rank variables based on some importance measure, which, however, requires threshold specifications. In order to get reliable results, cross-validation can be used for threshold selection and they become wrapper methods. In embedded methods variable selection is an integrated step of modeling involving internal cross-validation in most cases. It is likely that 'there is no such thing as an always best variable selection method since there is likely an interaction between method and the properties of the data' [106]. As it was observed [110] and recommended [106] in some reports, it is preferable to try out approaches with different properties to a given data problem. Two methods were used in this work, namely PLS variable importance in projection (VIP), and genetic algorithm for variable selection combined with PLS (GA-PLS).

VIP is a filter method initially introduced by [141] as 'variable influence in projection'. It accumulates the importance of each variable m given by $w_{am}/\|w_a\|^2$, where w_{am} is the loading weight of the m^{th} variable explained by the a^{th} component. The measure v_m of the VIP for the m^{th} variable is given by Eq.3.3.3.

$$v_m = \sqrt{P \sum_{a=1}^{A} [SS_a(w_{am}/\|w_a\|^2)] / \sum_{a=1}^{A} (SS_a)}. \tag{3.3.3}$$

Generally, for VIP values greater than 1, a variable should be selected. On the other hand, Chong et al. suggested that variables with VIP values within the threshold from 0.83 to 1.21 would be more relevant [142]. VIP values are often among results that are generated by the commonly used PLS algorithms. The VIP method was successfully used in variable selection [143, 144, 145], among other applications, and thus is a fit choice to validate other variable selection methods, such as GA used in this project. The theory about GA and applications to dimensionality reduction were explained in Section 2.11. The choice in GA was mostly based on the fact that two things can be achieved at once, namely simplification of the model while improving its predictive ability [113, 146]

Chapter 4

Fruit quality studies by ultra-low field SQUID-NMR

4.1 Introduction

Banana is a climacteric fruit which means that ripening can take place after harvesting. During the ripening process, the starch granules disappear and the concentration of soluble sugars rises. Along with that, there are changes in other quality attributes including total acids, firmness, and peel color that changes from green to yellow. The peel color is commonly used to distinguish between ripening stages of banana [147]. A traditional way of classification of banana based on their ripening stages, though subjective, was proposed by Von Loesecke in 1950 with respect to banana peel color [148] and is commonly used by other researchers. The aim of the study was to investigate the ripening process of banana using the SQUID-NMR technique as a non-destructive method. Banana is an ideal choice as the variation in many of its quality attributes during its ripening, present a wide range of variation. A large range of variation in quality attribute is necessary to ensure reliable data analysis when NMR relaxation processes are studied in reference with conventional fruit quality estimation. The problem of a small measured range is not new in quality measurement of horticultural products. Barreiro and coworkers, tried to solve the same problem by introducing new parameters to improve their prediction model [11]. Previous studies have been conducted to study the ripening process of banana using the method of relaxometry. Raffo et al. [83] used a combination of T_2 and water self-diffusion coefficient (D) measurements to study ripening associated changes on the sub-cellular level. The interpreting of relaxation data, based on a theoretical model of chemical and diffusive exchange, by Belton and Hills [149], made it possible to describe the distribution of sub-cellular water and to monitor its dynamics related to chemical composition [83]. Ribeiro et al. also combined T_2

and D to rule out the indirect correlation between them due to injury in banana samples during ripening [150]. They found that T_2 of the water in vacuoles decreases due to banana injury, hence a recommendation to use intact banana in such a study, to avoid injury biased results. T_2 increased during ripening, contrary to D. A hypothesis based on the reduction of Fe^{3+} and O_2 concentration was proposed as the origin of the observed increase in T_2. The reported studies of banana ripening by relaxometry have mostly been exploiting the transverse relaxation time, and rarely the longitudinal relaxation time.

Other non-destructive technologies that are currently in use include Fourier Transform Infrared (FTIR) spectroscopy [151], Laser-induced Fluorescence Spectroscopy (LIFS) [152], Time-Resolved Reflectance Spectroscopy [153], Proton Transfer Reaction Mass Spectrometry (PTR-MS) [154], and Near Infrared Spectroscopy (NIRS) [155]. Liew and Lau [147] studied banana during the ripening using NIRS and developed a multiple linear regression model for predicting ripening index, based on changes in firmness and soluble solid contents as banana ripens. According to their findings, NIR could be used to develop prediction models for internal quality of *Cavendish* banana [147]. In the above mentioned research findings and most of the others in the same context, full models for practical use are non-existing. A lot is also still to be investigated, such as meeting the exigences caused by the sorting speed and shielding on conveyor systems, miniaturization to a hand-held device among others, in order to bring this technique to full industrial use. In this work a SQUID-NMR system was used to probe internal quality of banana during ripening. The choice of this technique lies in the fact that it is an advanced system that is low cost and offers the flexibility of ultra-low field NMR techniques, which allows for scanning unprocessed inhomogeneous samples like fruit samples. The objectives were to probe the relationships between ultra-low field relaxation times T_1 and T_2, and banana attributes that change during ripening, such as color and sweetness.

4.2 Results and discussion

Various quality parameters were measured on ripening banana that were initially classified in three ripening stages (see Section 4.2.1). Banana samples at Ri1 were used for measurements taken in six instances over 10 days of storage and were the basis of the results reported in Section 4.2.2. Samples at Ri2 and Ri3 were respectively used for only four and two measurement instances, since they started decaying afterward. Daily average values of TSS, T_1 and a* showed a gradual increase as bananas ripened, while h gradually decreased. TSS measured values ranged

from 13 to 22.8 ^{o}Brix, T_1 values ranged from 0.53 to 0.99 seconds, a* between -15.41 and 7.05, and h varied between 112.88 and 79.38. The range of variation of all the measured parameters and their means are summarized in Table 4.1.

Table 4.1: Overview on measured values for banana quality parameters.

	Valid N	Mean	Minimum	Maximum	Std.Dev.
TSS (^{o}Brix)	32	18.68	13.03	22.83	2.32
T_1 (s)	32	0.79	0.53	0.99	0.12
T_2 (s)	32	0.53	0.43	0.71	0.07
pH	32	5.20	4.04	5.70	0.31
TA (%)	32	0.97	0.68	1.39	0.16
TSS/TA	32	19.69	11.09	25.84	4.12
Firmness (N)	28	68.42	30.03	121.68	19.79
L*	32	63.59	53.69	69.69	4.09
a*	32	-2.49	-15.41	7.05	6.05
b*	32	40.63	35.89	47.12	3.22
C*	32	41.17	36.43	47.59	3.09
h	32	93.40	79.38	112.88	8.63

4.2.1 Initial fruit quality

Banana samples were initially sorted subjectively, and placed in three ripening stages based on their apparent color. In this section a more objective classification is presented for validation purposes. PCA results (4.1) showed a clear separation between ripening stage 1 (Gy1) and the remaining two, with most of the variation explained by TSS, T_1, TSS/TA, h, a*, Firmness, and b*. It is also clear from Figure 4.1 that T_1 was highly correlated to TSS, a* and h; b* to TSS/TA; and C* to TA and pH.

Changes in some attributes are plotted against the ripeness stages, and a gradual variation is clear as shown in Figure 4.2. The analysis of variance in measured quality attributes showed that all mean values in different ripening stages were significantly different at 5% significance level in a*, h and T1, whereas for TSS, two groups (Ri1 and Ri2) had means signifficantly different from group 3 (Ri3). These results are based on a small range of ripening stages, and thus cannot be generalized to describe the entire ripening process. They do however, provide a separation between ripening stages concordant with that from the preceding subjective classification.

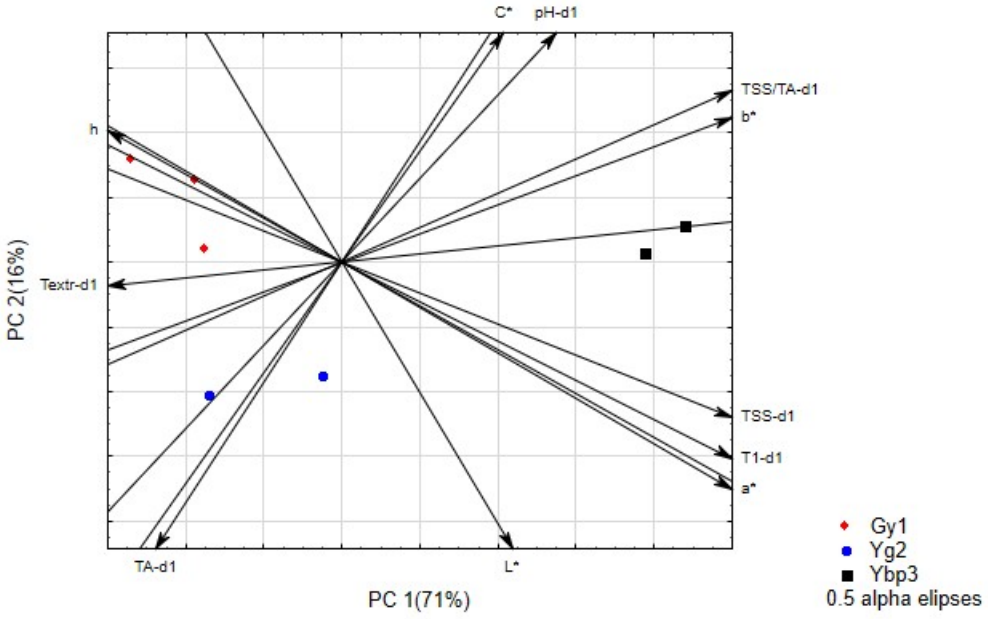

Figure 4.1: PCA results of analysis of banana at three ripening stages (Gy1 for green with some yellow peel, Yg2 for yellow peel with green tip and Ybp3 for yellow flecked peel with brown patches) on the first day of experiments.

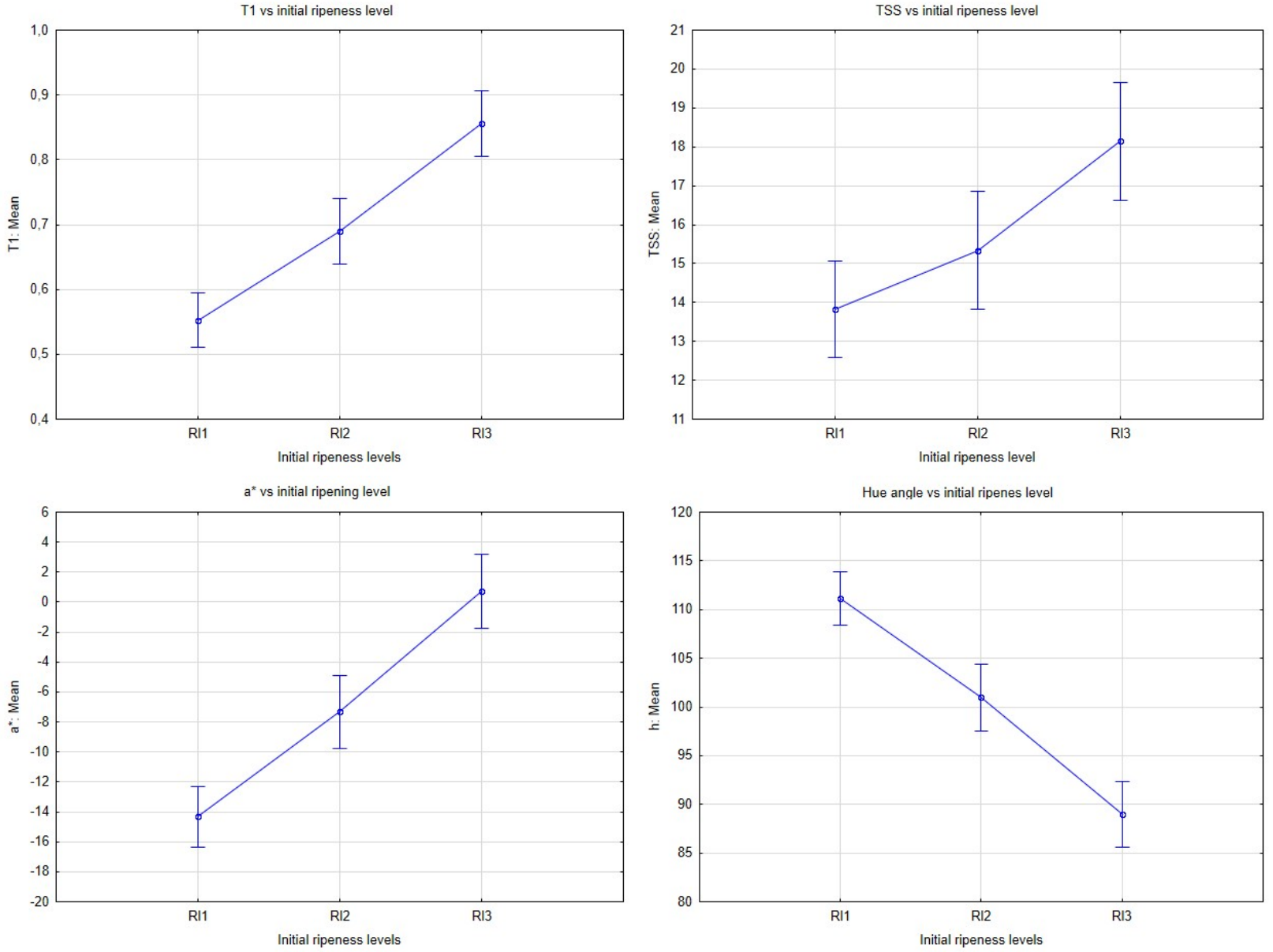

Figure 4.2: Initial fruit quality: change in T1, TSS, a* and h∗ according to the subjective classification. The intervals on the plot represent 95% confidence interval

4.2.2 Experimental results for the ripening experiment

Results of the analysis of experimental data, focusing uniquely on the earliest stage of ripeness are presented in this subsection. Banana samples that were still completely green were monitored during their ripening period, while stored at 15 ^{o}C and 85% RH. Results of PCA (4.3) show that day one was clearly different from all the other days, as explained mostly by TSS. This suggests that there was a rapid increase in TSS between measurement day one and day two (corresponding to the first four days of storage), relatively larger than the variation observed in other attributes within this same time period. This rapid increase suggests that the samples' ripening stage was suited for fast ripening in the storage conditions that were used. A clear separation of day one from day 5 and 6 was explained by T_1, TSS/TA, a* and h. All these attributes were highly correlated to each other as shown in Figure 4.3. It was also noted that day 2 was separated from day 5 and 6 by TA.

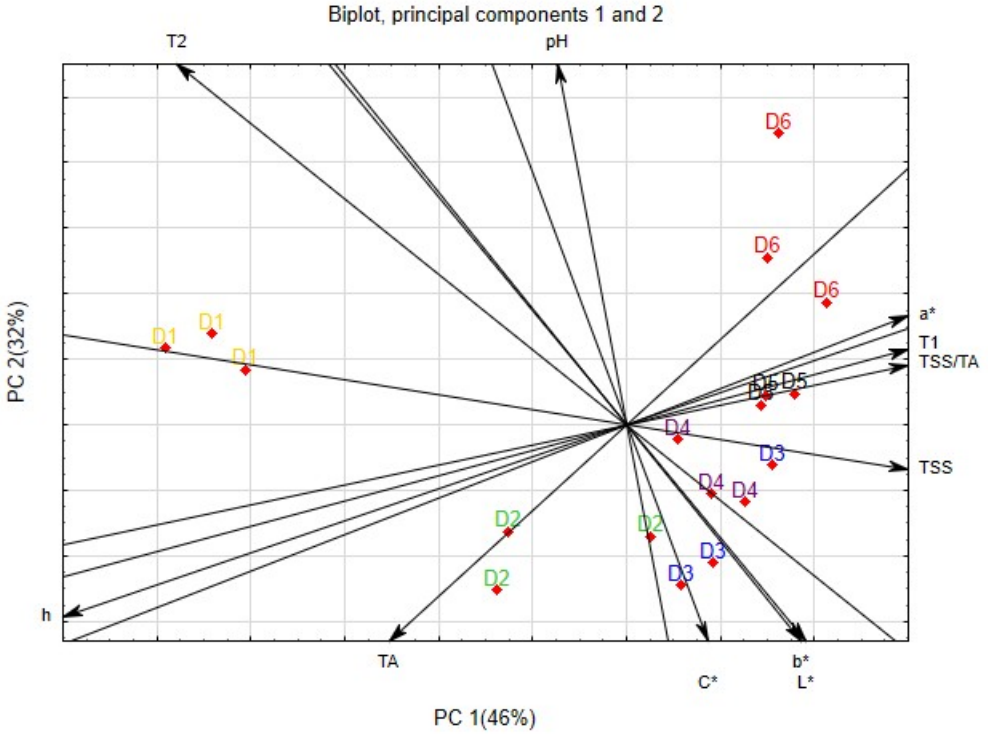

Figure 4.3: PCA analysis of the attributes measured progressively on ripening stage 1during the ripening period

4.2.2.1 Chemical attributes

It is shown, in Figure 4.4, how the measured attributes varied over the ripening period. TSS increased for the first six days in storage, after which it started declining slowly until storage day ten, which was the last day for measurements. TSS values ranged from 13.03 to 22.83 $^{o}Brix$, and the decline in TSS over the last four days of storage was estimated to be approximately 2.5% of the maximum attained as recorded at measurements day four (storage day six). A gradual increase was observed in TSS/TA from 12.36 to 25.84.

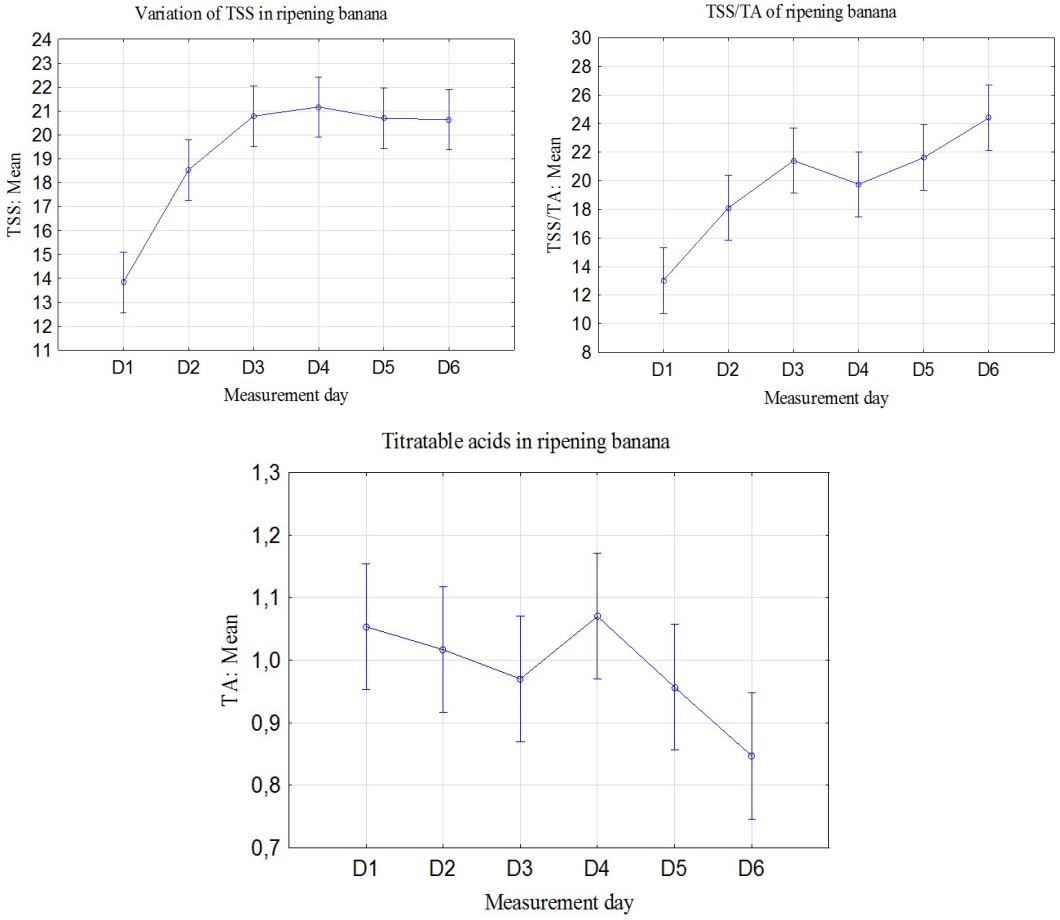

Figure 4.4: Changes in TSS, TA and sugar:acid ratio in ripening banana

The rapid increase in TSS during the first six days of storage was also observed by Kulkarni et al. [156] in their study of the effects of ripening involving ethrel treatments which induced fast ripening. On the other hand, Jaiswal et al. [157] managed to follow up on the ripening banana during 10 days of storage. The decrease observed in TSS of overripe bananas towards the end of storage could be due to the

continued enzymatic action associated with pectin breakdown and the beginning of tissue deterioration. Bailey reported a similar decrease from ripe yellow to over-ripe brown banana [158].

4.2.2.2 Firmness

Instead of a steady decrease in banana firmness during ripening [156], an irregular non-linear change was obtained (Figure 4.5). This was likely due to the experimental procedure, where the shape of the probe (5 *cm* diameter flat probe) and the positioning of the sample (banana fruit placed on a flat surface) were not a good fit for consistency in the measurements. Another issue was that banana samples didn't necessarily have the same diameter at the contact area, so the 7 *mm* displacement of the probe along which the banana resistive force was measured wasn't accurately repeatable procedure. For consistent results, a method such as measurement of shear force would be advisable [156, 157].

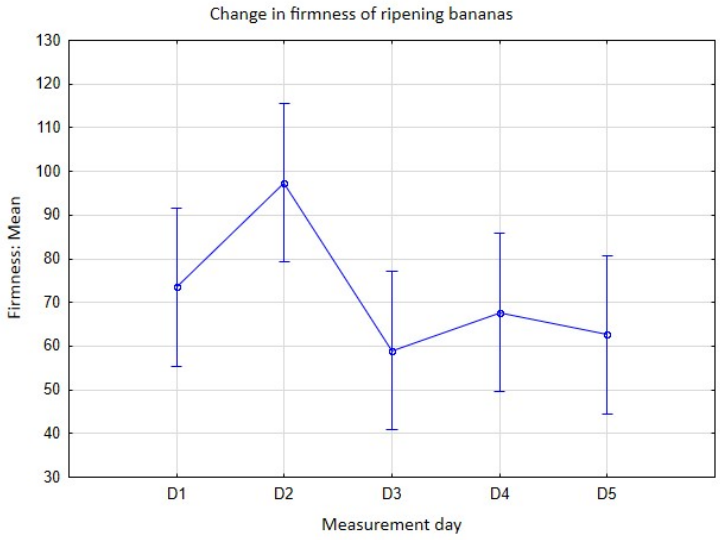

Figure 4.5: Variation in banana firmness during ripening period.

4.2.2.3 Color attributes

A gradual increase was observed in a*, whereas h decreased. The values of these attributes ranged from -15.41 to 7.05, and 112.88 to 83.98, respectively. It was observed that hue angle gradually varied from 111.15 (C* = 39.6) on day one to 83.27 (C* = 39.4) on measurement day 6, as measured on the batch initially considered at the earliest maturity stage. These values correspond to color change from yellow

green to yellow, which characterizes the ripening process of bananas. The chromaticity coordinate a* changed from -14.33 (b* = 36.88) on day one to 4.51 (b* = 39.03) at the last day of measurements, which correspond to green and yellow respectively, at lightness L of 57.79 and 58.57 with a peak of 67.67 at measurement day four (storage day six).

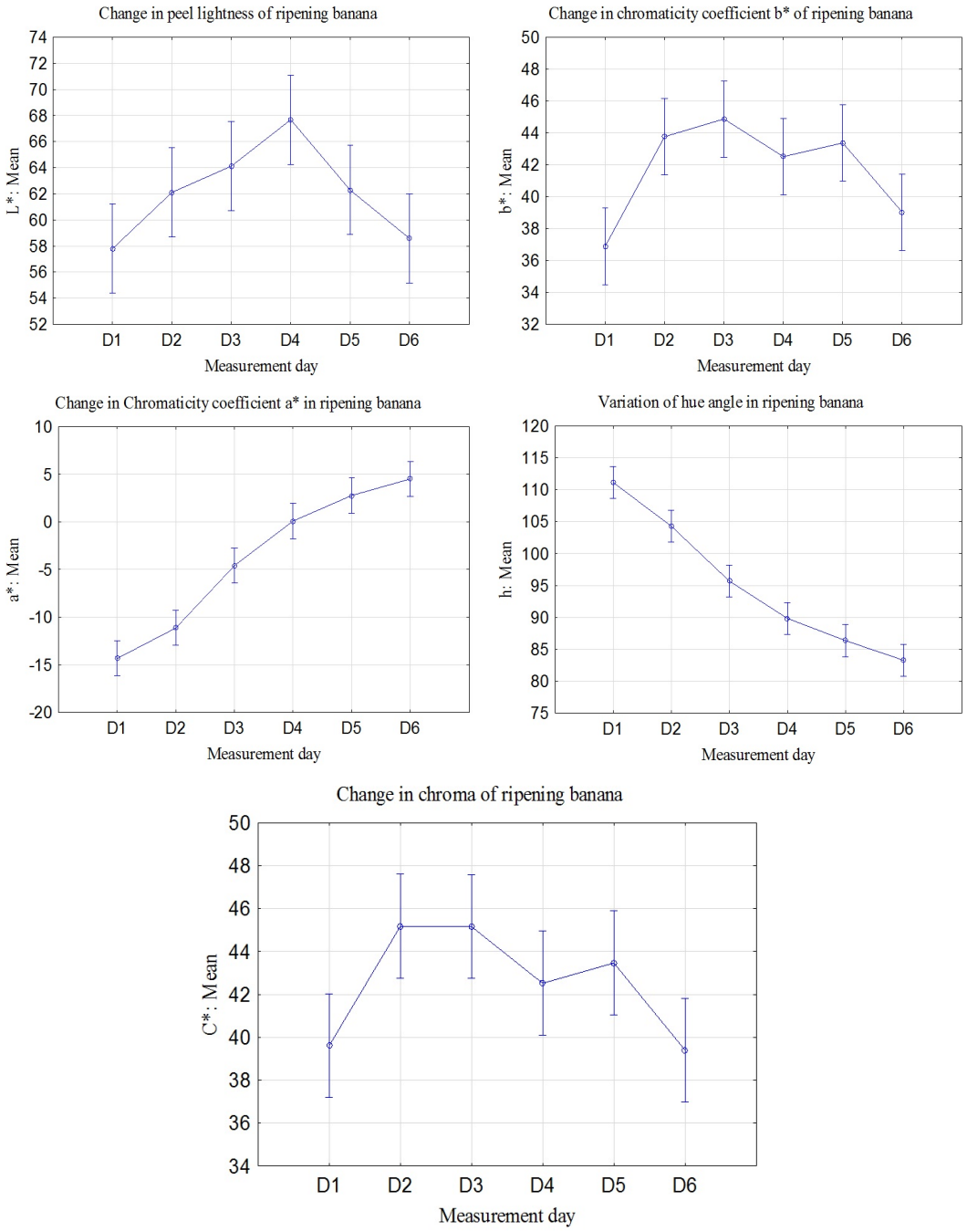

Figure 4.6: Color parameters measured during storage on ripening bananas.

From the above, it seems that lightness of the peel started to decrease quickly after sugars attains the maximum value and spots started developing on the fruit peels. The measured color parameters described well the changes in peel color during the ripening process of banana. It is however, worth noting that ethylene treatment of ripening banana allows to control spotting on the peel [156], hence improving the evenness of the color distribution. This would improve on accuracy in measurements of color indicators.

4.2.2.4 Total Color difference

The total color difference, as defined in [131] for ripening bananas, was calculated according to (3.1.3). Six stages of color difference (also corresponding to six measurement days) were considered, whereby the initial stage was used as control reference. Data measured on the batch that was initially classified at ripening stage 2, were averaged on a daily (measurement day) basis, and used for statistical analysis. Correlation analysis showed that TCD highly correlated with TSS, TSS/TA and T_1. The values of the correlation coefficient were 0.95, 0.92 and 0.94, respectively. From regression analysis, values of R^2 were 0.91, 0.83 and 0.89, respectively. Total soluble solids and their ratio to titratable acids increased with increasing total color difference until storage day six (measurement day 4). After storage day six the TCD didn't significantly change, hence the steadiness at the end of storage noticeable in Figure 4.7. Therefore, we recommend that in the same experimental conditions as in ours, more frequent measurements should be performed at the earliest stage of ripening in order to allow for recording more data points before fruits start to become overripe [156].

4.2.2.5 Relaxation characteristics

A number of cases in the literature reported about trends observed in NMR relaxation time(s) of ripening banana [83, 150], whereby transverse relaxation time of the water in banana cell vacuole T_{2vac} increased during ripening of banana fruit. Average T_2 and T_1 based studies of banana ripening remain unknown to the author and likely rare. In this work, measurements of T_2 did not give significant correlations with other attributes, in most cases. We will focus on the analysis involving T_1 as the NMR parameter. A gradual increase was observed in T_1 (0.529 - 0.91 sec) over 10 days of storage. Four (D3, D4, D5 and D6) out of five measurement days were significantly different from day 1 (D1), at 95% confidence level. The analysis of variance showed that the mean values of T_1 were not significantly different. A decline in values of T_2 during the first 4 days of storage was followed by a slight

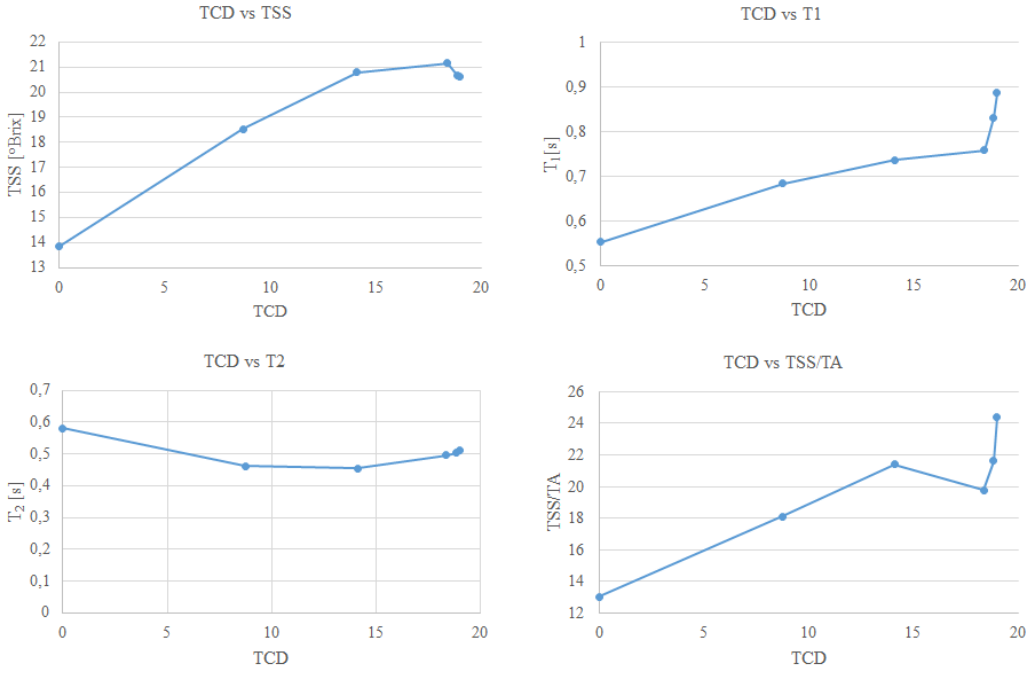

Figure 4.7: Total color difference plotted against relaxation times, TSS and TSS/TA

increase until end of storage with non significant statistical difference in mean values.

The trend observed in TSS, T_1, a* and h, as measured on day one, was also observed in the same attributes as measured on the earliest ripening stage (Ri1) according to the initial classification (ripening stage three as in [148]), over the whole ripening period. The ripening process was best described in the first six days of storage, during which four series of measurement were performed (measurement day 0 to day 4). After the sixth day of storage, dark spots started forming on banana peels, making the measured values of color parameter lightness L* to decrease from a peak (Figure 4.6), values of TSS to decrease (Figure 4.4), and values of total color difference to remain almost unchanged (see Figure 4.7).

Table 4.2: Cross-correlations between all quality attributes of interest. Marked correlations are significant at p <0.05 N=15 (Casewise deletion of missing data)

	Means	Std.Dev.	TSS	pH	TA	TSS/TA	Firm	L*	a*	b*	C*	h	TCD	Ri
T_1	0.71	0.11	0.72	-0.27	-0.52	0.82	-0.43	0.61	0.84	0.65	0.45	-0.85	0.94	0.89
T_2	0.49	0.06	-0.53	0.70	0.34	-0.54	0.038	-0.49	-0.32	-0.58	-0.49	0.36	-0.51	-0.27

Correlation analysis have shown that T_1 of ripening banana was highly correlated with TSS, TSS/TA, a*, and h (r= 0.72, r=0.82, r=0.84 and r=-0.85, respectively). A correlation was found also with L* (r=0.61), b* (r=0.65) and TA (r=-0.52),

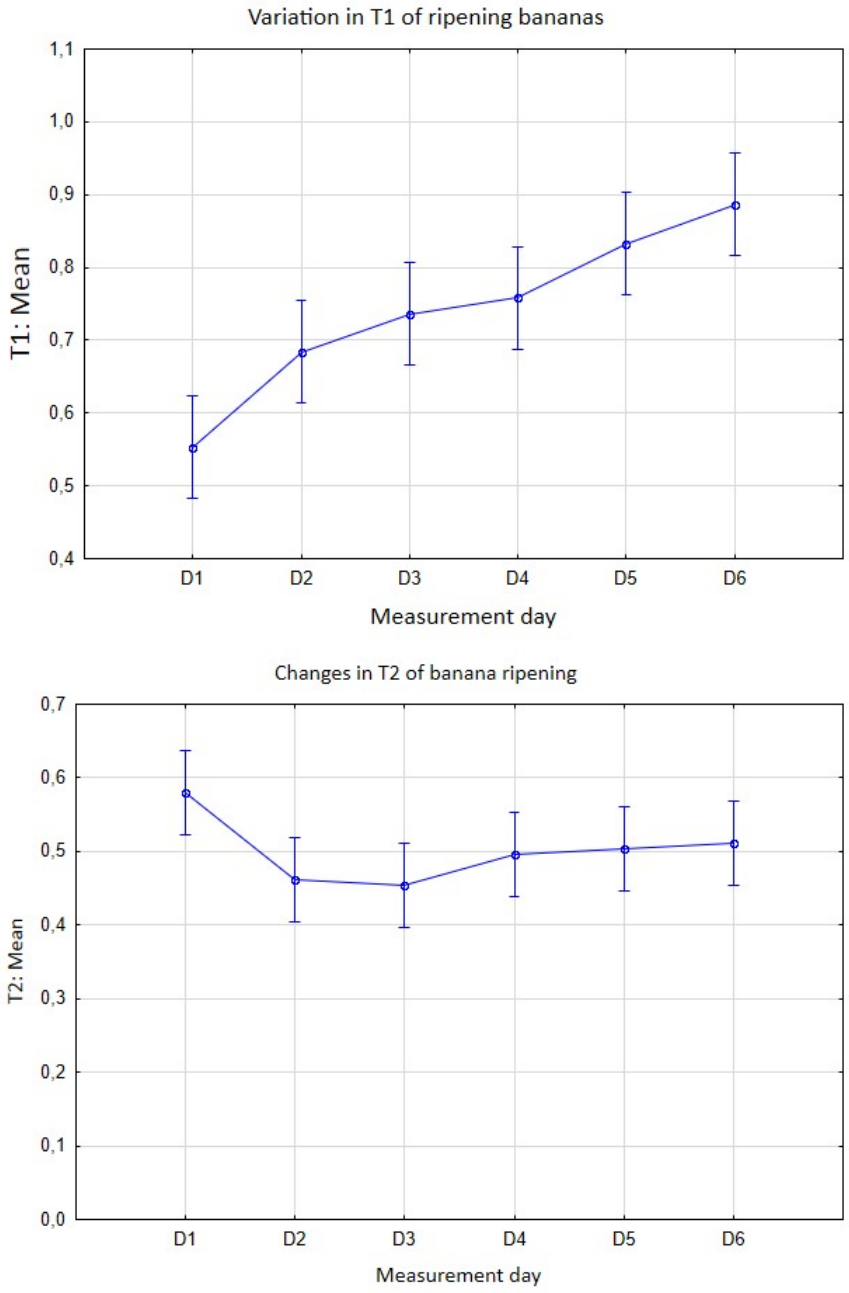

Figure 4.8: NMR relaxation characteristics of ripening banana.

all significant at $p<0.05$. On the other hand, T_2 showed a high correlation with pH ($r=0.70$) and an average correlation with TSS, TSS/TA and b* ($r=-0.53$, -0.54 and -0.58), all significant at $p<0.05$. A summary of correlation analyses between all the measured attributes is given in Table 4.2. All the values marked in red were significant at $p<0.05$. It should be noted that the analysis that rendered the results above, took the period after optimal ripening into consideration, which was characterized

by degradation of the samples quality and thus a change in the trend of changes in the measured attributes. For optimal results in a similar study of this ripening process, the author recommends to only use the data acquired until optimal ripening and thus before degradation of the samples.

4.2.2.6 Predicting ripening index

The degree of ripeness (ripening index, Ri) was defined according to the apparent change in peel color as bananas ripen. The ripening stages were classified as 3, 4, 5, 6, 7 and 7, as inspected on storage day 0, 2, 4, 6, 8, 10, respectively. The ripening index of banana is commonly defined based on color as in [148]. There was no noticeable difference in the appearance of banana samples from storage day 8 onwards, with dark spots developed all over the peels. From Figure 4.9, T_1 appeared to be highly correlated to Ri with a coefficient of 0.89. TSS, TSS/TA also highly correlate with the ripening index, with the coefficient R equal to 0.74 and 0.83, respectively. The ripening index was also very well described by color parameters a* and h with Spearman r equal to 0.98 and -0.98. T_2 showed no significant dependence on Ri.

It is worth noticing that Geya at al., in their study of the growth of pears using a low field (0.2 T) MRI system, found a good predictive ability of a 'cubic root' of fruit weight by components of bi-exponentiated T_2 [159]. In our case, only a reserved opinion can be given based on averaged (or bulk) T_2, and further studies are recommendable before drawing any conclusions of using average T_2 for predicting banana ripening. Average T_1, on the other hand, shows promising results at predicting banana ripening and it was achieved using the ultra-low field SQUID-NMR used in these experiments. However, as found in the literature, multi-exponentiation based relaxometry has allowed for some results in describing banana ripening [83, 150]. A multiexponentiation of relaxation data provides a distribution of relaxation times that would describe processes in different parts of the samples on a sub-cellular level [160], and thus providing a deeper understanding of the phenomena being studied. An extended look at NMR of ripening banana, using multiexponentiated T_1, is proposed in section 4.3.

4.3 NMR inverse Laplace transform

In experiments involving decaying signals, it is often desirable to analyze the data as a sum of exponential decays using the Laplace inversion method. An algorithm for uniform penalty inversion of multiexponential decay data (Upen ver.1.05) by

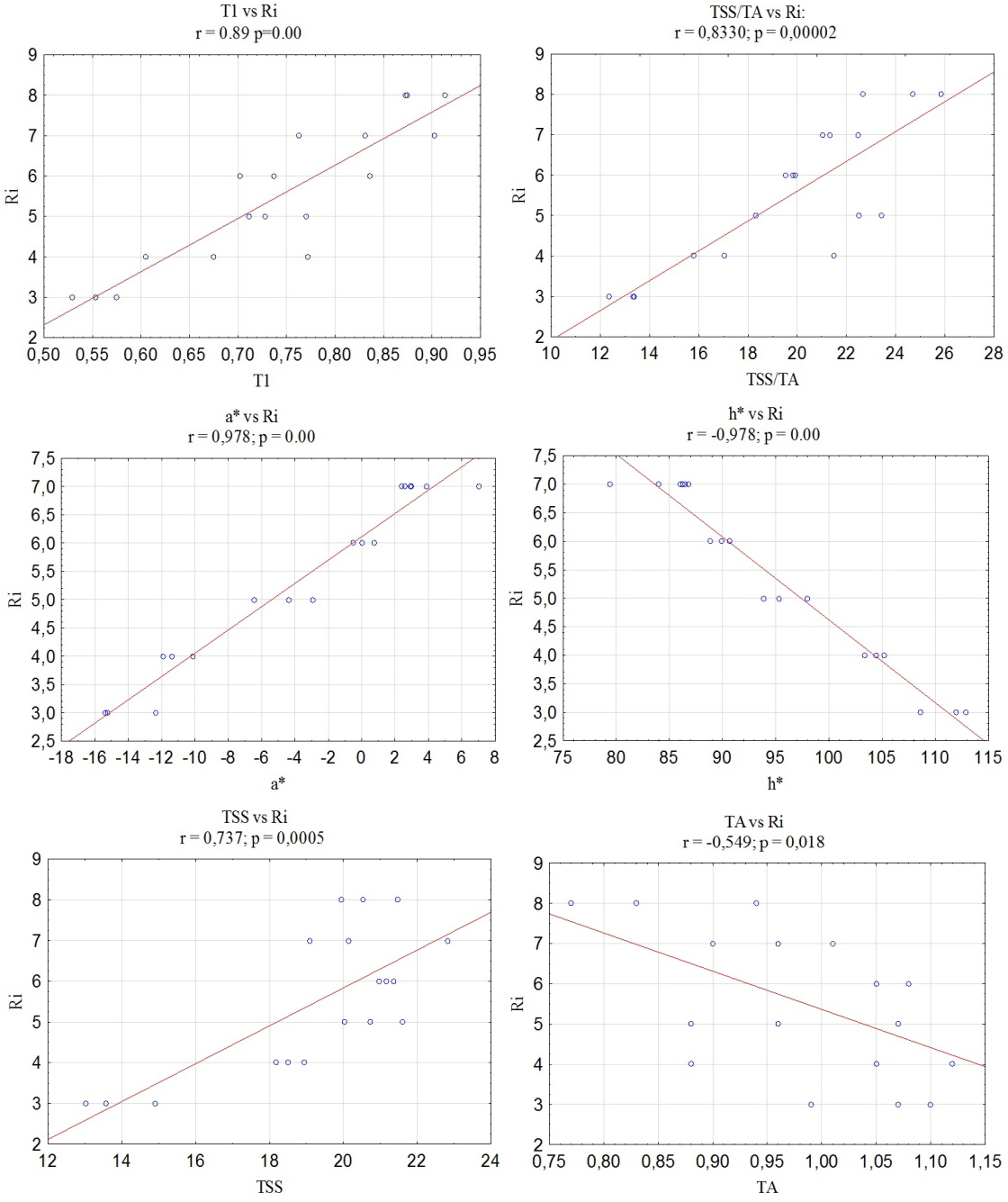

Figure 4.9: Regression analysis of ripening index against some quality parameters of ripening banana fruit

G C Borgia et al., was used to calculate the Laplace inversion of the NMR free induction decay signals (FIDs) [161, 160, 162, 46].

Four main peaks were obtained from the Laplace inversion NMR FIDs from banana samples. Only two, one or no peak was obtained after convergence of all the ILT generated solutions. Table 4.3 gives an overview of some results from ILTs

of inverse recovery NMR FIDs for some banana samples. The number of peaks in the solutions seemed to be random from sample to sample, and the final solution after convergence also showed some inconsistency in repeated measures of the FID per sample. In order to circumvent this hurdle, the initial FIDs were cut down to the time t where decay seemed to settle. Subsequently, these trimmed FID signals were refitted using cubic spline interpolation in order to obtain the data at equispaced times [163] and the data points reduced to 10000.

Table 4.3: Results of ILT for some banana samples. Only the first solutions before, convergence process starts, are shown.

sample ID	First ILT solution				Converged		
bna1-1b-Tp7	275	177	105	29	50		Rate
	22	67	40	100	100		Ampl
bna1-1a-Tp7		220	105	28	225	48	Rate
		100	22	61	100	20	Ampl
bna1-2b-Tp7	265	167	75				Rate
	100	86	13				Ampl
bna1-2a-Tp7	209	123	60		212		Rate
	100	12	5		100		Ampl
bna2-1a-Tp7	265	168	72				Rate
	100	80	9				Ampl
bna2-2a-Tp7	205	125	64		209		Rate
	100	12	22		100		Ampl
bna3-1a-Tp7	267	169	90				Rate
	100	92	8				Ampl
bna3-2a-Tp7	270	171	98	27	47		Rate
	74	100	19	24	100		Ampl

[1]

A distribution of spin-lattice relaxation times for bananas at three distinct stages of ripening is plotted in Figure 4.10. The earliest ripening stage (Ri=2 [148]) is plotted in blue diamonds, the second ripening stage (Ri=4) in red triangles and the last stage (Ri=7) in green hexagons. The curve is a plot of signal per Neper of relaxation time versus relaxation rate ($1/T_1$). Bananas at Ri=2 were characterized by two relaxation rates at 230 and $50s^{-1}$.

The calculation of the T_1 Laplace inversion at three ripening stages specified in Section 4.2.1 has led to two main relaxation rates within a small standard deviation, namely $232.9 \pm 3.3s^{-1}$ and $49.8 \pm 0.4s^{-1}$. In Figure 4.11 the signal per Neper of the spin-lattice relaxation time is plotted against the relaxation rate for all the three stages of ripeness.

No steady trend in either the values of T_1 components or peak area was noticed for the three ripening stages. For a more substantiated conclusion more data should

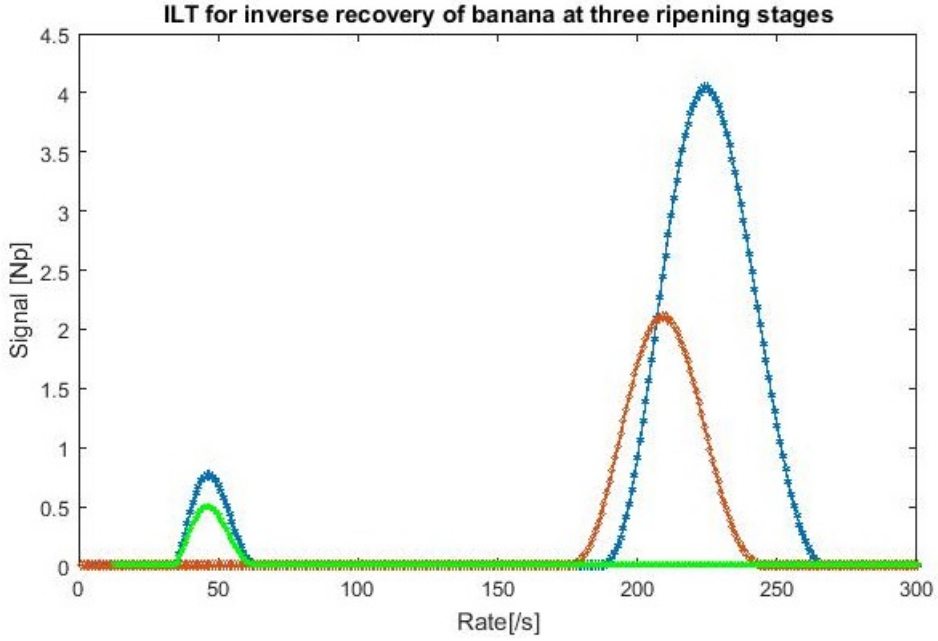

Figure 4.10: Inverse Laplace transformed T_1 relaxation time for banana at three ripening stages, namely stage 2 (blue diamonds), 4 (red triangles), and 7 (green hexagons).

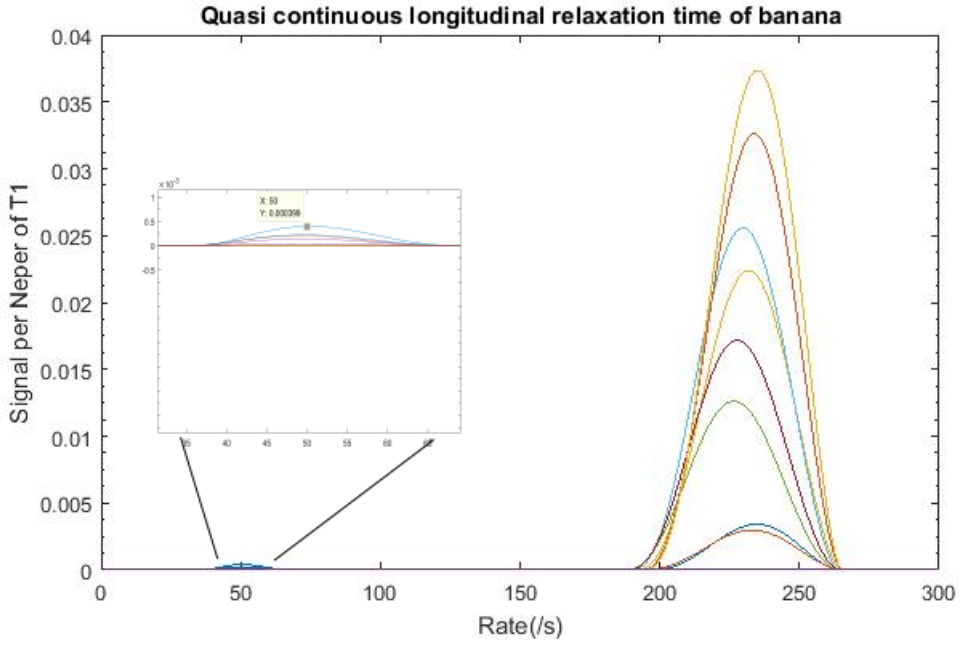

Figure 4.11: Quasi-continuous spin-lattice relaxation rates of banana at three of ripening stages

be used. The areas under the peaks are directly proportional to the concentrations of water proton pools corresponding to the peaks [164], and could be used as quan-

titative measures to track the changes occurring during ripening of banana using multiexponential T_1. In a process such as ripening of banana, changes in water concentration distribution should result in certain changes in the T_1 distribution or in the peaks areas or the area ratio per sample. It is envisaged that more comprehensive study that takes into consideration the ripening experiment used in this work (see section 4.2.2) would be carried out, and is expected to reveal trends related to the ripening index, and likely to the other quality attributes. An interpretation of such T_1 distribution as to characterizing water proton pools in unpeeled banana is to be investigated.

4.4 Conclusions

Banana ripening was studied by means of ultra low-field NMR technology. The NMR relaxation time parameters measured during the ripening of banana were compared to other conventional measures of quality attributes. Total sugars, sugar : acid ratio, and changes in color showed a high correlation with T_1, whilst T_2 did not show good correlations with other parameters. T_1 could thus be a good descriptor of the ripening process of banana. The trend of change in peel color of banana during ripening was best described by a*, h and TCD. The index of ripening, Ri, based on the apparent change in color, was highly correlated to a* and h. T_1 performed well at explaining ripening stages, where its correlation coefficient in relation to Ri was nearly 0.9. T_1 also increased with color change from green to yellow, while T_2 decreased with a significant correlation with Ri, of -0.48 at $p<0.05$. Given the working conditions of the work reported here, as discussed in the results section, these results should be easily reproducible for more extensive study on other climacteric products. More robust predictions should be obtained with a larger amount of data. The Ultra-low field SQUID NMR technique shows promise for fruit quality prediction based on averaged longitudinal relaxation time, T_1. A study of time resolved spin-lattice relaxation times of ripening banana was also conducted and resulted in two peaks that are characteristic of intact banana fruit. The dependency of peak intensities or areas on varying quality indicators in banana is still to be investigated. That opens the possibility of using a low-field NMR spectral data in the T_1 domain for further studies of banana quality and very likely other fruits as well.

Chapter 5

Fruit quality studies by NIR spectroscopy

5.1 Introduction

Spectroscopic methods have gained increasing interest in quality evaluation of foodstuff. Spectral data are transformed into useful information through chemometrics. It combines multivariate statistical analysis and spectral processing methods to establish relationships between quantifiable quality attributes and spectral data. The performance of calibration models developed from these spectroscopic methods and the effectiveness of statistical methods used can be limited by the experimental conditions, such as spectral acquisition system accuracy or precision. Various numerical methods for variable selection and optimization have been used in combination with multivariate statistical analysis in order to improve prediction models. Artificial neural networks were used in combination with genetic algorithms (GA-ANNs) for the nondestructive quantitative analysis of cefalexin based on NIR reflectance spectra [127]. Fei et al. [127] reportedly conveyed that as GA is a global search method, so it has less probability to be trapped at local minima. it's combination with ANNs, implemented as the fitness function for GA, should perform better than many other methods. Their study showed that GA improved the performance of ANNs, which, on the other hand, proved to give better models than PLS [127]. Genetic algorithms were used with multivariate regression to determine gelatine in historic paper using IR and NIR data. The model obtained using the GA was built on fewer data points (76 vs. 2150) and latent variables (4 vs 9) than that based on full spectra [112]. Optimization techniques can be used to improve prediction models and there is always room for improvement. One of the hurdles that hinders widespread use of NIR systems is that of calibration transfer. A calibration model developed on one instrument may not be directly used on another,

even if it is the same type of device. Having to construct the calibration model for every spectrophotometer is expensive and time consuming. These difficulties are associated to changes in the instrument response due to aging or maintenance and the climatic environment of the equipment, amongst others [165, 166]. Other than 'Standardization' methods that have proven to be useful [167, 168], in case of absorbance shift related problems, and when instrumental differences are small, there are alternative approaches to solve the transfer problem. Some of these approaches include using appropriate pre-processing methods, wavelength selection and including several instruments in the calibration [169, 170, 171].

In this chapter two NIR spectral acquisition modes, namely, the integrating sphere, IS and solid probe, SP of the multipurpose analyzer NIR spectrometer were used in order to assess the possibilities for calibration transfer by probing their predictive ability and spectral profile, relatively to those of the emission head (EH) of the Matrix-F spectrometer that has capabilities for online applications. Wavelength selection and pre-treatment methods were part of the methodology in predicting internal attributes of apple fruits, in order to assess the issues of transferability there associated.

5.2 Results and discussion

5.2.1 Spectral analysis

NIR spectra of all apple cultivars had a similar profile in all acquisition modes with four main peaks around 10230, 8330, 6890 and 5170 cm^{-1}. Figure 5.1 compares the average normalized spectra of 10 apples from three different acquisition modes: Blue line (MPA-solid probe), red (EH-Matrix-F) and green (MPA-IS). The spectra from the solid probe presented the most dominant peaks around 1923 nm and at 1449 nm, relatively to the other acquisition modes. Differences in absorbance values were noticed in the three acquisition modes, whereby the EH of the Matrix-F had the highest values in absorbance followed by the IS of the MPA. The SP of the MPA had the lowest values in absorbance except at it highest peaks that surpass the ones from the IS in amplitude. These differences can be attributed to the penetration depth and fruit surface area scanned specific for each acquisition mode. The peaks around 10230 and 6890 cm^{-1} corresponded to the 2^{nd} and 1^{st} vibrational overtones of OH stretching associated with water absorption [172, 173]. On the other hand, the peaks around 8330 and 5180 cm^{-1} correspond to the 2^{nd} and 1^{st} overtones of CH stretching, as well as the 3^{rd} overtone of OH, CH and CH_2 deformation associated with sugar solution [174].

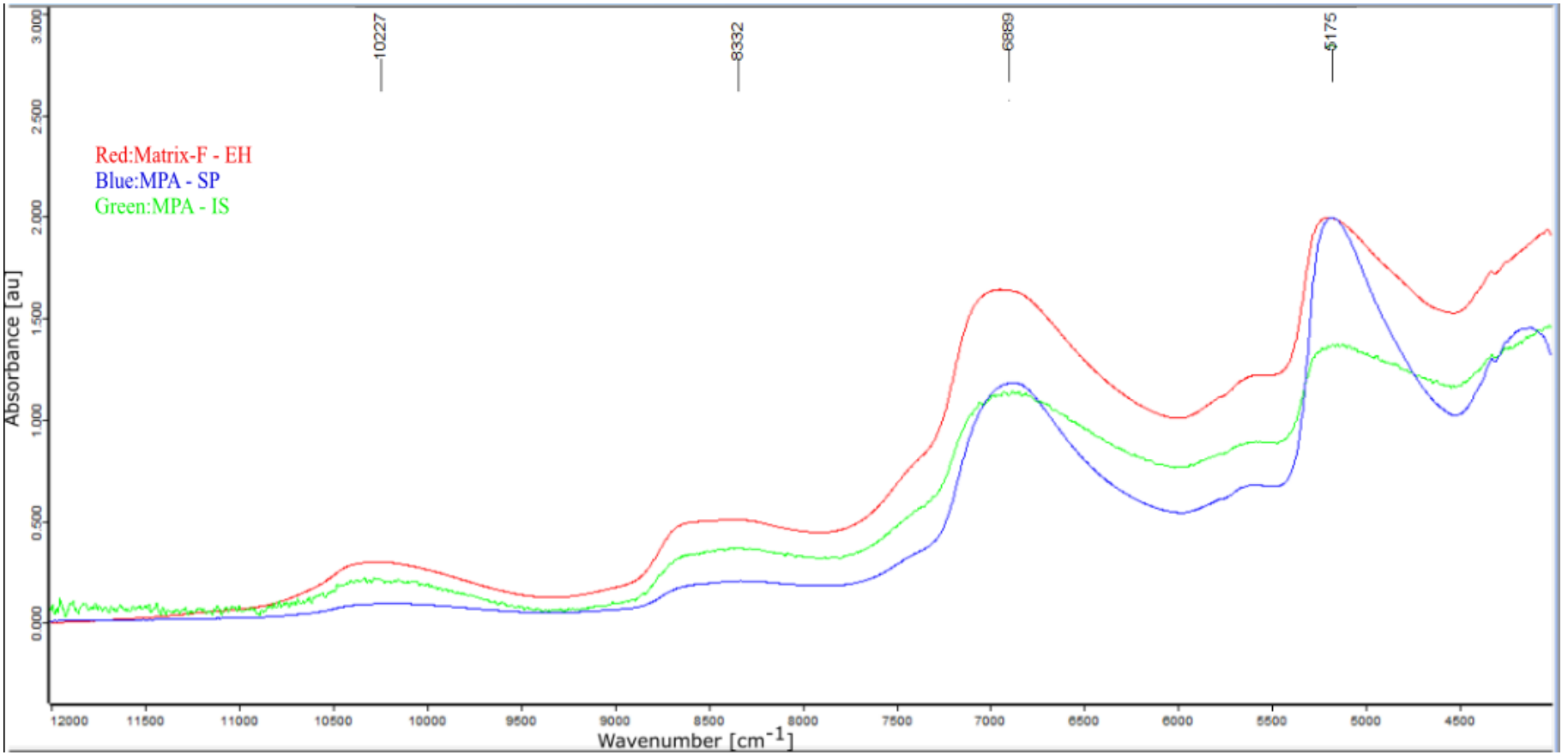

Figure 5.1: Comparison of spectra in three acquisition modes

5.2.2 Data distribution

Fruits were sourced from two different supermarkets in different monthly periods, spectral data acquired in different spectral acquisition modes and three reference quality parameters were measured destructively. Table 5.1 gives a brief overview of the quantitative measurements done on the entire dataset in different categories. Measures of soluble solids ranged from 8.8 to 18.3 ^{o}Brix, titratable acidity from 2.09 to 3.6%, both resulting in values of sugar:acid ration ranging from 2.5 to 7.5. In the batch of fruits bought from *Checkers*, the measures of TSS were also shown for different cultivars separately. *Royal Gala* apples had the highest mean value of TSS followed by *Golden Delicious* apples.

The reference values were normally distributed around the respective mean values and over a range that is large enough to constitute a good dataset for meaningful data analysis. TSS was spread over a range of 9.5 ^{o}Brix which is more than half the maximum of TSS values. A similar case was found in the values for the other reference quality attributes.

Table 5.1: An overview of the reference measurements for internal quality attributes

Source	Acq. mode	Attribute	Cultivar	N	Mean	SD	Range
FLM	EH / IS	TA	All	228	2,68	0,29	2,09 - 3,6
		TSS	″	″	13,41	1,92	9 - 18,3
		TSS/TA	″	″	5,09	1,02	2,5 - 7,5
Ch	EH / IS		GD	66	13,38	1,23	11,1 - 16,1
		TSS	GS	62	12,64	1,41	8,8 - 15,8
			RG	72	15,09	1,28	12,8 - 17,7
			All	200	13,77	1,67	8,8 - 17,7
	SP		GD	32	13,12	1,14	11,1 - 14,9
		TSS	GS	32	12,09	1,38	8,8 - 15,1
			RG	32	14,97	1,16	12,9 - 17,3
			All	96	13,39	1,72	8,8 - 17,3
All					13,54	1,43	8,8-18,3

FLM, *Food Lover's Market*; Ch, *Checkers* retail store; EH, 'Emission head' of the Matrix-F spectrometer; IS, 'integrating sphere' of the MPA spectrometer; SP, 'solid probe' of the MPA spectrometer; TSS, total soluble solids; TA, titratable acidity; TSS/TA, sugar:acid ratio; GD, *Golden delicious* apple cultivar; GS, *Granny Smith* apple cultivar; RG, *Royal Gala* apple cultivar; SD, standard deviation; Range, wavenumber region used for the actual prediction model.

Figure 5.2 shows clusters of samples differentiated with respect to mode of acquisition and sample sources. The first principal component separated samples

with respect to acquisition modes (green for 'MPA-probe' versus the rest for 'MPA-IS'). The second component helped distinguish between sample sources where samples from 'Ch' (purple) were clearly separated from those from 'FLM' (Cyan). Similar classes were obtained with the first two components, using most of the pre-processing methods, except for the first derivative and SLS methods, where the third principal component distinguished best between sample sources instead of the second. These PCA results showcase the fitness of the dataset used here for the purpose of external data validation reported in Section 5.2.

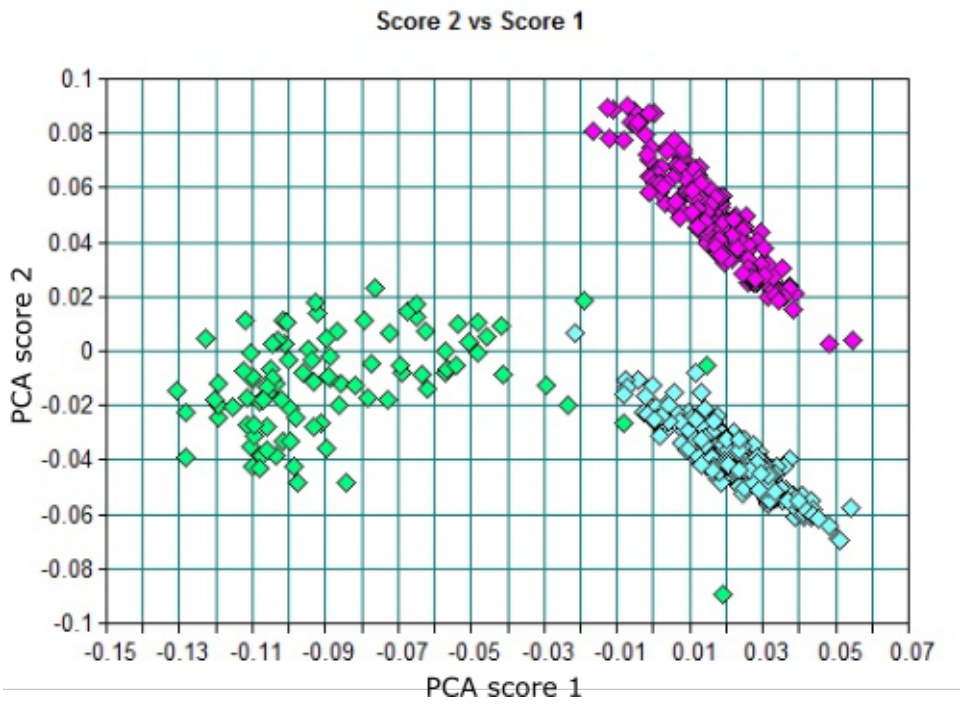

Figure 5.2: PCA scores plot for all spectral data acquired on the MPA separates fruit sources and modes of spectral acquisition.

5.2.3 Total soluble solids

The measured soluble solids content in apples were used to build prediction models by NIR spectroscopy in all the three acquisition modes, as introduced in section 3.2.3. The two spectra acquired per apple were averaged, as well as the TSS values from both scanned sides, and used as a single sample. A prediction model was built based on full spectral data and improved by means of spectral pre-processing. The best pre-processing method was rated according to the quality of the derived prediction model, and constituted the subject of the report presented here. The best performing pre-processing methods for TSS differed from those obtained in TA and

TSS/TA, and were also different with respect to sample sources. SLS (straight line subtraction) was the best pre-processing method for TSS in samples from *Checkers* ('Ch'), whilst for 'FLM' samples SNV (vector normalization) led to the best prediction model parameters (RMSEP, R^2, RPD and slope). Fruit samples from 'Ch' were used in models predicting soluble solids content (SSC or TSS) only. The prediction set was generated by selecting a block of two out of five consecutive samples up to a number that makes up to about 25% of all the samples. The remaining samples, approximately 75%, were used for model estimation. External validation of samples from IS for TSS used samples acquired from the MPA probe, and vice versa. Fruits from 'FLM' were used to build models based on TSS, TA and TSS/TA, using both the EH and IS acquisition modes. While SNV was the best performing pre-processing method for TSS and dominant in all the three attributes, SNV combined with first derivative was dominant in models involving TA (TA and TSS/TA).

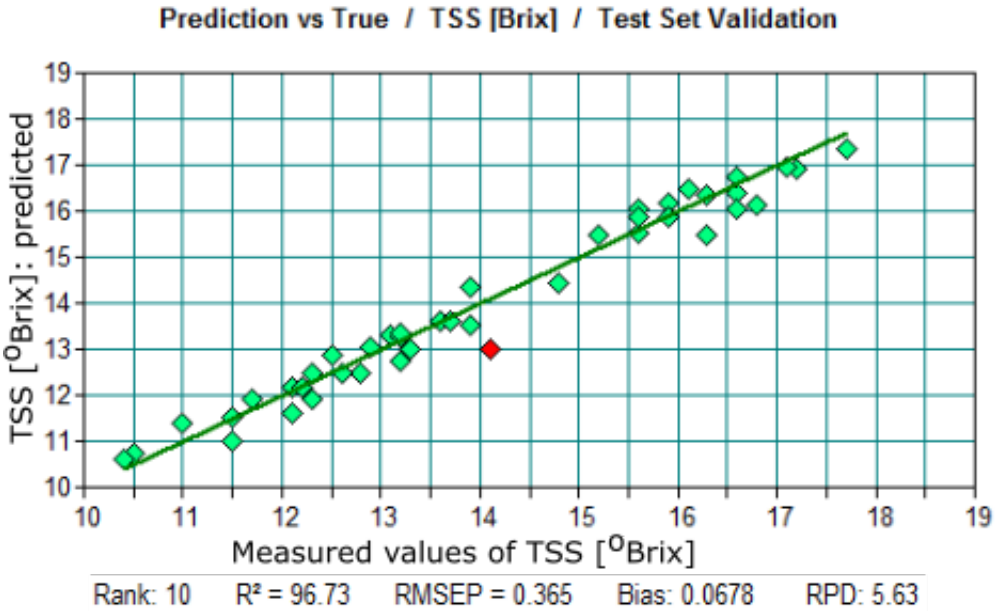

Figure 5.3: Prediction of soluble solids content in all three apple cultivars.

The plot shown in Figure 5.3 is a fit of measured versus predicted values of TSS with SNV as the pre-processing method of spectra acquired on the EH for all the three apple cultivars . The coefficient of determination in predicting TSS varied between R^2= 89.09% and 96.73%, the RMSEP between 0.365 and 0.40.

5.2.4 Titratable acidity

Predicting titratable acids based models was best achieved by using the first derivative as pre-processing method. The best model was obtained within restricted

wavelength regions (9403.5-7498.1 cm^{-1}; 6101.9-5774 cm^{-1}). Unlike TSS, TA models were very mediocre (R^2<50%) without any spectral pre-processing. A tremendous improvement in the prediction model was achieved after pre-processing, resulting in the value of R^2= 68.17 %, with a very low error of prediction of RMSEP=0.12, as shown in Figure 5.4.

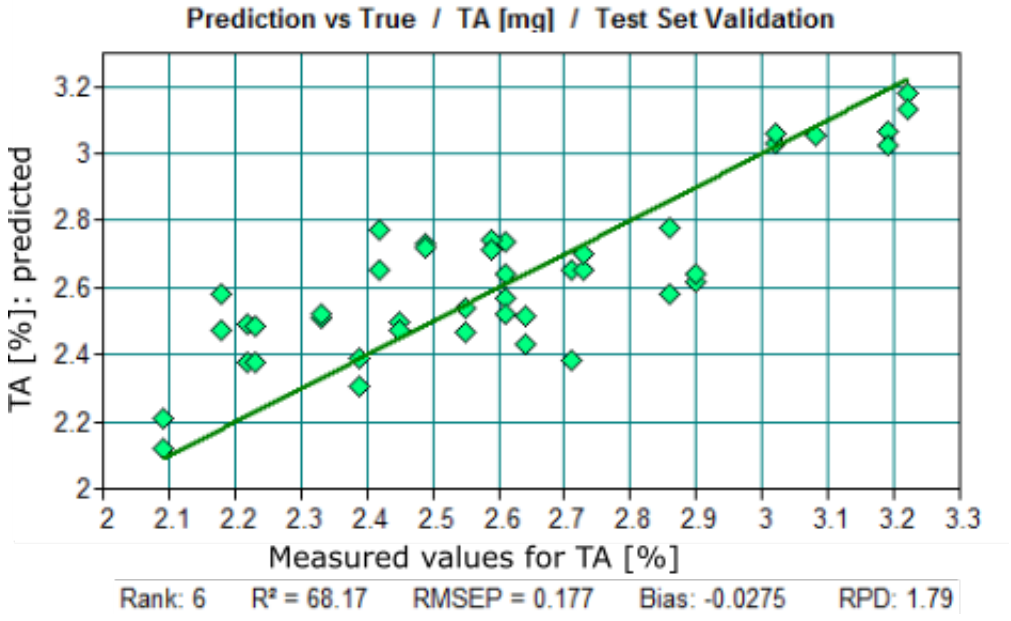

Figure 5.4: Prediction of total titratable acids in all three apple cultivars.

5.2.5 Soluble solids to titratable acids ratio (TSS/TA)

TSS/TA is commonly used as a good indicator of maturity in various types of fruit, including apples. It was used here as an additional internal quality indicator calculated by TSS/TA. The pre-processing method that resulted in the best prediction model for TSS/TA was the combination of both the best pre-processing methods for TSS and TA, i.e 1^{st} derivative and SNV. A good prediction model was obtained for TSS/TA, with R^2=82.62%, RMSEP= 0.43, etc.

Models plotted in Figures 5.3, 5.4 and 5.5 were based on the Matrix-F (EH) and models based on other instruments were summarized in Table 5.3. TSS models differed slightly with respect to the type of validation set (source or acquisition mode). It was noticed that lower RMSEP and higher RPD and R^2 values were obtained for samples from FLM, where the test set was from the same source and acquisition mode, than in the case where the test set was external (different source or acquisition mode). Therefore, external data validation induced more variability

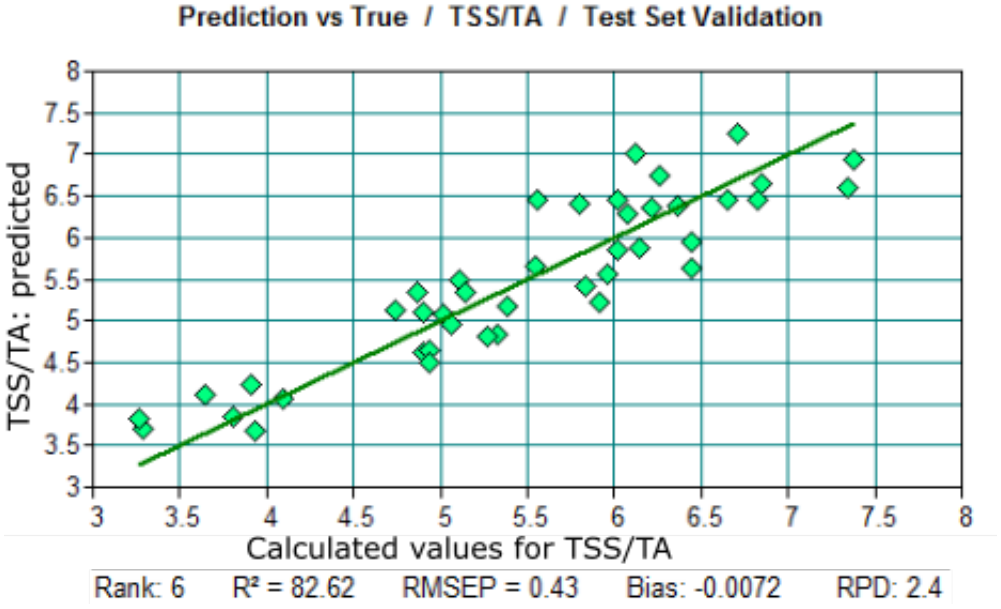

Figure 5.5: Prediction of sugar acid ratio in all three apple cultivars.

and slightly reduced the model performance, but as commonly understood, this contributes for model robustness [175, 147, 97].

Prediction models for TA had the lowest performance (lowest coefficients of determination, lowest RPD, slope farthest from 1, largest difference between prediction and calibration R^2 values) relatively to TSS and TSS/TA models. The EH had better predictive ability than the IS. In all cases, the three internal quality indicators in apple fruit (TSS, TA and TSS/TA) were well predicted by means of FT-NIR in different modes of acquisition.

5.2.6 Effect of cultivar on prediction models

Three apple cultivars were used in this work, namely *Golden Delicious* (GD), *Granny Smith* (GS) and *Royal Gala* (RG). There have been more studies on apple quality focusing on single cultivar than those combining many cultivars at a time. A combined study provides an inclusively more comprehensive understanding of the subject under investigation, given that there is always variability from one cultivar to another. The effect of apple cultivar on prediction of some internal quality attributes using FT NIR is discussed.

Table 5.2: A summary of FT-NIR prediction model parameters as related to apple cultivar

Source					Calibration			Validation				waveband (cm^{-1})
	Attribute	Cult	LV	preproc	R^2 (%)	RMSEC	Slope	R^2 (%)	RMSEP	RPD	Slope	
FLM	TSS (^{o}Brix)	GD	8	None	97,08	0,320	0,971	94,34	0,333	4,22	0,925	9403.7-6098.1 ; 5450.1-4246.7
		GS	8	M-Mnorm	96,95	0,271	0,969	91,48	0,374	3,44	0,903	9403.7-5446.3
		RG	8	M-Mnorm	95,91	0,305	0,959	86,49	0,483	2,73	0,834	6102-4246,7
	TA (%)	GD	6	1der+MSC	73,44	0,077	0,734	50,01	0,133	1,52	0,417	9403.7-8451; 5176.3-4246.7
		GS	6	None	54,09	0.123	0,541	31,21	0,196	1,35	0,359	5450.1-4597.7
		RG	7	1der+MSC	76,58	0,084	0,766	69,1	0,125	1,80	0,573	6102-5446.3; 4601.6-4246.7
	TSS/TA	GD	9	M-Mnorm	97,51	0,139	0,975	91,19	0,251	3,48	0,83	9403.7-7498.3; 5450.1-4246.7
		GS	8	None	81,79	0,212	0,818	71,48	0,225	1,95	0,795	9403.7-8451; 5450.1-5022
		RG	7	SLS	84,90	0,220	0,849	71,94	0,327	1,89	0,592	9403.7-7498.3; 6102-5446.3
Ch	TSS (^{o}Brix)	GD	5	1der + MSC	95,37	0,388	0,954	75,81	0,545	2,10	0,652	9403.7-5446.3
		GS	10	SLS	98,63	0,178	0,986	80,72	0,608	2,30	0,747	9403.7-6098
		RG	9	1der + SLS	95,61	0,328	0,956	85,61	0,442	2,64	0,85	9403.7-7498.3; 6102-5446.3

FLM, *Food Lover's Market*; Ch, *Checkers* retail store; TSS, total soluble solids; TA, titratable acidity; TSS/TA, sugar:acid ratio; Cult, cultivar; GD, *Golden delicious* apple cultivar; GS, *Granny Smith* apple cultivar; RG, *Royal Gala* apple cultivar; RMSEC, root mean square error of calibration; RMSEP, root mean square error of prediction; LV, latent variables ; Preproc, pre-processing method ; RPD, relative prediction deviation; SLS, straight line subtraction;.M-Mnorm, min-max normalization; MSC, multiplicative scatter correction; 1der, first derivative; None, no spectral pre-processing;

The values summarized in Table 5.2 are based on NIR spectral data that were acquired using the MPA (both IS and SP). Internal validation (25% test vs 75% calibration) was used on samples from 'FLM', whilst external validation was performed on the batch 'Ch' by choosing samples from the SP as test set and those from the IS as calibration set (see Figure 3.5). Best prediction models for TSS were found in GD followed by GS and then RG, for samples from 'FLM' (with internal validation), while this order was reversed in samples from Ch (with external validation). TA was best predicted in RG apples followed by GD and then in GS apples. A similar order to that in TSS (GD > GS > RG), but in a different scenario, was found in the prediction model for TSS/TA. The best model was obtained in GD, while the model parameters in the remaining cultivars were not outstandingly distinct. We argue that, even though the R^2 value in RG was slightly higher than that found for GS, it was noticed that GS had the lowest error of prediction of TSS/TA, a better RPD and Slope than the one obtained for RG. The difference between R^2 values for calibration and validation was also lower in GS than in RG. We therefore report the predictive model for GS as better than that for RG.

5.2.7 Comparison of spectral acquisition modes

It has not been possible to develop an 'all purpose' FT-NIR system, even though multiple functions or uses may be performed on the same system. It is understood that spectrometers designed differently might also perform differently, if used for the same tasks. However, there are ways of circumventing such hurdles with model optimization. For example, the EH of the Matrix-F used in this project was designed for process monitoring and allows for much larger sample sizes, while the MPA on the other hand, although it has many modes of acquisition, has disadvantages with very large sample sizes. It can be useful to compare measurements from different designs of the same analytical method for validation purposes and the development of new models. Here, we compare optimized prediction models that were built based on data from three different acquisition modes and two different FT-NIR spectrometers.

Table 5.3: A summary of prediction models internal. The '*' and '**' indicate where external validation based on acquisition mode and source were used, respectively.

Source	Attrib	Instr			Calibration			Validation				
			LV	Preproc	R^2 (%)	RMSEC	slope	R^2 (%)	RMSEP	RPD	Slope	waveband (cm^{-1})
CH		EH	6	SLS	90.47	0.53	0.905	89.05	0.487	3.09	0.872	9403.5-7498.1; 4601.5-4424.1
*	TSS	IS	10	COE	94.71	0.384	0.947	90.48	0.570	3.24	0.809	9403.7-7498.3; 6102-5446.3
*		SP	5	COE	85.66	0.674	0.857	81.87	0.573	2.73	0.931	9403.7-7498.3; 4601.6-4246.7
**		EH	10	1der	92.86	0.485	0.929	87.93	0.508	2.90	0.868	7502-5446.2
	TSS	EH	10	SNV	97.14	0.321	0.971	97.1	0.348	5.97	0.949	9403.7-5446.2; 4601.6-4246.7
		IS	10	SNV	97.97	0.274	0.98	97.21	0.315	5.99	0.979	9403.7-5446.2; 4601.6-4246.7
FLM												
	TA	EH	6	1der+SNV	72.11	0.157	0.721	68.17	0.177	1.79	0.646	9403.5-7498.1; 6101.9-5774
		IS	7	SLS	75.46	0.152	0.755	58.62	0.186	1.57	0.602	9403.5-7498.1; 6102-5446.3
	TSS/TA	EH	6	1der+SNV	86.83	0.370	0.868	82.62	0.430	2.40	0.859	9403.5-7498.1; 6101.9-5446.2
		IS	9	SNV	91.73	0.301	0.917	91.57	0.276	3.75	1.052	7425-5446.3; 4601.6-4424.1

FLM, *Food Lover's Market*; Ch, *Checkers* retail store; EH, 'Emission head' of the Matrix-F spectrometer; IS, 'integrating sphere' of the MPA spectrometer; SP, 'solid probe' of the MPA spectrometer; TSS, total soluble solids; TA, titratable acidity; TSS/TA, sugar:acid ratio; COE, constant offset elimination; SNV, vector normalization; RMSEC, root mean square error of calibration; RMSEP, root mean square error of prediction; LV, latent variables ; preproc, pre-processing method ; RPD, relative prediction deviation; SLS, straight line subtraction.

The prediction model parameters summarized in Table 5.3 are a comparative overview of the acquisition modes (EH, EH of the Matrix-F spectrometer; IS and SP modes for the MPA) used in this work. The relative predictive ability of the spectrometers was dependent on quality parameters. The SP mode had the lowest prediction ability for TSS (R^2=0.82, highest RMSEP=0.57 ^oBrix and lowest RPD=2.73) relatively to the EH (R^2=0.88, RMSEP=0.51 ^oBrix, RPD=2.9) and the IS (R^2=0.90, RMSEP=0.57 ^oBrix, RPD=3.24) with comparable slopes, where external validation was used. Nonetheless, the SP did give the lowest number of latent variables and the highest slope, which contributes to a relatively simpler model. In the case where internal validation was used, the IS performed consistently better (higher R^2 and slope, better RPD and lower RMSEP) than the EH in predicting both TSS and TSS/TA. However, the predictive parameters were very close (only different to the hundredth) in value and with the same optimal wavebands and pre-processing method, in the case of TSS. The IS and the EH displayed a near identical ability to predict TSS. On the other hand, the EH outperformed the IS in the measurements for predicting TA.

5.3 Application of GA-PLS for internal quality prediction

A genetic algorithm designed to optimize PLS regression models was used in order to study the improvement of model performance in different scenarios (two different spectral acquisition systems, three different apple cultivars) and for wavelength selection. First, GA-PLS was performed on full spectra, and variable selection was evaluated in comparison to previous research findings. Average contiguous spectral data were also used as an extended tool to confirm the accuracy of the free full spectrum based GA run. Figure 5.6 shows a graphical output of the genetic algorithm used in this study. Among other pieces of information, the frequency of selection of variables (A), the coefficient of determination (B), the spectra the model is based on (C) and the cross-validated error of prediction (D) are given and are all individually plotted against the sample number. The cutoff, indicating the best model, is indicated by a green line or point marker. The other models, under different conditions, are indicated in red or blue when a certain criterion of accuracy was specified.

Risks of over fitting may be encountered when the number of variables largely exceeds that of the observations, which is very likely to happen for spectral data like in NIRS. In order to check for the possibility that the GA calculations could have been impaired by the so-called 'large p problem' (for a "$n \times p$" data matrix X), the average contiguous wavelengths were used to reduce the spectral data to

less than 200 variables. The full spectra was reduced from 2074 to 188 variables (11 variables averaged to 1) for the IS (MPA) and from 2307 to 192 variables (12 variables averaged to 1) for the EH (Matrix). The results of variable selection in both cases led to model performances that were closely similar in either case (see Table 5.4).

Table 5.4: Full-spectrum PLS and GA optimized PLS model performance for predicting soluble solids and titratable acidity in apples

	R^2(%)	SD	Var	SD	LV	SD	RMSECV	SD		
EH	96,16	0,11	150,80	24,11	11.00	0,98	0,38	0,01	TSS	
IS	97,12	0,09	148,60	22,90	11.00	0,80	0,32	0,01		GA-PLS
EH	54,01	0,30	99,20	37,59	7.00	0,40	0,20	0,00	TA	
IS	59,78	1,73	106,80	42,50	7.00	0,00	0,19	0,00		
EH	95,69	0,10	61,80	9,52	12,00	0,80	0,40	0,00	TSS	Avcont
IS	96,86	0,04	85,40	17,67	12,00	0,98	0,34	0,00		
		Slope	Correl	Bias		RPD				
EH	91,23	0,91	0,96	-0,02	10,00	3,38	0,57		TSS	
IS	95,27	0,94	0,98	-0,02	10,00	4,60	0,42			PLSR
EH	42,06	0,46	0,65	0,00	6,00	1,31	0,21		TA	
IS	54,07	0,58	0,74	0,00	9,00	1,48	0,19			

'Avcont', Average contiguous wavelengths were used in the GA-PLS model development; 'SD', standard deviation; 'correl', correlation coefficient between predicted and real values; 'Var', number of variables used in the final model; LV, latent variables.

The values in Table 5.4 give a comparative overview of model performance when GA was (sections 'GA-PLS' and 'Avcont') or wasn't (section 'PLSR') applied to PLS regression. These values were averaged over five individual runs and standard deviations are indicated. For the PLS principal components (LV), the statistical mode was indicated instead. The PLSR models were built using 10-fold cross-validation, without any pre-processing methods, but outliers were deleted from the models. The following summarizes the results in Table 5.4:

- The % cross-validated explained variance expressed by the coefficient of determination (R^2) was relatively higher in all GA models than the full spectra PLSR models.
- The number of variables in the GA models was reduced by more than a factor of 12 relative to the full spectra models.

- GA did not reduce the number of latent variables, but remained comparable in the same attributes.
- The error of cross-validation expressed as RMSECV was improved (reduced by 30% for the EH and by 24% for the IS) by GA in models for TSS, but remained relatively the same in models for TA.
- The performance of models that were built based on average contiguous variables was relatively the same as those based on the original variables.
- The IS consistently provided better models than those based on the EH for both modeling approaches and both quality attributes. Nonetheless, both instruments displayed a relatively close performance in predicting these attributes.

It is worth noticing that the relative performance of the acquisition modes discussed here was also realized for external validation involving optimization based on pre-processing of spectra reported in Table 5.3.

5.4 Conclusion

This chapter reported on predicting internal quality of apple fruit non-destructively, using three acquisition modes from two FT-NIR spectrometers. The main objective was to assess the performance of the EH of the Matrix-F spectrometer, intended for online applications, by comparing it to the usual laboratory standard MPA and envisaging to assess some issues of calibration transferability.

It was shown by simple PCA score plots, that fruit samples were distinct in relation to their respective sources and they were distinguishable with respect to spectral acquisition modes.

NIR spectral data were used to build models to predict apple internal quality indicators (TSS, TA and TSS/TA). Various case scenarios were used to assess the performance of models, namely the effect of cultivar and acquisition modes on the models' performance. The models were also optimized by using different pre-processing techniques in various wavelength regions of the entire spectra.

Relative prediction performances with respect to cultivars varied depending on validation approach. Validation based on source (cal: 100% FLM + 50% Ch; val: 50% Ch) resulted in the following order for prediction of TSS: GD > GS > RG ('>' signifies 'better model performance than'). The same order was obtained in predicting TSS/TA, using internal validation (up to 30% of the dataset was used for validation). The acquisition mode based validation (cal: 100% Ch(IS); val: 50% Ch(SP))

resulted in a reversed order from above (RG > GS > GD). The large gap (10% to $\approx$ 20%) between the predictive and calibration values of R^2 suggests that there is a considerable divergence between the respective spectral data, even though they were acquired on the same samples. It is, however, possible that inclusion of part of the test data in the calibration dataset could improve the prediction results. Internally validated TA showed the best prediction in RG and the worst in GS.

The comparison of acquisition modes revealed that, although the IS seemed to outperform the EH in predicting TSS and TSS/TA and the opposite in predicting TA, the model parameters were close in value in most of the cases and both modes performed relatively better than the SP of the MPA. Similar results were obtained in the GA optimized models.

In light of the demonstrated performance of the EH of the Matrix-F and the IS mode of the MPA, it is likely that the transferability of calibrations from the IS mode to the EH mode will present less challenges than usually encountered in this subject matter.

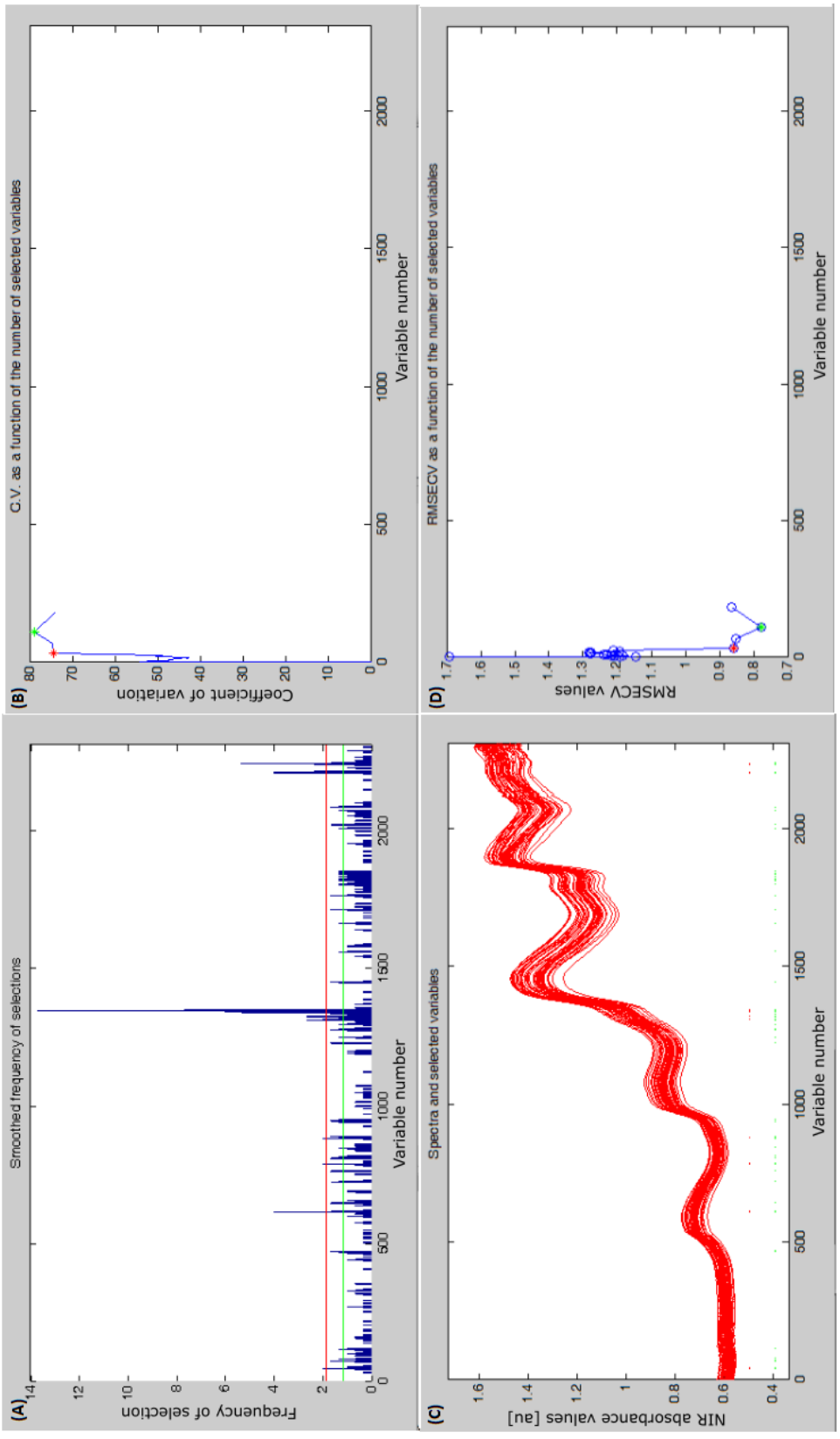

Figure 5.6: A typical graphical output of the GA used in this project

Chapter 6

Advances in prediction of bruise severity in apples: Model optimization using GAs

6.1 Introduction

Bruising is one of the most common surface defects in apples. Their main causal effects are compression and collision forces. When a physical strain is applied to a fruit, resulting in tissue damage, there may occur changes in texture, colour and flavour [176]. The severity of the damage depends much upon the amount of mechanical energy applied and absorbed by the fruit [177, 178]. Bruises can take a long time to appear and can be internal during development. They are thus an example of latent damage [179]. It can thus be said that damage severity can be time-dependent. Time after bruising is related to color and tissue deterioration. Therefore, they can be used for bruise detection, i.e. in the sorting process.

It would be interesting to be able to detect bruises at an early stage of development and thus foretell the later state of fruit quality in terms of tissue damage. Vahid Rostampour and coworkers developed a model that can predict the apple bruise volume in transport condition. By using vibration frequency and acceleration, apple mass, curvature radius and acoustic stiffness as input parameters for a neural network, they were able to make predictions with near-one-values of R^2 and an RMSE of 4.21 [180]. Zarifneshat et al. studied the prediction of bruise volume as a function of radius R, temperature T, acoustical stiffness S and impact energy (f(R,T,S,E)) or contact force (f(R,T,S,F)). In their findings, they brought to light the relative performance of different training algorithms for ANNs in bruise volume prediction, and concluded that their method was objective, accurate and fast to

lead to a practical solution for estimating apple bruise volume [181]. In other research reports, different wavelength regions of interest were reported as preferable for bruise detection. Amongst others, wavebands were 720 - 840nm in *Red Delicious* apples [182], 750 - 800nm in *Golden Delicious* apples [183] and 850 - 1030nm in imaging *Golden Delicious* apples [184].
A visual inspection of the spectral curves and correlation coefficients [185], stepwise regression [142], analyzing divergences between spectra and the average spectrum [186], principal component analysis [187], and others [188], are some of the strategies used for significant wavelength selection, but no standard method exists. ElMasry et al. used partial least squares (PLS) and stepwise discrimination analyzes to reduce high dimensionality of the spectral data, and obtained a few essential wavelengths representing the whole spectrum. The input of the two methods was the raw spectral data extracted from both normal and bruised surfaces, whereby the effective wavelengths were selected using PLS, with the variable importance in projection (VIP) scores on the one hand, and the effective wavelengths resulted from stepwise discrimination analysis, as described in [144], on the other hand. In most of the research that was reported on studying bruising by NIR, the focus was on segregating damaged tissue from healthy tissue [189, 144]. In this study an important additional feature to classification was investigated. The objective was to predict bruise severity, as a tentative way of detecting bruises at their earliest stage of development, before they are detectable by the human senses, such as sight and touch. This study aimed at applying genetic algorithms to PLS regression models in order to improve and simplify the predictive ability of the models.

6.2 Results and Discussion

6.2.1 Exploratory data analysis

In Figure 6.1, PCA scores of NIR spectral data of bruised apple tissue are plotted for the two first components. Scores of samples as measured after 1 hour of bruising, 1 week and 2 weeks of storage are clearly separated into clusters along the first component. Scores for spectral observations of 1 day, 1/2 and 1 week old bruises were dispatched in clusters overlapping with both the clusters predominated by scores from data taken after both 1 hour and 2 weeks. It was, however, difficult to conclude whether the clusters had to do with bruise development or not. Since the same clusters were not confirmed by measurements done on a different spectrometer (the MPA), we can only conclude that they are likely due to some changes in the measurements' physical setup on different days.
NIR spectral data were inspected for any trends related to storage time. In some

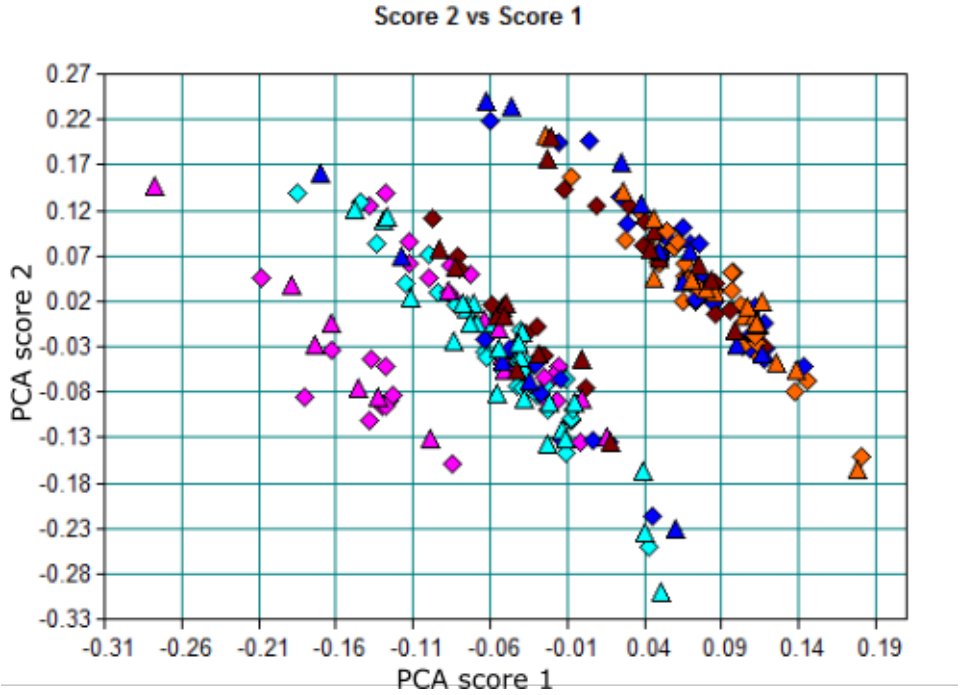

Figure 6.1: PCA scores plot of NIR spectral data on bruised tissue acquired using the Matrix-F system. 1 hour, 24 hours, 1/2 week 1 week, 2 weeks

cases spectral inspection revealed that differences in absorbance values in some spectral regions were related to time elapsed after bruise induction. This was only detected for apples bruised at the lowest impact energy used in this work (drop height=20cm). In Figure 6.2 average normalized spectra of a random sample from a bruised *Royal Gala* apple was plotted and such a trend is shown. Two regions around wavenumber 10200cm^{-1} and 8400cm^{-1} are marked, and show a decrease in absorbance with storage time.The same test was performed on unbruised apples but no such a change in absorbance values was observed. It was therefore concluded that the decrease in absorbance values with elapsed storage time was not due to overall moisture loss in apples that would be expected to happen during storage. The marked regions are associated with the 2^{nd} overtones of water OH stretching, CH and CH_2 stretching [190]. Bobelyn [173] and others [15, 172] also found that strong carbohydrate absorbance bands exist around 10200cm^{-1} and they are convoluted with the strong water band at 10300cm^{-1} to give the observed broad peak. It is likely that the observed decrease in absorbance is associated to the variation in carbohydrates and water content resulting from bruising. The same phenomenon was noticed in spectra acquired on *Golden Delicious* apples, whereas no clear conclusion could be drawn in the case of *Granny Smith* apples. This may suggest that the sensitivity of the absorbance in bruised tissue to storage time is

lower in *Granny Smith* apples than in the other two cultivars.

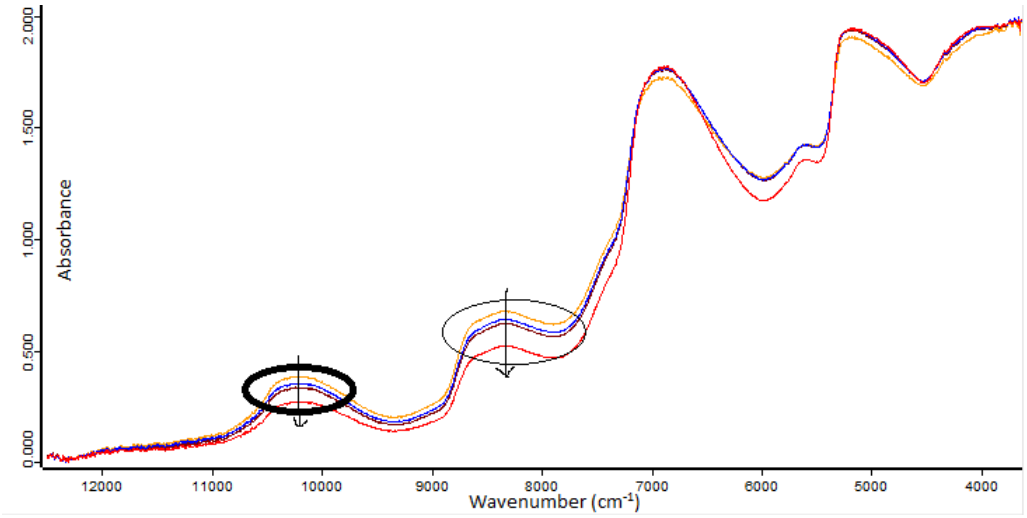

Figure 6.2: Storage time influence on absorbance in NIR spectra of *Golden Delicious* apple bruised tissue. The arrow indicates the direction of increasing storage time.

6.2.1.1 Bruise measurement

Table 6.1 summarizes the range of bruise measurement values in relation to three bruising energy levels and apple cultivar. Bruise diameter values ranged from 11.38 to 16.73mm, 11.41 to 17.54mm and 10.4 to 15.53mm in *Golden Delicious*, *Granny Smith* and *Royal Gala* apples, respectively. Bruise sizes were generally comparable in *Golden Delicious* and *Royal Gala* apples in the two lower bruising energy levels, whereas bruises were mostly bigger in *Granny Smith*. Bruises in *Royal Gala'* apples were relatively more difficult to identify visually, than in the green cultivars.

Table 6.1: Measured values of reference attribute and their correspondence with calculated impact energies and cultivar classes. E_i is the energy of impact in Joule (J); BD, the bruise diameter in mm; and N, the number of samples used in respective categories shown in the table. The apple cultivars *Golden Delicious*, *Granny Smith* and *Royal Gala* are respectively denoted by GD, GS and RG.

E_i (J)	N	BD *mm*)		Cultivar								
		Average	Stdev	N			Average (BD)			Stdev		
0,23	62	11,89	0,47	21	21	20	11,48	12,55	11,64	0,11	0,89	0,97
0,39	90	13,58	0,44	30	30	30	14,13	13,54	13,07	0,27	0,85	0,37
0,74	79	16,02	0,77	25	27	27	16,01	16,97	15,09	0,53	0,42	0,51
				GD	GS	RG	GD	GS	RG	GD	GS	RG

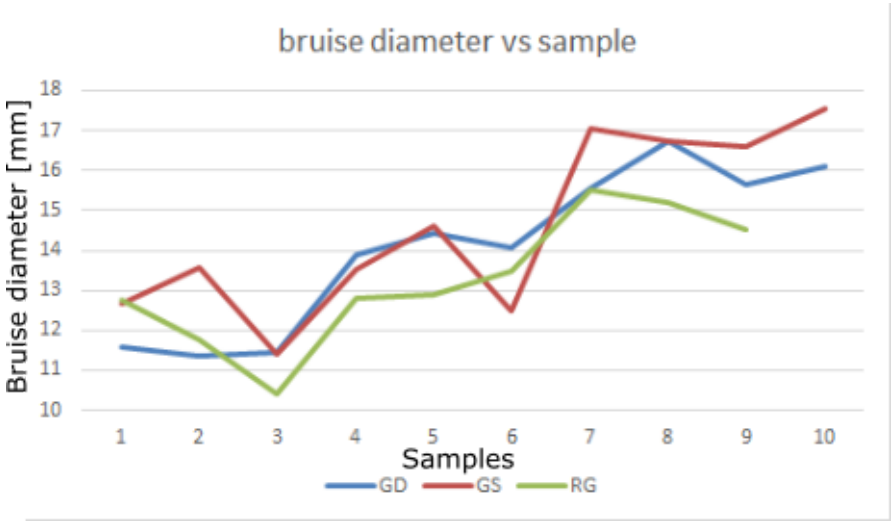

Figure 6.3: Bruise diameter plotted against three slots of samples bruised at different drop heights

A comparison of bruise diameter in the respective apple cultivars showed a slight generalized difference at the same drop heights. *Royal Gala* apples had the lowest bruise diameters, whereas *Golden Delicious* and *Granny Smith* apples had more or less comparable measures of bruise diameter, with fluctuating values for *Granny Smith*.*Golden Delicious* and *Granny Smith* apples fruit sizes appeared to be bigger than *Royal Gala* apples, which may explain the difference in bruise sizes whereby at 'high impacts', the larger the radius of curvature the bigger the bruise would be [191]. The variation in bruise diameter with respect to impact energy was more consistent in *Golden Delicious* and *Royal Gala* apples than it was for the *Granny Smith* cultivar. Figure 6.3 displays the variation in bruise diameter with respect to different drop heights. On the horizontal axis are the samples grouped in intervals of 1 to 3, 4 to 6 and 7 to 10 for drop heights of 0.2, 0.35 and 0.65 m, respectively. The vertical axis shows values of bruise diameter in mm.

6.2.2 Bruise detection

The discriminant analysis of data from the MATRIX-F spectrometer is displayed in Figure 6.4, with bruised tissue (shown in green) is clearly differentiated from healthy tissue (shown in blue). The scatter plot of the scores t1 vs t1o, which is in the X space of independent variables (spectral data in this case), is important in the analysis of a two-class separation (discrimination) problem. Here we used the healthy tissue as a control group and the bruised tissue as a treatment group. The discrimination between the two classes occurs in the horizontal direction (t1) and the discrimination within class occurs in the vertical direction (along t1o). The

method used for segregating bruised from healthy apple tissue is orthogonal PLS discriminant analysis (OPLS-DA) and 71.91% of bruised tissues versus 85.9% of healthy ones were correctly classified. The remaining percentage fell in the overlapping region.

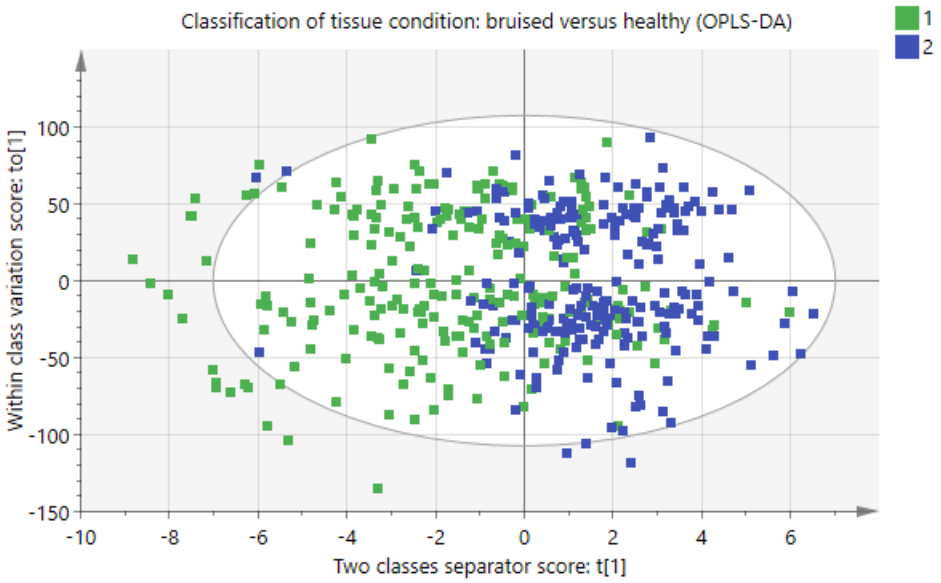

Figure 6.4: Scores plot for healthy and bruised apple tissue. Spectra were acquired on the Matrix-F spectrometer. Category '1' (green) is for bruised apples and category '2' (blue) is for sound apples.

An even greater discrimination was obtained on data acquired on the MPA in integrated sphere mode, whereby 89.87% of bruised apple tissue and 96% of healthy tissue were correctly classified. The total quality of classification was 92.92%.The scores plot for discriminant analysis orthogonal PLS is shown in Figure 6.5.
A discriminant analysis was also conducted to see if there was a difference between the samples classified according to respective applied impact energies (the figure's legend is according to drop heights). Figure 6.6 depicts the score plots of the OPLS-DA, where three groups are fairly differentiated according to impact energies. The classification results are summarized in Table 6.2.
The correctness in classification increased with the drop height as seen in Table 6.2. The analysis shows that the spectral data acquisition method (open non-contact Matrix-F system) captured the differences in absorbance due to levels of tissue damage. The apples bruised at 65cm drop height were relatively greatly segregated from the rest (those of which drop height was either at 20 or 35cm). The misclassification among the two groups at low drop heights was high, where more than half the samples at 20cm drop height were not properly classified. This suggests that

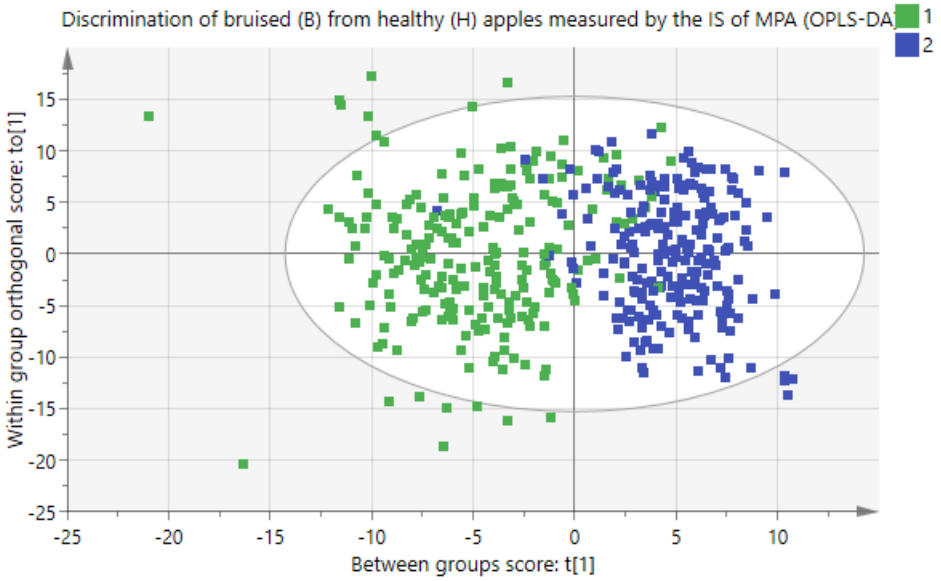

Figure 6.5: Scores plot for healthy and bruised apple tissue. Spectra were acquired on the MPA system. Category '1' (green) is for bruised apples and category '2' (blue) is for sound apples.

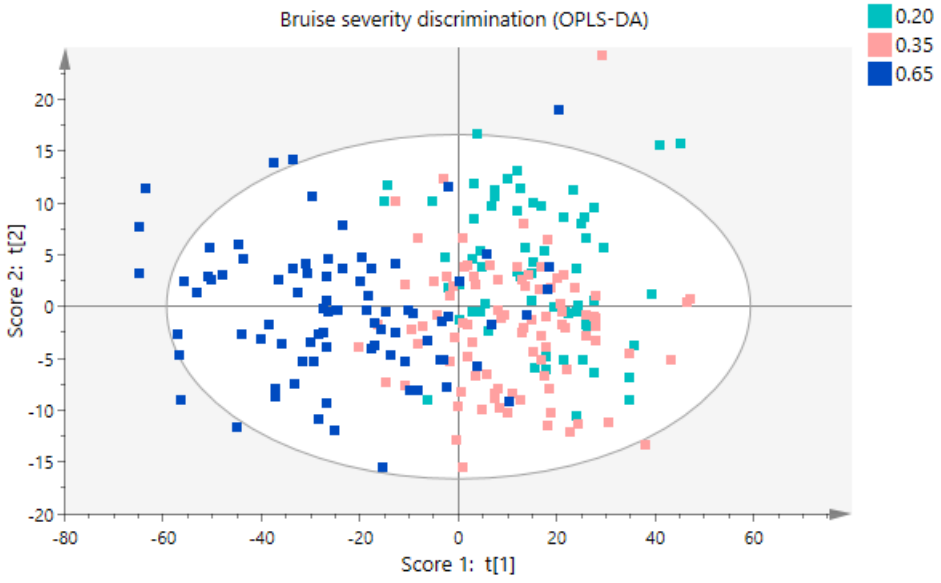

Figure 6.6: Scores plot showing segregation of apple samples with respect to drop height/energy of impact based on spectral data acquired on the Matrix-F spectrometer. Classified categories are labeled according to respective drop height (expressed in m) used to induce the bruises.

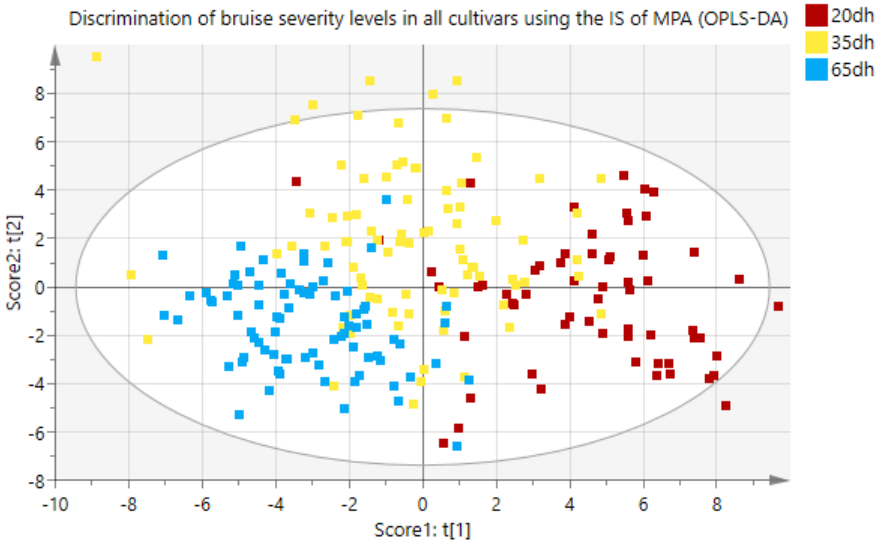

Figure 6.7: Scores plot showing segregation of apple samples with respect to drop height/energy of impact on data from the MPA. Classified categories are labeled according to respective drop height; 20dh, 35dh and 65dh for 20 *cm*, 35 *cm* and 65 *cm* of drop height used in inducing the bruises, respectively.

the spectrometer used in this case (Matrix-F) may be relatively less sensitive to less severe bruises than it is to severe ones.

Table 6.2: Misclassification table for three levels of bruise from spectral data acquired on the Matrix-F.

	Members	Correct	0.20	0.35	0.65	No class (YPred <= 0)
0.20	65	49.23%	32	29	4	0
0.35	90	71.11%	11	64	15	0
0.65	83	83.13%	4	10	69	0
No class	0		0	0	0	0
Total	238	69.33%	47	103	88	0
Fisher's prob.	$1.3\ e^{-006}$					

In Figure 6.7 MPA acquired bruise spectra were considered. The segregation between bruise severity is improved compared to the previous case (see Figure 6.7). However, unlike in the previous case, the greatest misclassification was obtained in bruises induced from a drop height of 35cm.

The findings in these results from spectral data analysis suggest that spectral data from the two NIR spectrometers used in this work differ from each other. Therefore, this would imply that the individual sensitivity of either of these devices to bruises in apples, is relatively different. The classification results summarized in

Table 6.3: Misclassification table for three levels of bruise from spectral data acquired on the MPA.

	Members	Correct	20dh	35dh	65dh	No class (YPred <= 0)
20dh	62	0.84	52	6	4	0
35dh	82	0.58	11	48	23	0
65dh	81	0.98	0	2	79	0
No class	227		183	43	1	0
Total	452	0.79	246	99	107	0
Fisher's prob.	$1.7\ e^{-6}$					

Table 6.3 show that differentiation between bruise severity levels was better in data from the MPA than that from the Matrix-F spectrometer by 10%.
The effect of cultivar on bruise detection is displayed in Figure 6.8. The correctness of classification in individual cultivars was better than when they were combined, and amounted to 96.15% for *Golden Delicious* (A), 94.08% for *Granny Smith* (B) and 95.83% for *Royal Gala* (C). Therefore, it is clear that better results were obtained when apple bruises were analyzed on individual cultivars. In all three cases, a wider spatial spread is noticed in the cluster of bruised tissues than in healthy tissues. This variance is likely due to the difference in bruise severity, and will be explored later in prediction models.

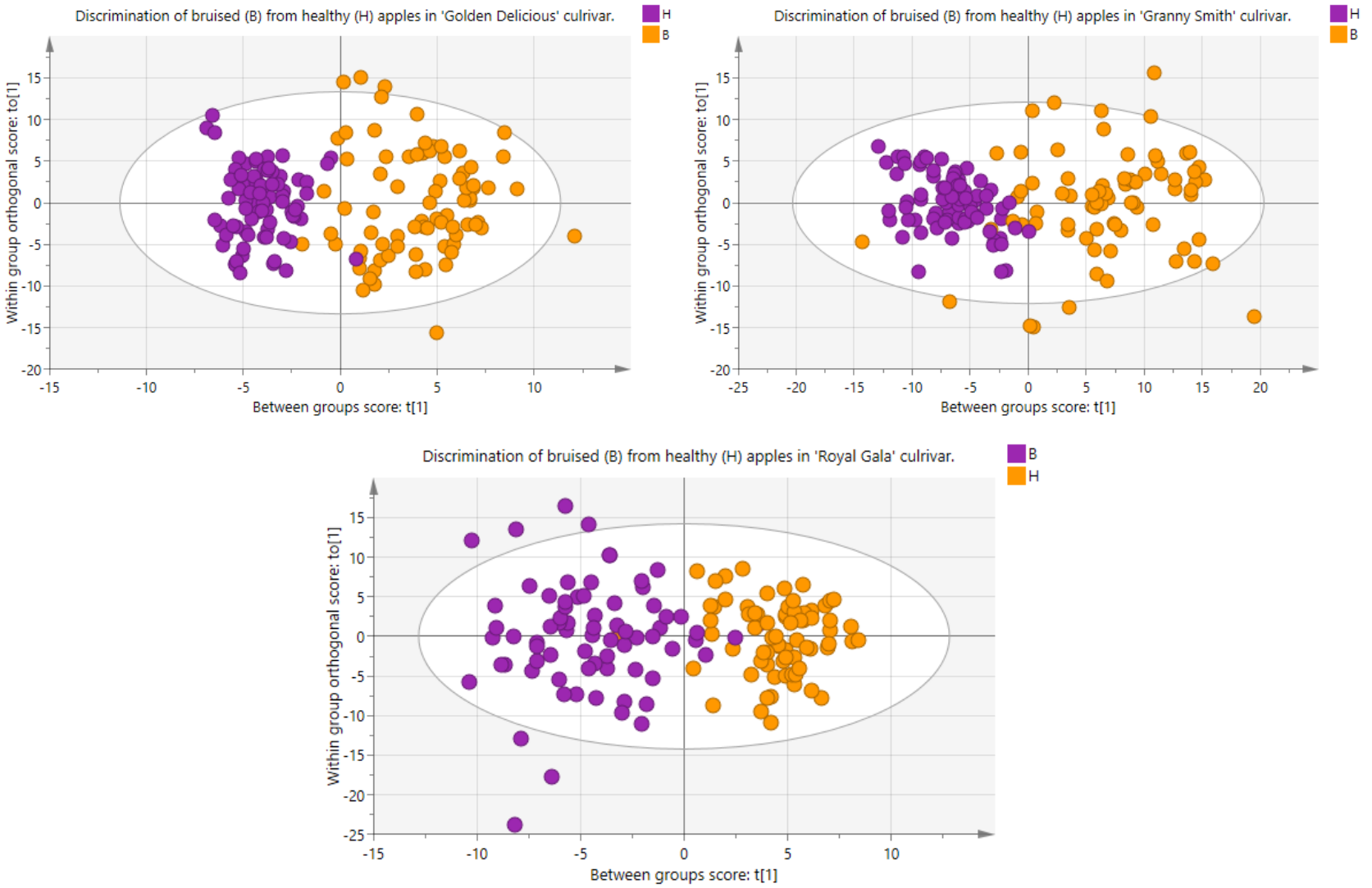

Figure 6.8: Scores scatter plot to discriminate between bruised and healthy apple tissue in the three cultivars. In the figures legends, H and B stand for 'healthy' and 'bruised' apples, respectively

6.2.3 Bruise level prediction

Pre-processing of NIR spectra was done using Opus software/Quant package prior to quantitative analysis. PLS regression was performed to entire spectra with no pre-processing method at first, and then the data was subjected to a model optimization process by applying diverse pre-processing methods to them. Opus software applies multiple pre-processing methods, one at a time, and to different regions of the spectra. The pre-processing method that gave the model with the lowest RMSECV, was selected as the best one and used for establishing the optimal model. In Table 6.4 we presented a few cases where model optimization was attempted by applying different pre-processing methods.

Table 6.4: Spectral pre-processing and prediction model performance there derived.

Instr	Stor time	Calibration		Validation				preproc
		R^2	RMSEE	R^2	RMSECV	RPD	Bias	
EH	1h	71.57	0.88	55.93	1.02	1.51	-0.007	None
	1d	67.96	1.1	64.83	1.12	1.69	-0.003	"
	4d	74.27	0.77	69.53	0.802	1.81	-0.002	"
	1w	95.58	0.393	81.6	0.708	2.33	0.008	"
	All	58.07	1.2	46.29	1.3	1.37	0.14	None
	1h	78.69	0.766	51.87	1.06	1.44	0.001	COE
	1d	86.63	0.682	78.43	0.839	2.15	0.012	der2
	4d	94.29	0.387	80.17	0.647	2.25	0.013	
	1w	98.32	0.25	87.51	0.591	2.83	-0.027	der1
	2w	95.98	0.391	69.07	1.01	1.8	0.007	der2
	All	59.95	1.18	40.01	1.26	1.32	-0.258	der1+MSC
IS	1h	94.82	0.431	72.66	0.847	1.91		None
	1d	59.63	1.25	39.05	1.43	1.28		"
	4d	20.56	1.35	3.75	1.43	1.02	-0.015	"
	1w	29.66	1.57	14.35	1.66	1.08	-0.03	"
	2w	93.12	0.575	75.67	0.956	2.03	-0.017	"
	All	76.94	0.928	59.85	1.17	1.58	0.005	None
	1h	80.36	0.771	67.38	0.909	1.75	0.056	SLS
	1d	79.29	0.927	63.58	1.11	1.66	-0.044	Loc
	4d	82.46	0.716	36.29	1.16	1.26	-0.074	Loc
	1w	96.08	0.389	64.34	1.07	1.67	0.0044	SLS
	2w	89.77	0.695	70.68	1.07	1.85	0.037	der1 + SLS
	All	75.27	0.961	70.51	1	1.84	0.029	Loc

None, full spectrum with no preprocessing; COE, constant offset elimination; der1/2, first/second derivative; MSC, multiplicative scattering correction; SLS, straight line substraction; Loc, localised waveband with no preprocessing.

In many cases, models were improved upon applying a pre-processing method which, in some cases, consisted only in restricting the model to a certain region of

wavelengths. In some other cases, the best model performance was obtained by using the entire spectrum. It was also noticed that pre-processing methods that best optimized the models varied depending on the type of cross-validation used. Figure 6.10 displays the predictability of 1 to 2 hours old bruise damages in apple tissue by NIR spectroscopy, by using 'Multiplicative scatter correction' as the pre-processing technique. In comparison to a non pre-processed data based model in Figure 6.9, it is noted that the PLS regression prediction model performance error was improved by almost 11%.

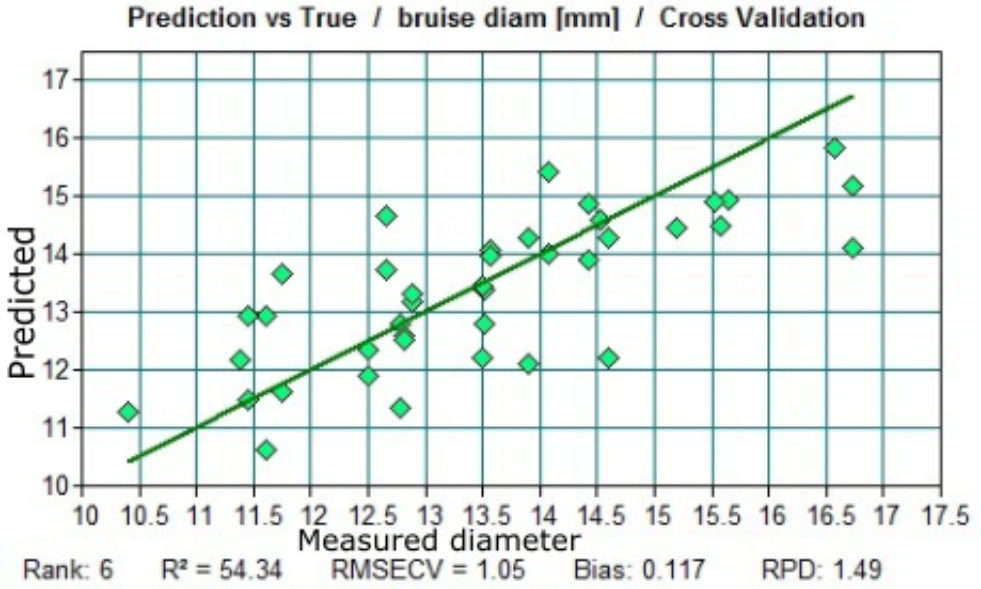

Figure 6.9: Cross-validated model to predict 1-2h old bruises in apple tissue using full spectra of the Matrix-F spectrometer.

Figures 6.11, 6.12 and 6.13 represent a typical example where a model is best without any pre-processing. In Figure 6.12 the model is improved by simply removing outliers in the calibration (model estimation) step, whereas in Figure 6.13 a relatively smaller improvement of the original model (Figure 6.11) was obtained by applying a straight line subtraction to the spectra as a pre-processing method. It is to be understood that applying pre-processing methods always lead to restraining the model to some regions of the spectra, but in some cases such as this, the best performance of the model was obtained by using the whole region of the spectrum.

6.2.3.1 Cultivar specific analysis

Various factors and their effects on bruise prediction were investigated, namely apple cultivar, storage time, and all inclusive dataset. In Figure 6.14(A) measured

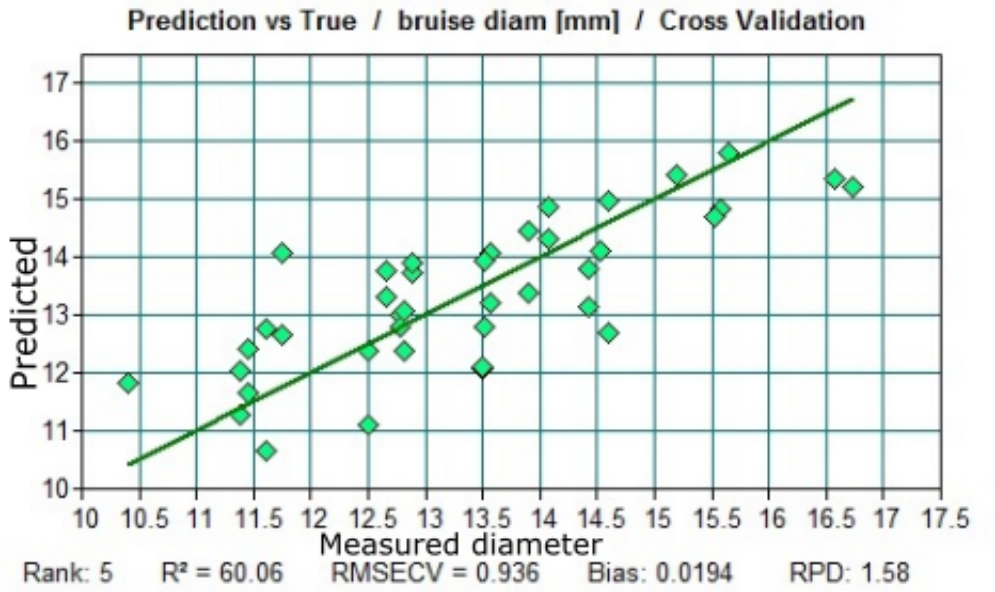

Figure 6.10: Cross-validated model to predict 1-2h old bruises in apple tissue using Multiplicative scatter correction to pre-process spectra from the Matrix-F spectrometer.

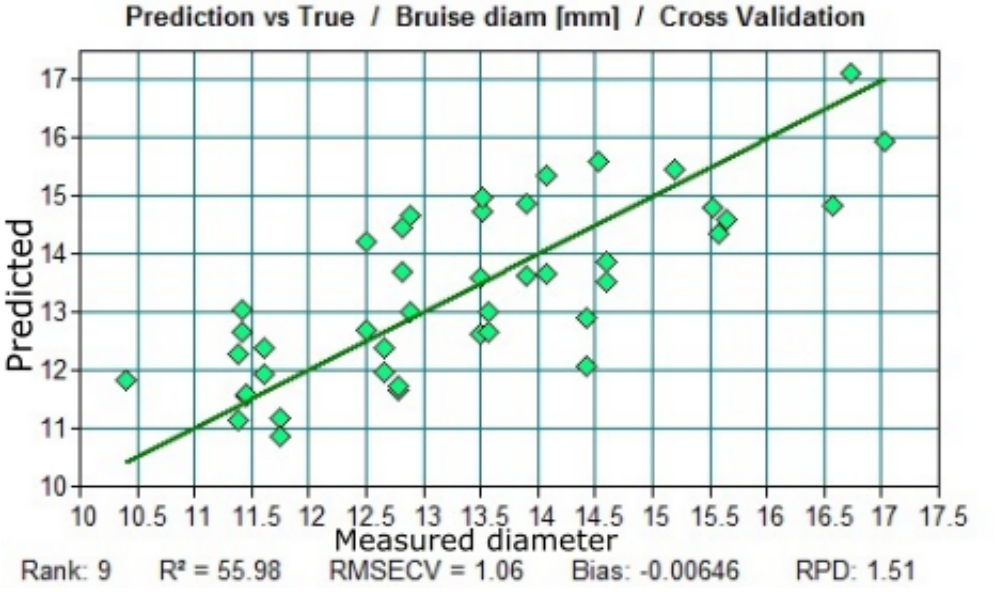

Figure 6.11: Cross-validated model to predict 1-2h old bruises in apple tissue using whole spectra from the integrated sphere of the MPA NIR spectrometer

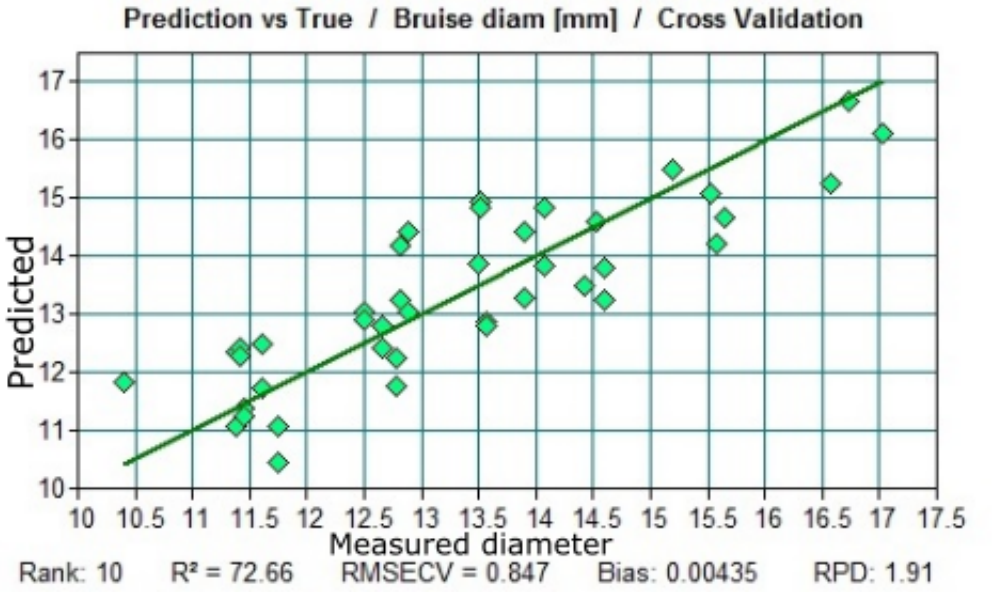

Figure 6.12: Cross-validated model to predict 1-2h old bruises in apple tissue after outlier deletion. The spectral data was acquired by using the integrated sphere of the MPA NIR spectrometer

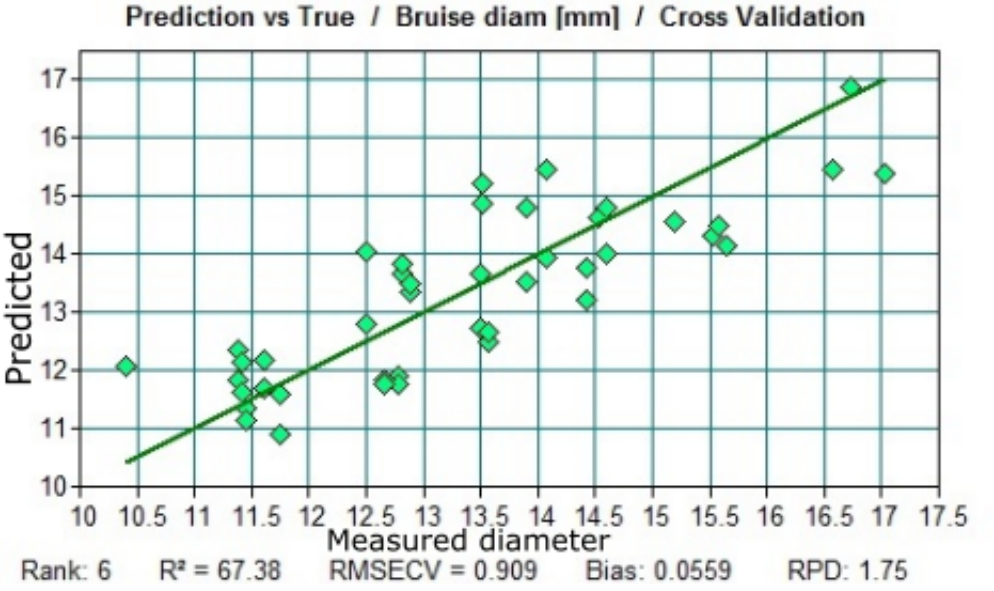

Figure 6.13: Cross-validated model to predict 1-2h old bruises in apple tissue using Straight line subtraction to pre-process spectra from the integrated sphere of the MPA NIR spectrometer.

bruise diameters are plotted against predicted bruise diameters. The error of cross-validated prediction is 1.35 and with a 48.55% goodness of fit for all the cultivars combined. However, bruise predictability was more effective whithin single cultivars. Figure 6.14, (B), (C) and (D) display the plot of observed versus predicted values of bruise size in *Golden Delicious*, *Granny Smith* and *Royal Gala*, respectively. A good prediction performance was obtained in all the three cases, whereby the R^2 values were 63.37% for *Royal Gala*, 77.8% for *Granny Smith* and 72.1% for *Golden Delicious*. The best prediction error was found in *Royal Gala*, followed by *Golden Delicious* apples. The cross-validated prediction error values ranged from 1.086 to 1.226.

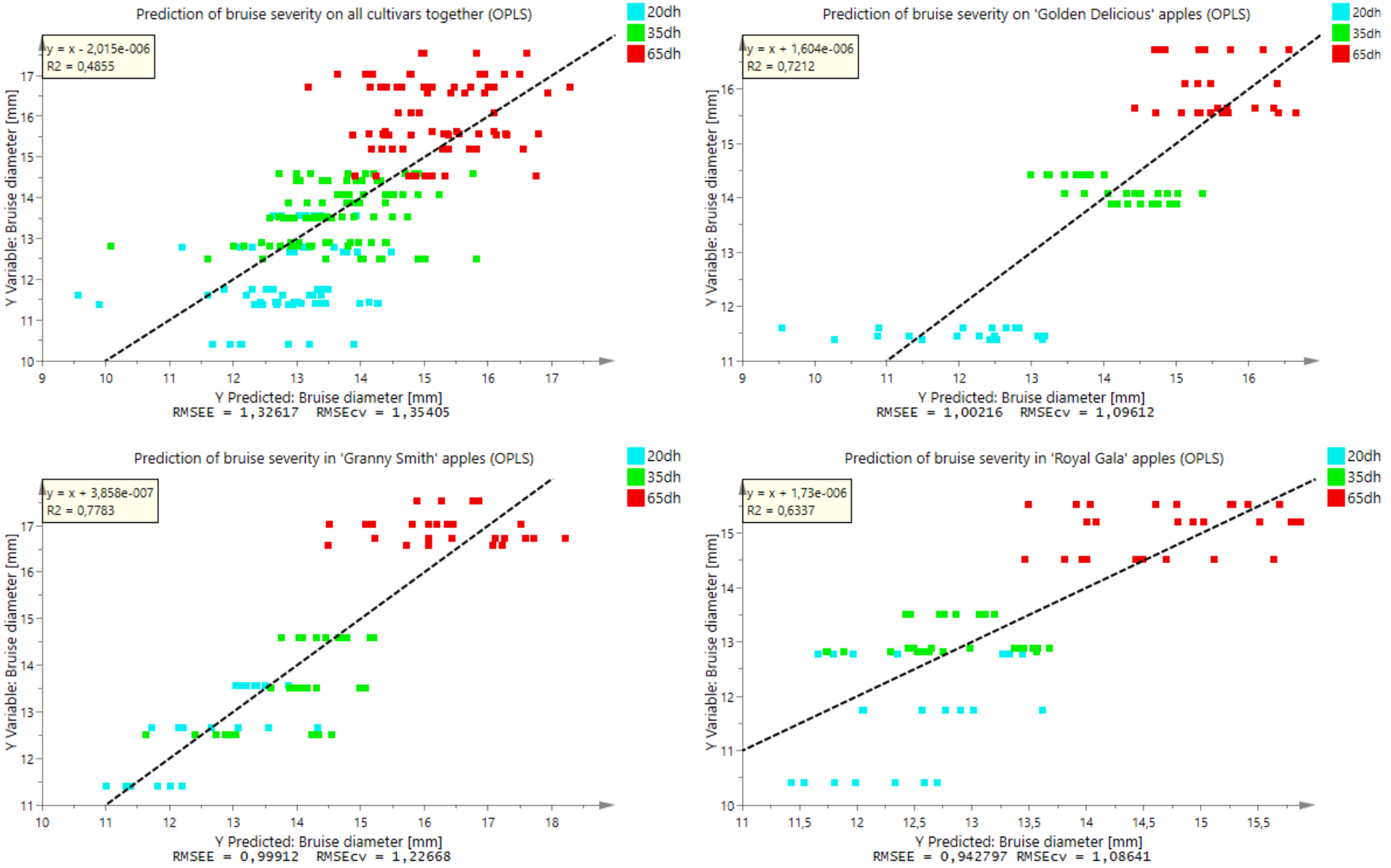

Figure 6.14: Observed versus predicted values of the bruise size. Predictor data were acquired with the Matrix-F spectrometer.

Table 6.5 summarizes the performance of PLS regression models developed on apple bruises with respect to individual cultivars separately. The results of prediction model performance were similar in the sense that in both modes of data acquisition (Matrix-F and MPA) the best model performance was found in *Golden Delicious* and *Royal Gala*. By considering the RMSECV as of higher importance than R^2 in determining the model performance, we argue that *Golden Delicious* apples' low RMSECV on the Matrix-F side and lowest on the MPA side set it as markedly better model performance in both modes of acquisition and highest overall, followed by *Royal Gala*. The model performance obtained in *Granny Smith* apples was rated lowest of all the cultivars, with the highest RMSECV in both acquisition modes.

Table 6.5: Apple cultivar effect on bruise prediction models.

		R^2	RMSECV	LV
Matrix-F	GD	0,72	1,09	1+5
	GS	0,78	1,23	1+8
	RG	0,63	1,09	1+5
	All	0,49	1,35	1+5
MPA	GD	0,93	0,61	1+7
	GS	0,62	1,32	1+3
	RG	0,74	0,99	1+6
	All	0,62	1,29	1+5

The latent variables (LV) were presented in terms of OPLS projection (1 predictive component + orthogonal components).

It is also to be noted that the model predictive ability for the all inclusive dataset was better on the MPA data than it was for the Matrix-F.

6.2.4 Variable importance

In NIR spectroscopy of bruised apple tissue, spectral data are determined from the response of certain chemical compounds and various textural features to different wavelengths in the NIR region. Some wavelengths will inspire specific responses that best describe the attributes in question and their contribution to PLS models differ from the others'. The measure of variable importance in projection (VIP) was used to determine the effective wavelengths for the PLS models. VIP values were calculated for each variable by summing the squares of the PLS loading weights, weighted by the amount of sum of squares explained in each model component. Figure 6.15 shows the importance of variables both to explain X and to correlate to Y, sorted from high to low. Important variables have values that are larger than

one. In the PLS model generated from the all inclusive batch (the three cultivars put together), these variables were marked in red. From Figure 6.15(B) it seems that only important variables in both *Granny Smith* and *Royal Gala* were also important for the all inclusive batch, whereas no important variables for *Golden Delicious* did contribute for the latter.

Over 800 variables were found to have values larger than 1 and thus important, in each case model. In Figure 6.16 VIP values greater than 1 are plotted against their corresponding variables. Figure 6.16(A) shows the plot based on variables that are most involved in the PLS model for the all inclusive batch (marked in yellow), and shows how these same variables are represented in individual apple cultivar based models. It is noticeable that wavelengths in the regions from 800 to 1150 *nm*, 1240 to 1286 *nm*, 1881 to 1885 *nm* and 2764 to 2770 *nm* were the most important for the prediction model of the all inclusive batch. It also shows that these wavelength regions were also important for the *Golden Delicious* model. The two last regions are, however, not important for the other two cultivars, given that the VIP values corresponding to them are smaller than 1. From these results, it is advisable that apple bruise PLSR models that include all these three cultivars would perform better in their common wavelength region, that is 800-1150 *nm*.

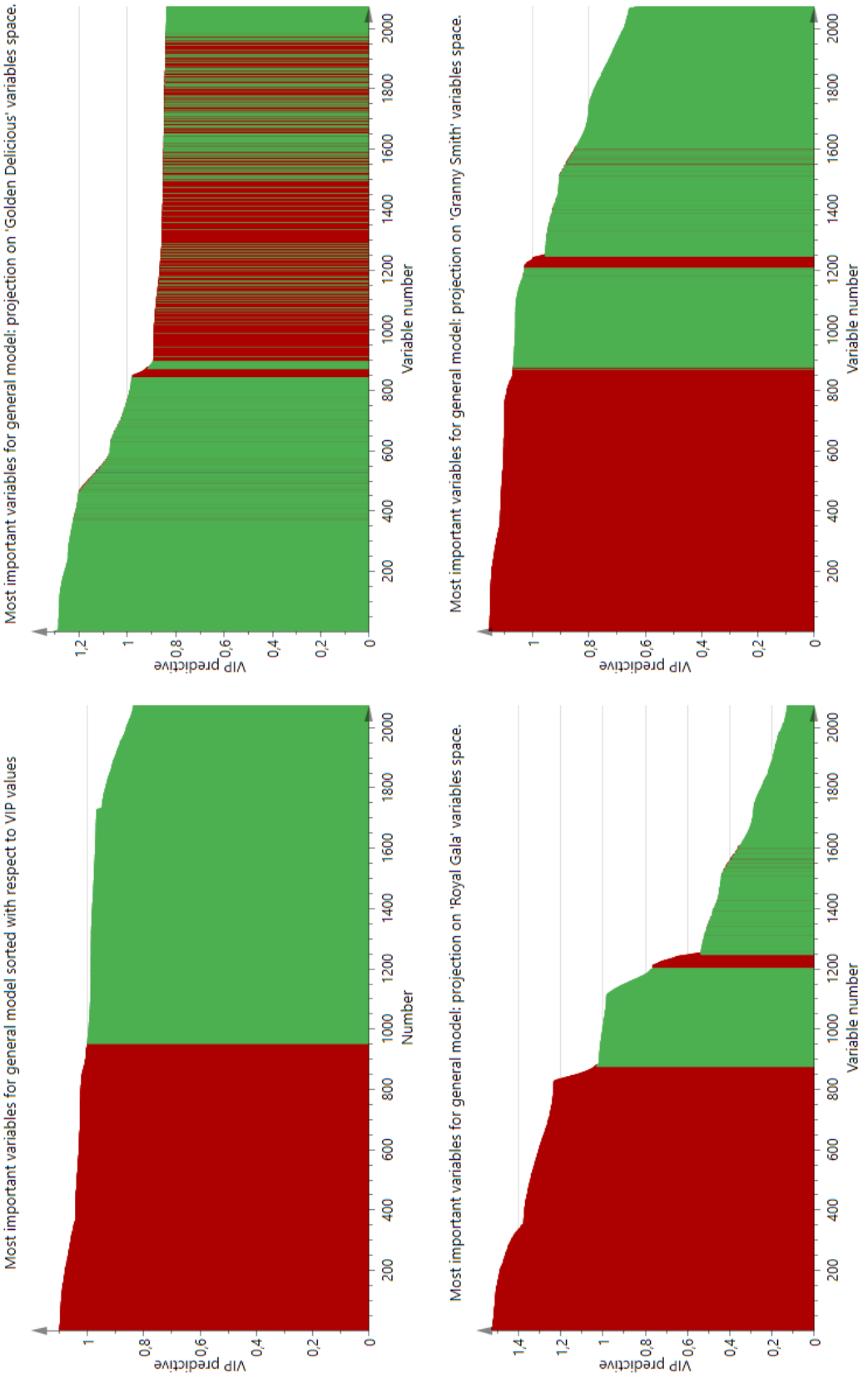

Figure 6.15: Variable importance for the projection plotted against variable number, sorted from largest to smallest value. VIP values for the all inclusive model (A) larger than 1 are marked in red and the corresponding variables are marked for individual batches (B), (C) and (D). The latter correspond to *Golden Delicious*, *Royal Gala* and *Granny Smith* cultivars, respectively. The spectral data were acquired on by the Matrix-F spectrometer.

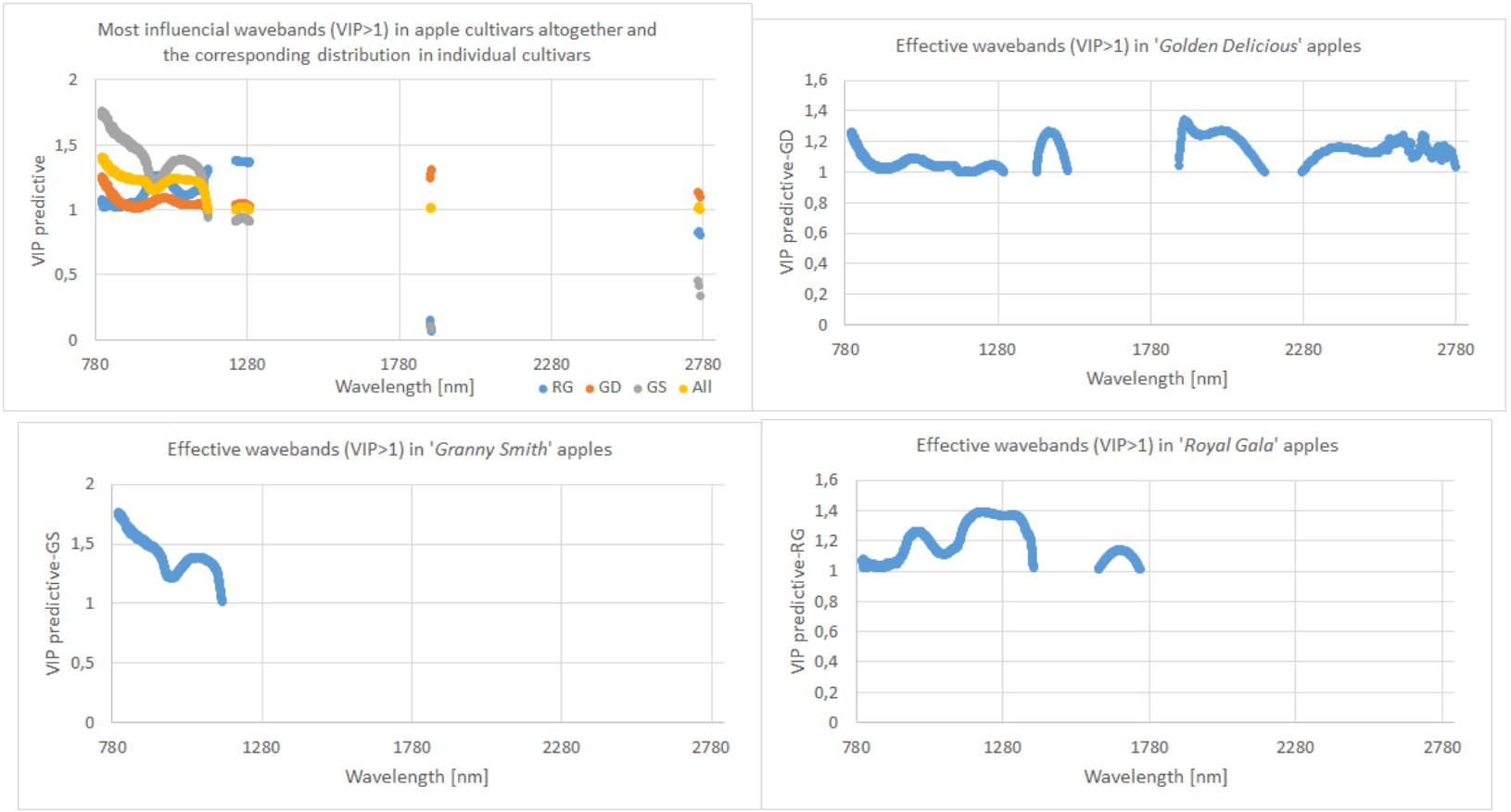

Figure 6.16: Variable importance for the projection plotted against wavelengths in nm. (A) Important variables for the all inclusive batch model, with the same variables plotted for individual batches. In (B), (C) and (D) are important variables specific for individual batches, namely *Golden Delicious*, *Granny Smith* and *Royal Gala* cultivars respectively. The spectral data were acquired by the MPA spectrometer only.

VIP values were used to determine the wavelength regions that are most influential in predicting bruise severity. As seen in Figures 6.16(B), 6.16(C) and 6.16(D), favored wavelength regions are 800-1300nm, 1406-1508nm, 1872-2152nm and 2274-2780nm for *Golden Delicious*, 800-1146nm for *Granny Smith*, and 800-1385nm and 1605-1748nm for *Royal Gala*, respectively.

6.2.5 Regression using genetic algorithm: GA-PLS

In this study, the GA described in [114] was used. The dataset was comprised of two parts, namely the reference values (Y=bruise size) and the spectral data (X). The dataset was sorted according to the Y variable so as establish a similarity in the range and dispersion of the Y variable in each deletion group.The cross validation used the 'venetian blind' technique with 5 leave-out groups.
The genetic algorithm toolbox contains five main programs, and the following steps were followed. A function that returns an average percent variance explained in cross validation was used to determine whether it is suitable to use GA on the dataset. Values that are <10 are acceptable, and in our case values <5 were obtained. This function also offers an option to determine how many evaluations are safe to use, in order to avoid overfitting [114]. This check was also performed and different values were obtained in different instances, and thereafter used with the function that implements the GA-PLS method. The latter was then run on the dataset to generate optimal PLS models upon applying the GA.
GA-PLS analysis of data from the Matrix-F spectrometer yielded high regression coefficients of up to R^2 = 73.98% and very low errors of prediction RMSECV between 1.43 and 0.96 for spectra acquired after 2 weeks and 24 hours, respectively. An improvement of up to 20% in error of prediction was achieved, in comparison to full spectrum based models.
On the other hand, the analysis conducted on data acquired using the MPA (integrated sphere mode) showed that the GA-PLS method improved data by a margin of 33%, with R^2 values of up to 88.69% and RMSECV between 1.22 and 0.61.

6.2.6 Variable selection

The genetic algorithm used here generates, as part of the outputs, the frequency of selection for variables used in developing the model. Given that the GA method involves randomized processes, it was necessary to get a global view by compiling the results from five consecutive runs. A plot was also generated to showcase the regions of the spectra that were favored by the selection process. Figure 6.19 is an example of such a plot. Figure 6.17 shows the variable selection frequency plotted against the variable IDs for spectra acquired with the integrated sphere mode of the

Table 6.6: A comparison of results obtained from GA-PLS and whole spectrum PLSR analysis, from both the Matrix-F and MPA NIR spectral data of bruise.

Instrument		Full spectra			GA			
		R^2(%)	RMSECV	LV	R^2(%)	RMSECV	LV	var
Matrix-F	1hour	22.08	1.56	5	56.67	1.17	5	57
	1day	67.88	1.07	4	73.98	0.96	4	137
	1week	50.07	1.21	8	75.03	0.84	10	180
	2weeks	35.48	1.37	6	43.32	1.42	5	38
MPA	1hour	52.46	1.18	6	87.67	0.61	10	58
	1day	38.94	1.43	8	64.01	1.1	6	25
	1week	67.45	1.02	7	80.28	0.74	11	117
	2weeks	35.16	1.59	5	65.41	1.17	5	76

MPA after two weeks of storage. The cutoff value for the best model is indicated by the green line. Variables most favorably selected and used in final models ranged from 800-850 *nm*, 890-980 *nm*, 1740-1860 *nm* and 2137-2700 *nm*, for spectra acquired on the MPA.

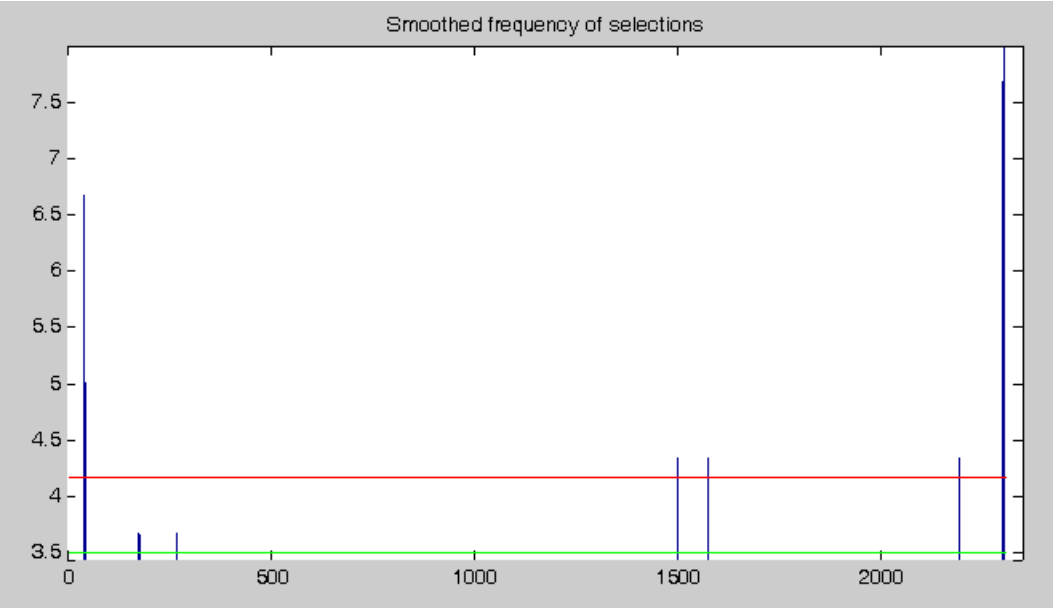

Figure 6.17: Plot of frequency of selection for variables in the NIR spectra from the MPA after two weeks of storage.

As for spectra acquired with the MATRIX-F spectrometer, Figure 6.18 shows the frequency for variable selection plotted against the variable number. Wavelengths were calculated from wavenumbers corresponding to favored regions of the spectra. It was noted that variables ranging from 11990 to 10415 cm^{-1} ($\approx$ 830- 960 *nm*),

1010 to 1020 nm, 4000 to 4050 cm^{-1} ($\approx$ 1770 - 1830 nm) and 1900 to 2050 nm were favored in PLS-GA models of bruised tissue, for spectra acquired on the MATRIX-F spectrometer.

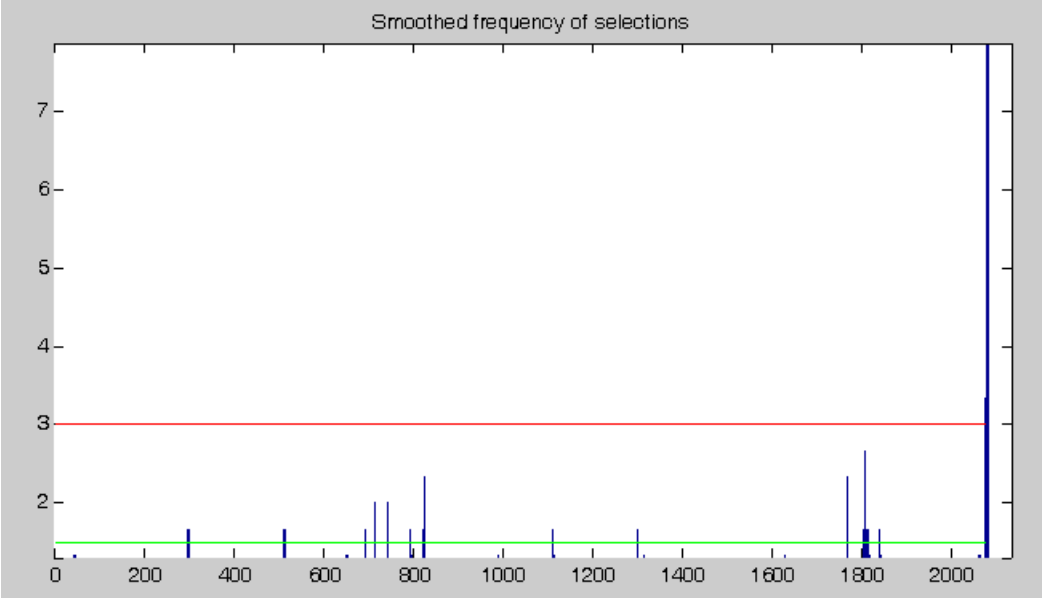

Figure 6.18: A typical plot of frequency of selection for variables in the NIR spectra from the Matrix-F spectrometer. 31 variables were selected for the best model.

It has been noted that different opinions concerning the NIR wavebands characteristic of bruises in apples were reported in the past. Geola et al. proposed a procedure for detection of damaged tissue in *Golden Delicious* apples, a classification function was obtained in the region of 750 to 800 nm [183]. More apple tissue classification studies based on reflectance spectra were conducted where, in most cases, the most significant wavelengths were found in the range of 690 - 850 nm [182, 192, 193]. Kleynen et al., working with a VIS/NIR spectrometer developed a method to detect defects on bicolour apple fruit (*Jonagold*). The most significant wavelengths were found in the NIR range (700-920 nm or 14.285-10.869 cm^{-1}) [194]. According to Lammertyn and associates, the light penetration depth of NIR radiation in *Jonagold* apple tissue was the highest in the region 700-900 nm [195]. Hence, Kleyman associated their observations to the latter wavelength region.

The variable selection from the Matrix-F spectral data resulted in favored wavebands that generally coincided with those obtained from the spectra acquired with the MPA. In both cases, there is an agreement with the reported findings on wavebands that most influence bruise detection in various apple cultivars. In Figure 6.19 favored wavebands selected in five different GA runs in averaged contiguous wavelengths are marked.

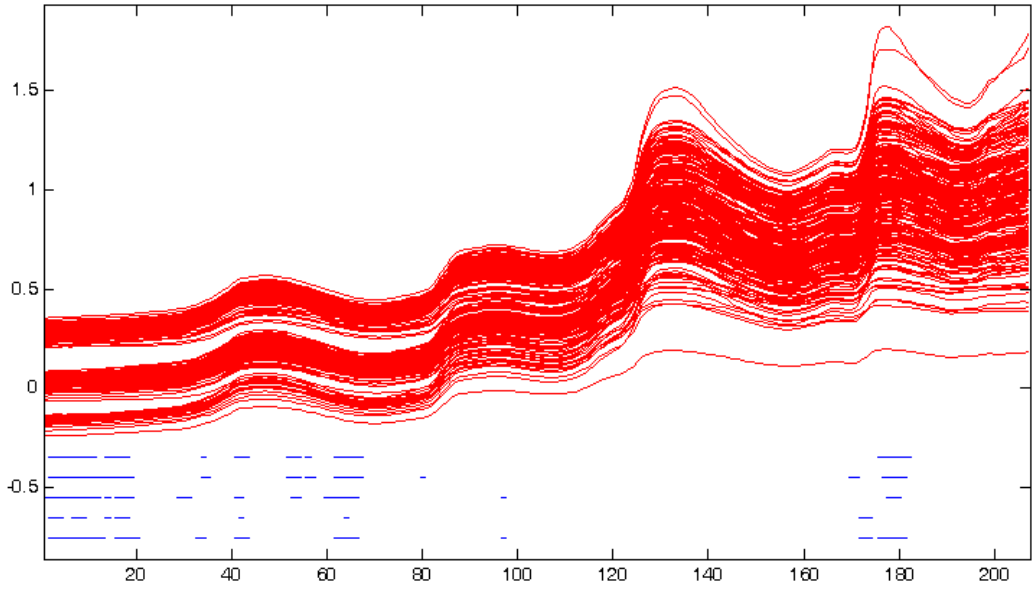

Figure 6.19: A typical plot of regions of the spectra that were favored by variable selection using GA-PLS

6.3 Conclusions

A study of apple bruising was conducted on three apple varieties. Bruises were physically introduced in the apple tissues in a controlled manner, and their sizes used as reference measurements. Two configurations of NIR spectroscopy were used for data acquisition and the spectral data used for bruise detection studies and as predictor of bruise size. The study of bruise detection, using orthogonal partial least squares discriminant analysis, revealed that fruit cultivar had an influence on bruise detectability. *Golden Delicious* apples proved to be the easiest of the three cultivars in allowing discrimination of bruised apple tissues from healthy ones. Prediction of bruise severity was conducted by studying the cross-validated PLS models performance estimated by the RMSECV. The two modes of NIR spectral acquisition proved to have comparable predictive abilities in general, but time-wise best predictions were obtained on data from different days of apple storage on either spectrometer.

Prediction of bruise severity was done using PLS regression models and genetic algorithms combined with PLS. A good model performance was obtained in full spectra based PLSR, with cross-validated error of up to 1.02. Cultivar influence on model performance was also evaluated, and best model performance was obtained for *Golden Delicious* in both acquisition modes. The storage time influence on model performance led to inconclusive results. It is, however, possible that a study of

the evolution of chemical changes in the bruised tissue during storage could shine more light on this. A comparison of both modeling methods (full spectra based PLSR and GA-PLS) revealed that GA-PLS improved model performance by at least 10% and up to 40% , relative to full spectrum PLS.

Variable selection was used to determine effective wavelengths for predicting bruises in apple tissue. Two methods were used in order to ensure consistency in the results of the selection. The variable selection methods used were based on VIP values and GA-PLS. The VIP method resulted in four, one and two effective wavelength regions of the spectra for *Golden Delicious*, *Granny Smith* and *Royal Gala*, respectively. All the cultivars had one common region, namely 800-1150nm, in which is also represented, the wavelength region (750-900nm) repeatedly reported in previous research reports as the best wavelength region to describe bruises in apples. We have comparatively shown that effective wavelengths in modeling apple bruises differ in apple cultivars and what they are for these three cultivars. Results from variable selection by using the GA-PLS method, on the other hand, mainly favored four wavebands located at the lower, middle and higher wavelength regions of the used spectra. The MPA had wider bands in all spectral regions and both acquisition modes had two wavebands in common, namely 830-960nm and 1770-1830nm. Future studies may focus on specificity about the rarely reported wavebands in this regard.

From an industrial application point of view, understanding the exact factors that chemically set the apple bruise apart from healthy tissue will add value to improve accuracy in bruise detection or even external defect identification. It is suggested that, for future studies, chemical changes in the bruised tissue would be investigated in relation to NIRS of bruises.

Chapter 7

General summary and conclusions

Two major analytical tools for non-destructive quality evaluation of agricultural products were used in this project. The objective was to bring to light some of their unexplored potential and use current advanced and exhaustive techniques to maximize the performance in prediction methods, in order to pave the way for future developments needed for their industrial use.

The SQUID detected ULF NMR was used to study various quality parameters in banana during ripening. Relaxation times (longitudinal and transverse) were the NMR parameter that were correlated to physico-chemical attributes measured using traditional standard laboratory methods. Averaged T_1 proved to be better in characterizing the ripening process of banana fruit than T_2. Attributes indicating changes in color (a, h and TCD), soluble solid content, sugar:acid ratio were the best at describing the ripening process, with the best correlation to the NMR parameter T_1, and also the best prediction of ripening index. A time resolved distribution of relaxation time was obtained on bananas at different degrees of ripeness, using an algorithm that implements the inverse Laplace transform and designed for NMR relaxation decays. Two peaks were obtained in general, and were characteristic of one slow and one fast relaxation time. The results of the Laplace inversion were somehow irregular, whereby replicated NMR free induction decays (FIDs) of the same sample didn't necessarily result in the same distribution of relaxation times, i.e. different peak amplitudes or relaxation component values. There was no evident change in values of the relaxation time components with respect to differences in the degrees of ripening. It was left out as a further investigation of determining to which degree the inaccuracy of the transform may be associated to either the convergence algorithm used or the acquisition system.

Non-destructive prediction of internal quality of apple fruit used three acquisition modes from two FT-NIR spectrometers. The main objective was to assess the performance of the emission head (EH) of the Matrix-F spectrometer, intended

for online applications, by comparing it to the usual laboratory standard MPA and envisaging to assess some issues of calibration transferability.

A PCA scores plot showed that fruit samples were distinguishable with respect to spectral acquisition modes and source.

Prediction of apple internal quality indicators (TSS, TA and TSS/TA) was done taking into account different scenarios, such as the effect of cultivar and acquisition modes on the models' performance. The models were also optimized by using different pre-processing techniques in various wavelength regions of the entire spectra.

Relative prediction performances with respect to cultivars varied depending on validation approach. Validation based on source (cal: 100% FLM + 50% Ch; val: 50% Ch) resulted in the order, GD > GS > RG, for the prediction of TSS, where '>' stands for 'better model performance than'. The same order was obtained in predicting TSS/TA, using internal validation (up to 30% of the dataset was used for validation). The acquisition mode based validation (cal: 100% Ch(IS); val: 50% Ch(SP)) resulted in a reversed order from above (RG > GS > GD). The large gap (10% to $\approx$ 20%) between the predictive and calibration values of R^2 suggested that there is a considerable divergence between the respective spectral data, even though they were acquired on the same samples. It is, however, possible that inclusion of part of the test data in the calibration dataset will improve the prediction results. Internally validated TA showed the best prediction in RG and relatively worst prediction in GS.

The comparison of acquisition modes revealed that, although the IS seemed to outperform the EH in predicting TSS and TSS/TA , with the opposite true in predicting TA, the model parameters were close in value in most of the cases and both modes performed relatively better than the SP of the MPA. Similar results were obtained in GA optimized models.

In light of the demonstrated performance of the EH of the Matrix-F spectrometer and the IS mode of the MPA, it is likely that the transferability of calibrations from the IS mode to the EH mode would present fewer challenges than usually encountered in this subject matter.

Part of the project that was conducted using the FT-NIR technique, focused on the study of mechanical damages physically induced in apples. Distinguishing between bruised and intact tissue of apple fruit was achieved with high classification accuracy (up to 96%) using OPLS-DA applied on NIR spectral data. PLS score plots were able to clearly segregate between spectra characteristic of bruises at different degrees of severity. Bruised tissue discrimination was cultivar sensitive, whereby the best discriminating power was obtained in *Golden Delicious* apples, followed by

Royal Gala and *Granny Smith*, in descending order. The same order was obtained in the prediction of bruise severity, with the model performance assessed according to cross-validated error of prediction (RMSECV).

Genetic algorithm optimized models were significantly improved in prediction error, relative to the full spectrum models. Variable selection was performed using both VIP values and GA. VIP values revealed that individual cultivars had particular wavebands that were most favorably descriptive of bruising in them, but also one wavelength region was common to all three cultivars. Genetic algorithm variable selection revealed an almost similar set of wavebands for both acquisition modes and maintained the common region to all the three cultivars as found in the VIP method.

7.1 Summary of original contributions

The aim of this project was to apply advanced methods in spectroscopic techniques that are considered to be on top of the chain in non-destructive techniques as far as spectroscopy is concerned. The endgame was to bring about the possibilities for future applications that would be especially relevant for the South African horticultural sector.

7.1.1 Fruit quality studies by ultra-low field SQUID-NMR

Nuclear magnetic resonance is considered as holding immense potential in probing material properties, versatile in non-destructive measurements and proven to be a successful tool for studying the properties of vegetal tissue. Practical applications in line with the horticultural sector are mainly based on relaxation measurements at low magnetic fields. Developmental progress towards industrial applications have been addressing both hardware and acquisition techniques, and data interpretation related issues, in order to meet the industrial conveniences. In most reports of previous case studies, relaxation data were extracted from MRI images and/or largely focused on transverse relaxation time (T_2), were completely or partly destructive and were usually limited to studying changing trends in values of T_2. In this work, intact banana fruits were used and attention was given to longitudinal relaxation time (T_1). It was shown that average T_1 was a good descriptor of the ripening process of banana fruit, a potentially good predictor of the ripening index of banana and most highly related to specific changes in color indicators including total color difference. It was also shown that flavor related attributes in banana, such as total soluble solids which are mainly composed of sugars, and sugar:acid ratio were highly related to T_1. The measurement of average relaxation data is relatively

faster than acquisition of data for image processing and the use of this approach could contribute in saving processing time as another step forward in addressing the sorting speed of industrial conveyor systems. A rough profile of multicomponent T_1 was produced, and should be useful in further investigations to understand the microchanges that occur in banana during ripening. The methodology used here should be easily reproducible for other fruits or similar food stuff.

7.1.2 Fruit quality studies by NIR spectroscopy

It is widely recognized that near infrared spectroscopy and imaging are powerful tools in studying the properties of material. They have been used in both destructive and non-destructive measurements of food related things quite reliably and extensively. In the horticultural industry, NIRS is seen as a potential tool for fruit sorting based on internal quality. In hyperspectral imaging for internal quality, image processing is relatively time consuming, and is better fit for damage and defects. The NIRS, though fit for chemical attributes, it still faces challenges that include high sorting or processing speeds, selective performance relative to sample (fruit) sizes and structure. Building calibrations based on selective wavelengths is a contributing solution towards solving the issue of processing speed, and calibrations that are inclusive of biological and instrumental variability are a significant basis for alleviating the issues of selective performance and promoting a collaborative network with other users, to facilitate calibration transfers.

A variety of FT-NIR acquisition modes was used together with three cultivars of apple fruit, to build prediction model of some internal quality features. Variable selection was proven to be crucial to achieving good prediction of titratable acids. Total soluble solids were highly predictable with FT-NIR, but also prediction performance improved through variable selection. Variable selection was done using both model optimization implemented in Bruker Opus software and genetic algorithm combined with PLS (GA-PLS). Different scenarios for validation, that involved combination of fruit cultivars, source and/or spectral acquisition modes were used for testing the models. It was found that there is a high similarity in the spectral profile (little signal shift) and predictive ability of flavor related attributes in apples by both the integrating sphere of the FT-NIR MPA and the emission head of the FT-NIR Matrix-F. The latter has been undergoing tests for an effective use inline (in some packing houses in the region), since long exposures turned into samples heating quickly, which affects spectral data. The heating rate, however reduced by exposing the samples with fewer lamps (i.e. 2 instead of 4). Therefore, the similarities demonstrated between both spectrometers modes could be a contributing factor in easing constraints related to calibration transfer between the two

systems.

7.1.3 Prediction of bruise severity in apples

External appearance is of key importance in determining consumer choices, and external defects in apples are the main factors that lead to product depreciation in the market place. Therefore, they represent a high-value feature in fruit sorting. Bruise damages are the most common external defects in apple fruit. They were studied on many accounts, as previously reported, using NIR spectroscopy. Reports have highlighted either a number of individual wavelengths or wavebands that contribute for the detection of bruises. In most studies, single cultivar or multiple cultivars (with individual models) were used, and also a great deal of studies used the VIS/NIR range, where the NIR range was partially used. In general, it has been shown that variable selectivity is inherent with effective bruise detection in apples.

Here we investigated both the detection of bruise and prediction of bruise severity in three apple cultivars and their individual effects on variable selectivity, using a full range of NIR spectrum. All inclusive (all three cultivars combined) and exclusive (individual cultivar considered) models were considered. In both detectability and prediction studies, exclusive models were found to have better performance than all inclusive ones. Also, individual cultivars had unique favored wavebands whereas, altogether, a common favored waveband was found that coincided essentially with the wavebands, most commonly reported as having the main effects on bruise damage in apples. In other words, we have shown the specificity of apple cultivar on variable selection in bruise damage related studies. Variable selection consisted in two methods, namely, variable importance in projection (VIP) and GA which follow different approaches, for validation purposes.

Our study of apple quality, both internal and external using NIR spectroscopy, adds value to the board of knowledge in line with non-destructive measurements of quality attributes of horticultural products and falls in line with developmental trends towards industrial applications.

7.2 Limitations and future prospects

This project originally started with a focus on the application of SQUID-NMR techniques to the horticultural industry. The aim was to further the knowledge in understanding low resolution NMR studies of quality in agricultural products, to develop models for quality testing of fruits and address the issues that hinder the industrial applications of the low-field NMR in horticulture and similar fields, such

as foods in general. The hope was to advance the practical aspects of nondestructive applications of the SQUID-NMR, especially in relevance to the horticultural industry in the region.

Before the end of the first year in this project, the SQUID-NMR system that was intended for this project, for some reason, broke down and the process of insurance claiming for reparations took more than 8 months, followed by the additional time thereafter for parts ordering, fixing and shipping the NMR sensor (SQUID probe) back from Taiwan. A year passed within which very little significant work was done that directly contributed to this thesis. Even after the SQUID probe was received, it did not perform as well as was expected, probably due to improper transportation during shipping.

Since this SQUID-NMR spectrometer was the only one in the region that could allow for the study in question and was not operational, this project could not continue as originally planned. An alternative solution had to be found, and a new proposal had to be devised, which would allow to further the work without greatly jeopardizing the overall objective of the project.

NIR spectroscopy offered non-destructive capabilities with advanced prospects for industrial use, such as low cost and/or inline applications. Therefore both advanced techniques, namely the SQUID-NMR and NIRS, were incorporated in the initial objective framework of the project.

The SQUID-NMR studies brought some new findings to light, but not without difficulties. The average spin-spin relaxation time T_2 had poor predictive ability for banana ripening. However, as previously reported in the literature [196], the multicomponent relaxation based approach found that the T_2 component pertaining to water in the vacuole, described the ripening process in banana fairly well. The calculation of multicomponent T_2 distribution was not successfully achieved in this project and hence couldn't be used for further analysis. The issue was mostly due to the presence of high noise levels between the echoes of the spin-echo signal, which made the Laplace inversion algorithm that was used unable to properly calculate the transforms. Pre-processing of the echo signal, by cutting off the trenches of noise, would likely improve the quality of the raw data. Most, if not all multicomponent T_2 based studies used signals with hundred or thousands of echoes. The design or optimal capabilities of our spectrometer allowed for 10 echoes at best, and this would still diminish the richness of information possibly extractable from the T_2 resolved spectra, especially in complex foods. Optimising the time between the π pulses would seem like another option to circumvent this hurdle, but the noise in the echo signals seemed to change from day to day. It was thought that there could have been some electromagnetic disturbances in the surrounding

area or else some functions were not optimal, since the spectrometer was still in its infancy, as far as commercial SQUID-NMR availability was concerned.

The study based on the spin-lattice relaxation time, however, showed promise. Good description of banana ripening and correlation to ripening associated changes in attributes, such as some color features and sugar content, amongst others, were obtained. Calculation of the T_1 resolved distribution of relaxation times for multi-component based studies was carried out by trying out adjusting various parameters to ensure stable transforms. Two main T_1 components were found to pertain to intact banana, but the transforms were mostly consistent per single NMR raw signal (single FID). An alternative multicomponent generation method, such as in [45, 197], amongst others, would be beneficial to determine whether the consistency in the transforms had to do with the nature of the data or the accuracy of the algorithm used.

Multicomponent NMR relaxation time studies are the way forward in low-resolution NMR methods, one- and multi-dimensional. There has been a number of studies on porous media [198] and vegetal tissue [199] and there is still plenty of room for research to help understand the embedded properties of water containing material, describe processes on a micro-cellular level, address the issues of peak assignments and more features that are only available through NMR at low fields.

It has also to be noted that, for more practical purposes, this work was done on 'intact bananas' with higher variability in sampling, since, unlike many studies where a banana was left to ripen while small parts of it were progressively cut off for analysis [83]. Such a procedure exposed bananas to injury-like tissue textural changes and tissue degradations on the edge that was cut off. The sampling in this project consisted of randomly choosing intact bananas from a larger cluster on each measurement day, in order to also represent variability that may occur in a batch during the ripening process. This contributes for a value-added on a more realistic, non-destructive study for practical/industrial uses and is in accord with previous recommendations by Ribeiro and coworkers to rather use intact banana for such a study [150]

As argued in Chapter 1, NIRS shows a lot of promise, and has been used extensively. New developments and applications are found year after year [145, 200]. Online use of NIR spectroscopy is an invaluable attraction in the horticultural field, as well as user friendly handheld devices. PLS models are very commonly used in NIR spectroscopy for various purposes [201, 122, 202]. The high dimensionality of the NIR spectral data induces model complexity, but since not all wavelengths (x variables) are always necessarily relevant to the problem at hand, variable selection methods can be used, thus reducing the high dimensionality problem. Opti-

mal model performance can also be achieved when some optimization methods are used. Another problem often encountered is that of calibration transfer, whereby a model developed on one instrument rarely works on another instrument, even that of the same type [15].

The study of some internal quality indicators of apple was investigated in three apple cultivars and three different Fourier transform NIR (FT-NIR) acquisition modes. The influence of cultivar and that of spectral acquisition mode on model performance was studied. By involving the variability induced by both the variety of acquisition modes used here and the different apple cultivars and sources, strong calibration models were developed and it was found that the emission head (EH) of the Matrix-F spectrometer had properties that would increase the models' compatibility between itself and the integrating sphere mode (IS) of the MPA. In other words, results indicate that calibration transfer between the EH and IS is likely to be relatively simpler than in many cases. Since the EH was intended for online applications, calibration transfer from the more commonly used, more available MPA gives many opportunities for database construction and with relatively reduced challenges to face in the process.

Model optimization for internal quality used pre-processing, and genetic algorithms (GA) validated the influences of instruments on prediction model performances. There exist alternative variable selection and optimization methods, but all have individual limitations. However, combinations of some algorithms can compensate for individual methods' limitations and may improve the performance (computing time and precision) in some cases [106]. For advanced variable selection methods and optimization, a combination of methods is advisable [203].

In the study of mechanical damage (bruising) in apple fruits, various softwares were used, each of which had limitations and slight variations in the algorithms used. The 'Bruker'OPUS Quant2 method is a purely PLS-based tool, and discrimination of bruises from sound tissue was impossible. Also the suggested latent variables in the final models were, in some cases, corresponding to the model with the lowest error, according to the RMSECV (P) versus rank plot. Also, even when outliers had been removed from the PCA plot, there were cases where more data points were marked as outliers, even though it didn't seem to be the case. It was up to the author to decide on what ought to be treated as such and discarded from the model. In this vein, we had to compare models built in another software package, called SIMCA (from *Umetrics*). The latter was also used to carry out discriminant analysis. SIMCA favors orthogonal PLS, and has shown to perform better than the usual PLS, even though it concentrated most important variance in one component and the rest in components that are orthogonal to the first.

Bruise prediction models had poor performance and thus optimization and variable selection was an eminent solution to adopt. Model optimization by pre-processing was done using OPUS, but this presets some wavelength regions and juggles around with pre-processing methods and their combinations within those preset regions. Even though it has been found to improve models in most cases, some important variables may be left behind. A genetic algorithm was used in combination with PLS to further optimize the models and proved to be very effective. Since variable selection seemed crucial to NIR bruise prediction [140], the variable importance in projection (VIP) method was also used to select effective wavelengths and thereby used to validate GA's variable selection results.

Both GA and VIP methods resulted in wavelength regions that were spread from the beginning to the end of the spectra. These wavebands were not completely the same, but had commonalities and especially, one consistently common waveband, regardless of the cultivar considered. Nonetheless, only VIP values higher than 1 were considered and corresponded to highly influential variables. Some authors considered 'medium influence' variables, of which VIP values are situated between 0.8 and 1 [143]. This considered, the favored wavebands could be extended but, of course, would not affect the results found in this work. The challenge remains to develop a method to quantitatively assess accurately the extent of internal damage to fruits induced by external force [204]. Also, additional investigation using other variable selection methods can be used if one intended to raise the level of precision and maybe make a final decision on the selected wavelengths specific for their application. For future reference, it should be noted that for practical applications, bruise detection or fruit segregation based on bruises can be achieved by setting up thresholds for bruise/healthy tissue conditions and customization routine for the selection system (in sorting lines for instance). The margins could be set for one tissue condition, and the test would be done for identifying the other.

This project used practical experimental studies of fruit quality using two advanced [205] analytical spectroscopy techniques to further research towards non-destructive and online application of NIRS and SQUID-NMR. Insight is given on future prospects for industrial applications.

Bibliography

[1] S. A. Fresh Produce Exporters Forum, "Fpefsa statistics," November 2016. [Online]. Available: http://fpefsa.co.za/statistics/

[2] A. A. Kader, "Plenary speech at the Postharvest symposium Africa," CIGR technical symposium, Stellenbosch, South Africa, November 2012.

[3] D. Slaughter, "Nondestructive maturity assessment methods for mango: A review of literature and identification of future research needs," *National Mango Board, Orlando, FL, USA*, 2009.

[4] M. Ruiz-Altisent, L. Ruiz-Garcia, G. Moreda, R. Lu, N. Hernandez-Sanchez, E. Correa, B. Diezma, B. Nicolaï, and J. García-Ramos, "Sensors for product characterization and quality of specialty crops: A review," *Computers and Electronics in Agriculture*, vol. 74, no. 2, pp. 176–194, Nov. 2010.

[5] Y. Zhang, L. Q. Qiu, H.-J. Krause, H. Dong, A. I. Braginski, S. Tanaka, and A. Offenhaeusser, "Overview of low-field NMR measurements using HTS rf-SQUIDs," *Physica C: Superconductivity*, vol. 469, no. 15, pp. 1624–1629, 2009. [Online]. Available: http://dx.doi.org/10.1016/j.physc.2009.05.085

[6] B. P. Hills and C. J. Clark, "Quality assessment of horticultural products by NMR," *Annual Reports on NMR Spectroscopy*, vol. 50, pp. 75–120, 2003.

[7] Y. Hatsukade, T. Abe, S. Tsunaki, M. Yamamoto, H. Murata, and S. Tanaka, "Application of Ultra-Low Field HTS-SQUID NMR/MRI to Contaminant Detection in Food," *Applied Superconductivity, IEEE Transactions on*, vol. 23, no. 3, p. 1602204, 2013.

[8] S. Fukumoto, S. Tsunaki, T. Chigasaki, Y. Hatsukade, and S. Tanaka, "ULF-NMR system using HTS-SQUID and permanent magnet," *Physica C: Superconductivity*, 2012.

[9] A. N. Matlashov, V. S. Zotev, R. H. Kraus, Jr., H. Sandin, A. V. Urbaitis, P. L. Volegov, and M. A. Espy, "SQUIDs for Magnetic Resonance

Imaging at Ultra-low Magnetic Field," *PIERS Online*, vol. 5, no. 5, pp. 466–470, 2009. [Online]. Available: http://piers.mit.edu/piersonline/piers.php?year=2009{&}volume=5{&}number=5{&}page=466

[10] F. Dalitz, M. Cudaj, M. Maiwald, and G. Guthausen, "Process and reaction monitoring by low-field NMR spectroscopy," *Progress in Nuclear Magnetic Resonance Spectroscopy*, vol. 60, no. 2012, pp. 52–70, 2012. [Online]. Available: http://dx.doi.org/10.1016/j.pnmrs.2011.11.003

[11] P. Barreiro, a. Moya, E. Correa, M. Ruiz-Altisent, M. Fernández-Valle, a. Peirs, K. M. Wright, and B. P. Hills, "Prospects for the rapid detection of mealiness in apples by nondestructive NMR relaxometry," *Applied Magnetic Resonance*, vol. 22, no. 3, pp. 387–400, Sep. 2002. [Online]. Available: http://link.springer.com/10.1007/BF03166119

[12] H. Yan, D.-L. Lu, B. Chen, and W. G. Hansen, "Development of a hand-held near infrared system based on an android os and micronir, and its application in measuring soluble solids content in fuji apples," *NIR news*, vol. 25, no. 4, pp. 16–19, 2014.

[13] T. Genkawa, "Development of an online near infrared/mid-infrareddual-region spectrometer and its application," *NIR news*, vol. 25, no. 2, pp. 13–14, 2014.

[14] P. Vermeulen, J. A. F. Pierna, H. P. van Egmond, P. Dardenne, and V. Baeten, "Online detection and quantification of ergot bodies in cereals using near infrared hyperspectral imaging," *Food Additives and Contaminants: Part A - Chemistry Analysis Control Exposure & Risk Assessment*, vol. 29, no. 2, pp. 232–240, 2012.

[15] M. C. Alamar, E. Bobelyn, J. Lammertyn, B. M. Nicolaï, and E. Moltó, "Calibration transfer between NIR diode array and FT-NIR spectrophotometers for measuring the soluble solids contents of apple," *Postharvest Biology and Technology*, vol. 45, no. 1, pp. 38–45, 2007.

[16] F. R. Harker, F. A. Gunson, and S. R. Jaeger, "The case for fruit quality: an interpretive review of consumer attitudes, and preferences for apples," *Postharvest Biology and Technology*, vol. 28, no. 3, pp. 333–347, 2003.

[17] M. Ladaniya, "Citrus fruit: biology, technology and evaluation," *Academic Press*, 2010.

[18] J. F. I. Nturambirwe, "Non-destructive measurement of internal fruit quality using SQUID-NMR techniques," Master's thesis, Stellenbosch, 2012.

[19] L. S. Magwaza, U. L. Opara, L. a. Terry, S. Landahl, P. J. Cronje, H. Nieuwoudt, A. M. Mouazen, W. Saeys, and B. M. Nicolaï, "Prediction of 'Nules Clementine' mandarin susceptibility to rind breakdown disorder using Vis/NIR spectroscopy," *Postharvest Biology and Technology*, vol. 74, no. 2012, pp. 1–10, 2012. [Online]. Available: http://dx.doi.org/10.1016/j.postharvbio.2012.06.007

[20] J. Létal, D. Jirák, L. Šuderlová, and M. Hájek, "MRI 'texture' analysis of MR images of apples during ripening and storage," *LWT - Food Science and Technology*, vol. 36, no. 7, pp. 719–727, Nov. 2003.

[21] M. Koizumi, S. Naito, N. Ishida, T. Haishi, and H. Kano, "A Dedicated MRI for Food Science and Agriculture," *Food Science and Technology Research*, vol. 14, no. 1, pp. 74 – 82, 2008.

[22] P. Barreiro, C. Ortiz, M. Ruiz-altisent, J. Ruiz-cabello, and M. E. Ferna, "Mealiness assessment in apples and peaches using MRI techniques," *Magnetic Resonance Imaging*, vol. 18, pp. 1175–1181, 2000.

[23] M. Musse, S. Quellec, M. Cambert, M. Lahaye, M.-F. Devaux, and F. Mariette, "Monitoring the postharvest ripening of tomato fruit using quantitative MRI and NMR relaxometry," *Postharvest Biology and Technology*, vol. 53, no. 1-2, pp. 22–35, Jul. 2009. [Online]. Available: http://linkinghub.elsevier.com/retrieve/pii/S0925521409000581

[24] G. Nesbitt, "Principles of NMR microscopy," *TrAC Trends in Analytical Chemistry*, vol. 11, no. 6, p. XVIII, 1992.

[25] J. Stepisnik, "Spectroscopy: NMR down to Earth." *Nature*, vol. 439, no. 7078, pp. 799–801, 2006.

[26] L. F. Gladden, "Nuclear magnetic resonance in chemical engineering: principles and applications," *Chemical Engineering Science*, vol. 49, no. 20, pp. 3339–3408, 1994.

[27] N. Blog, "Low Field NMR Spectroscopy and Applications." [Online]. Available: http://nanalysis.com/wp/?p=113

[28] J. Dabek, J. O. Nieminen, P. T. Vesanen, R. Sepponen, and R. J. Ilmoniemi, "Improved determination of FID signal parameters in low-field NMR." *Journal of Magnetic Resonance (San Diego, Calif. : 1997)*,

vol. 205, no. 1, pp. 148–60, Jul. 2010. [Online]. Available: http://www.ncbi.nlm.nih.gov/pubmed/20471879

[29] B. P. Hills, "Applications of Low-Field NMR to Food Science," *Annual Reports on NMR Spectroscopy*, vol. 58, pp. 177–230, 2006.

[30] B. P. Hills, K. M. Wright, and D. G. Gillies, "A low-field, low-cost Halbach magnet array for open-access NMR," *Journal of Magnetic Resonance*, vol. 175, no. 2, pp. 336–339, aug 2005. [Online]. Available: http://www.ncbi.nlm.nih.gov/pubmed/15935715

[31] B. Manz, B. J. Parkinson, and P. T. Callaghan, "A mobile one-sided NMR sensor with a homogeneous magnetic field : The NMR-MOLE," *Journal of Magnetic Resonance*, vol. 183, pp. 25–31, 2006.

[32] A. N. Matlachov, P. L. Volegov, M. a. Espy, J. S. George, and R. H. Kraus, "SQUID detected NMR in microtesla magnetic fields." *Journal of Magnetic Resonance*, vol. 170, no. 1, pp. 1–7, Sep. 2004. [Online]. Available: http://www.ncbi.nlm.nih.gov/pubmed/15324752

[33] Y. Hatsukade, S. Tsunaki, M. Yamamoto, T. Abe, J. Hatta, and S. Tanaka, "Feasibility study of contaminant detection for food with ULF-NMR/MRI system using HTS-SQUID," *Physica C: Superconductivity*, vol. 494, no. 2013, pp. 199–202, Nov. 2013.

[34] S. Tsunaki, M. Yamamoto, J. Hatta, Y. Hatsukade, and S. Tanaka, "Development of contaminant detection system based on ultra-low field SQUID-NMR/MRI," *Journal of Physics: Conference Series*, vol. 507, no. PART 4, 2014.

[35] M. Espy, A. Matlachov, P. Volegov, J. Mosher, and R. Kraus, "SQUID-Based Simultaneous Detection of NMR and Biomagnetic Signals at Ultra-Low Magnetic Fields," *IEEE Transactions on Appiled Superconductivity*, vol. 15, no. 2, pp. 635–639, Jun. 2005.

[36] M. Espy, A. Matlashov, and P. Volegov, "SQUID-detected ultra-low field MRI." *Journal of Magnetic Resonance*, vol. 228, no. 2013, pp. 1–15, Mar. 2013.

[37] L. Q. Qiu, Y. Zhang, H.-J. Krause, and A. I. Braginski, "SQUID-detected NMR in Earth's magnetic field," *Journal of Physics: Conference Series*, vol. 97, p. 012026, feb 2008. [Online]. Available: http://stacks.iop.org/1742-6596/97/i=1/a=012026?key=crossref.4e676c805458a0fc18ab507571952189

[38] L. Qiu, Y. Zhang, H. J. Krause, A. I. Braginski, and A. Offenhäusser, "Low-field NMR measurement procedure when SQUID detection is used," *Journal of Magnetic Resonance*, vol. 196, no. 2, pp. 101–104, 2009. [Online]. Available: http://dx.doi.org/10.1016/j.jmr.2008.09.009

[39] F. Mariette and J. Guillement, "Continuous relaxation time distribution decomposition by MEM," *Data Handling in Science . . .* , 1996. [Online]. Available: http://scholar.google.co.za/scholar?lookup=0&q=Continuous+relaxation+time+distribution+decomposition+by+MEM&hl=en&as_sdt=0,5#0

[40] K. L. Kuhlman, "Review of inverse Laplace transform algorithms for Laplace-space numerical approaches," *Numerical Algorithms*, vol. 63, no. 2, pp. 339–355, 2013.

[41] C. J. Bakker and J. Vriend, "Multi-exponential water proton spin-lattice relaxation in biological tissues and its implications for quantitative NMR imaging." *Physics in medicine and biology*, vol. 29, no. 5, pp. 509–18, 1984. [Online]. Available: http://www.ncbi.nlm.nih.gov/pubmed/6330769

[42] D. W. Marquardt, "An algorithm for least-squares estimation of nonlinear parameters," *Journal of the society for Industrial and Applied Mathematics*, vol. 11, no. 2, pp. 431–441, 1963.

[43] M. Musse, S. Quellec, M. M.-F. Devaux, M. Cambert, M. Lahaye, and F. Mariette, "An investigation of the structural aspects of the tomato fruit by means of quantitative nuclear magnetic resonance imaging." *Magnetic Resonance Imaging*, vol. 27, no. 5, pp. 709–19, Jun. 2009. [Online]. Available: http://www.ncbi.nlm.nih.gov/pubmed/19144488http://dx.doi.org/10.1016/j.mri.2008.11.005http://www.sciencedirect.com/science/article/pii/S0730725X08003676

[44] W. Windig and B. Antalek, "Direct exponential curve resolution algorithm (DECRA): A novel application of the generalized rank annihilation method for a single spectral mixture data set with exponentially decaying contribution profiles," *Chemometrics and Intelligent Laboratory Systems*, vol. 37, no. 2, pp. 241–254, Jun. 1997. [Online]. Available: http://linkinghub.elsevier.com/retrieve/pii/S0169743997000282

[45] H. T. Pedersen, R. Bro, and S. r. B. Engelsen, "Towards Rapid and Unique Curve Resolution of Low-Field NMR Relaxation Data: Trilinear SLICING versus Two-Dimensional Curve Fitting," *Journal of Magnetic*

Resonance, vol. 157, no. 1, pp. 141–155, Jul. 2002. [Online]. Available: http://linkinghub.elsevier.com/retrieve/pii/S109078070292570X

[46] P. Fantazzini, S. Mengoli, L. Pasquini, V. Bortolotti, L. Brizi, M. Mariani, M. Di Giosia, S. Fermani, B. Capaccioni, E. Caroselli, F. Prada, F. Zaccanti, O. Levy, Z. Dubinsky, J. A. Kaandorp, P. Konglerd, J. U. Hammel, Y. Dauphin, J.-P. Cuif, J. C. Weaver, K. E. Fabricius, W. Wagermaier, P. Fratzl, G. Falini, and S. Goffredo, "Gains and losses of coral skeletal porosity changes with ocean acidification acclimation." *Nature Communications*, vol. 6, no. October, p. 7785, 2015.

[47] P. Fantazzini and R. J. S. Brown, "Initially linear echo-spacing dependence of 1/T2 measurements in many porous media with pore-scale inhomogeneous fields," *Journal of Magnetic Resonance*, vol. 177, no. 2, pp. 228–235, 2005.

[48] C. Casieri, F. De Luca, and P. Fantazzini, "Pore-size evaluation by single-sided nuclear magnetic resonance measurements: Compensation of water self-diffusion effect on transverse relaxation," *Journal of Applied Physics*, vol. 97, no. 4, pp. 1–11, 2005.

[49] F. Z. Ribeiro, L. V. Marconcini, I. B. de Toledo, R. B. de Vasconcellos Azeredo, L. L. Barbosa, and L. A. Colnago, "Nuclear magnetic resonance water relaxation time changes in bananas during ripening: a new mechanism." *Journal of the Science of Food and Agriculture*, vol. 90, no. 12, pp. 2052–7, Sep. 2010. [Online]. Available: http://www.ncbi.nlm.nih.gov/pubmed/20586083

[50] J. H. Lee, C. Labadie, C. S. Springer, and G. S. Harbison, "Two-dimensional inverse Laplace transform NMR: altered relaxation times allow detection of exchange correlation," *Journal of the American Chemical Society*, vol. 115, no. 17, pp. 7761–7764, 1993. [Online]. Available: http://pubs.acs.org/doi/abs/10.1021/ja00070a022

[51] R. Lamanna, "On the inversion of multicomponent NMR relaxation and diffusion decays in heterogeneous systems," *Concepts in Magnetic Resonance Part A: Bridging Education and Research*, vol. 26, no. 2, pp. 78–90, 2005.

[52] V. Viti, E. Massaro, L. Guidon, and P. Barone, "The Use of the Maximum Entropy Method in NMR Spectroscopy," *Journal of Magnetic Resonance*, vol. 393, pp. 379–393, 1986.

[53] G. J. Daniell and P. J. Hore, "Maximum entropy and NMR - a new approach ," *Journal of Magnetic Resonance*, vol. 84, no. 3, pp. 515–536, 1989.

[54] J. H. Lee, C. Labadie, C. S. Springer Jr, and G. S. Harbison, "Two-dimensional inverse Laplace transform NMR: altered relaxation times allow detection of exchange correlation," *Journal of the American Chemical Society*, vol. 115, no. 17, pp. 7761–7764, 1993.

[55] L. Venturi and B. Hills, "Spatially resolved multidimensional cross-correlation relaxometry," *Magnetic Resonance Imaging*, vol. 28, no. 2, pp. 171–177, 2010.

[56] S. W. Provencher, "A constrained regularization method for inverting data represented by linear algebraic or integral equations," *Computer Physics Communications*, vol. 27, no. 3, pp. 213–227, 1982.

[57] ——, "Contin version 2. part 1: Users manual," pp. 1–62, 1984.

[58] B. Hills, A. Gravelle, K. Wright, N. Marigheto, and D. Hibberd, "Developing NMR probes of the microscopic water distribution in food," *http://iufost.edpsciences.org*, 2006. [Online]. Available: http://dx.doi.org/10.1051/IUFoST:20060597

[59] E. Miguez, M. I. B. Tavares, and C. Spinola, "The Use of Low-Field Solid-State NMR Relaxation to Study the Latex Extracted from Brosimum Parinarioides," in *Macromolecular Symposia*, vol. 299. Wiley Online Library, 2011, pp. 254–256.

[60] J. Bent, J. Lee, and T. Benson, "A T_2d TDNMR study of skin," *The Open-Access Journal for the Basic Principles of Diffusion Theory, Experiment and Application*, vol. 14, pp. 1–5, 2011.

[61] R. J. S. Brown, F. Capozzi, C. Cavani, M. A. Cremonini, M. Petracci, and G. Placucci, "Relationships between< sup> 1</sup> H NMR Relaxation Data and Some Technological Parameters of Meat: A Chemometric Approach," *Journal of Magnetic Resonance*, vol. 147, no. 1, pp. 89–94, 2000.

[62] Y.-Q. Song, L. Venkataramanan, M. D. Hürlimann, M. Flaum, P. Frulla, and C. Straley, "T_1-T_2 Correlation Spectra Obtained Using a Fast Two-Dimensional Laplace Inversion," *Journal of Magnetic Resonance*, vol. 154, no. 2, pp. 261–268, 2002.

[63] S. Ghosh, K. M. Keener, and Y. Pan, "A simulation based method to assess inversion algorithms for transverse relaxation data." *Journal of Magnetic Resonance (San Diego, Calif. : 1997)*, vol. 191, no. 2, pp. 226–30, Apr. 2008.

[64] C. Fotakis, D. Christodouleas, K. Kokkotou, M. Zervou, P. Zoumpoulakis, P. Moulos, M. Liouni, and A. Calokerinos, "NMR metabolite profiling of Greek grape marc spirits." *Food Chemistry*, vol. 138, no. 2-3, pp. 1837–46, Jun. 2013.

[65] M. Anastasiadi, A. Zira, P. Magiatis, S. A. Haroutounian, A. L. Skaltsounis, and E. Mikros, "H NMR-based metabonomics for the classification of Greek wines according to variety, region, and vintage. comparison with HPLC data," *Journal of Agricultural and Food Chemistry*, vol. 57, no. 23, pp. 11 067–11 074, dec 2009. [Online]. Available: http://www.ncbi.nlm.nih.gov/pubmed/19904930

[66] J. M. Ribó, J. Crusats, Z. El-Hachemi, M. Feliz, P. Sanchez-Bel, and F. Romojaro, "High-resolution NMR of irradiated almonds," *JAOCS, Journal of the American Oil Chemists' Society*, vol. 81, no. 11, pp. 1029–1033, 2004. [Online]. Available: http://www.scopus.com/inward/record.url?eid=2-s2.0-12744278788{&}partnerID=tZOtx3y1

[67] N. Marigheto, L. Venturi, and B. Hills, "Two-dimensional NMR relaxation studies of apple quality," *Postharvest Biology and Technology*, vol. 48, no. 3, pp. 331–340, Jun. 2008. [Online]. Available: http://linkinghub.elsevier.com/retrieve/pii/S0925521407003857

[68] V. T. Povlsen, A. . Rinnan, F. Van Den Berg, H. J. Andersen, and A. K. Thybo, "Direct decomposition of NMR relaxation profiles and prediction of sensory attributes of potato samples," *LWT - Food Science and Technology*, vol. 36, no. 4, pp. 423–432, 2003.

[69] M. Musse, M. Cambert, and F. Mariette, "NMR study of water distribution inside tomato cells: Effects of water stress," *Applied Magnetic Resonance*, vol. 38, no. 4, pp. 455–469, 2010.

[70] M. Bunzel and J. Ralph, "NMR characterization of lignins isolated from fruit and vegetable insoluble dietary fiber," *Journal of Agricultural and Food Chemistry*, vol. 54, no. 21, pp. 8352–8361, oct 2006. [Online]. Available: http://www.ncbi.nlm.nih.gov/pubmed/17032051

[71] E. Vigneau and F. Thomas, "Model calibration and feature selection for orange juice authentication by 1H NMR spectroscopy," *Chemometrics and Intelligent Laboratory Systems*, vol. 117, pp. 22–30, aug 2012. [Online]. Available: http://linkinghub.elsevier.com/retrieve/pii/S0169743911001080

[72] G. E. Pereira, J. P. Gaudillere, C. V. Leeuwen, G. Hilbert, M. Maucourt, C. Deborde, A. Moing, and D. Rolin, "1H NMR metabolite fingerprints of grape berry: Comparison of vintage and soil effects in Bordeaux grapevine growing areas," *Analytica Chimica Acta*, vol. 563, no. 1-2 SPEC. ISS., pp. 346–352, 2006.

[73] B. P. HILLS and C. J. Clark, "Quality Assessment of Horticultural Products by NMR," *Annual Reports on NMR Spectroscopy*, vol. 50, pp. 75–120, 2003.

[74] P. Barreiro, A. Moya, E. Correa, A. Peirs, K. M. Wright, and B. P. Hiils, "Prospects for the Rapid Detection of Mealiness in Apples by Nondestructive NMR Relaxometry," *Applied Magnetlc Resonance*, vol. 400, pp. 387–400, 2002.

[75] R. R. Ruan, P. L. Chen, and S. Almaer, "Nondestructive analysis of sweet corn maturity using NMR," *HortScience*, vol. 34, no. 2, pp. 319–321, 1999.

[76] A. K. Thybo, I. E. Bechmann, M. Martens, and S. B. Engelsen, "Prediction of Sensory Texture of Cooked Potatoes using Uniaxial Compression, Near Infrared Spectroscopy and Low Field ^{1}H NMR Spectroscopy," *LWT-Food Science and Technology*, vol. 33, no. 2, pp. 103–111, 2000.

[77] A. K. Thybo, H. J. Andersen, A. H. Karlsson, S. Donstrup, and H. Stodkilde-Jorgensen, "Low-field NMR relaxation and NMR-imaging as tools in differentiation between potato sample and determination of dry matter content in potatoes," *LWT-Food Science and Technology*, vol. 36, no. 3, pp. 315–322, 2003.

[78] A. K. Thybo, P. M. Szczypi'nski, A. H. Karlsson, S. Donstrup, H. S. Stodkilde-Jorgensen, and H. J. Andersen, "Prediction of sensory texture quality attributes of cooked potatoes by NMR-imaging (MRI) of raw potatoes in combination with different image analysis methods," *Journal of Food Engineering*, vol. 61, no. 1, pp. 91–100, Jan. 2004. [Online]. Available: http://linkinghub.elsevier.com/retrieve/pii/S0260877403001900

[79] B. Hills, A. Costa, N. Marigheto, and K. Wright, " T1-T 2 NMR Correlation Studies of High-Pressure-Processed Starch and Potato Tissue," *Applled Magnetic Resonance*, vol. 27, pp. 13–27, 2005.

[80] E. Miguez, M. I. B. Tavares, and C. Spinola, "The Use of Low-Field Solid-State NMR Relaxation to Study the Latex Extracted from Brosimum Parinarioides," *Macromolecular Symposia*, vol. 299-300, no. 1, pp. 254–256, Jan. 2011. [Online]. Available: http://doi.wiley.com/10.1002/masy.200900076

[81] B. Hills, S. Benamira, N. Marigheto, and K. Wright, "T1-T2 Correlation Analysis of Complex Foods," *Applled Magnetic Resonance*, vol. 560, pp. 543–560, 2004.

[82] S. S. Tu, Y. J. Choi, M. J. McCarthy, and K. L. McCarthy, "Tomato quality evaluation by peak force and NMR spin-spin relaxation time," *Postharvest Biology and Technology*, vol. 44, no. 2, pp. 157–164, 2007.

[83] A. Raffo, R. Gianferri, R. Barbieri, and E. Brosio, "Ripening of banana fruit monitored by water relaxation and diffusion 1H-NMR measurements," *Food Chemistry*, vol. 89, no. 1, pp. 149–158, jan 2005. [Online]. Available: http://linkinghub.elsevier.com/retrieve/pii/S0308814604001888

[84] V. Beaten and P. J. A. Fernandez, "Spectroscopy and chemometrics training," November 2016.

[85] M. Blanco, "Influence of temperature on the predictive ability of near infrared spectroscopy models," *J. Near Infrared Spectroscopy*, vol. 126, pp. 121–126, 2004.

[86] B. M. Nicolaï, K. Beullens, E. Bobelyn, A. Peirs, W. Saeys, K. I. Theron, and J. Lammertyn, "Nondestructive measurement of fruit and vegetable quality by means of NIR spectroscopy: A review," *Postharvest Biology and Technology*, vol. 46, pp. 99–118, 2007.

[87] J. J. Workman JR, P. R. Mobley, B. R. Kowalski, and R. Bro, "Review of chemometrics applied to spectroscopy: 1985-95, part i," *Applied Spectroscopy Reviews*, vol. 31, no. 1-2, pp. 73–124, 1996.

[88] B. R. Kowalski, *Chemometrics: Mathematics and Statistics in Chemistry*. Springer Science & Business Media, 2013, vol. 138.

[89] E. Stella, R. Moscetti, R. P. Haff, D. Monarca, M. Cecchini, M. Contini, and R. Massantini, "Review: Recent advances in the use of non-destructive near infrared spectroscopy for intact olive fruits," *Journal of Near Infrared Spectroscopy*, vol. 23, no. 4, pp. 197–208, 2015.

[90] R. Guidetti, R. Beghi, and L. Bodria, "EVALUATION OF GRAPE QUALITY PARAMETERS BY A SIMPLE VIS/NIR SYSTEM," *Transactions of the ASABE*, vol. 53, no. 2, pp. 1–8, 2010.

[91] A. J. Daniels, "Development of infrared spectroscopic methods to assess table grape quality," Master's thesis, 2013. [Online]. Available: http://scholar.sun.ac.za/handle/10019.1/80369

[92] A. Kurenda, A. Zdunek, O. Schlüter, and W. B. Herppich, "VIS/NIR spectroscopy, chlorophyll fluorescence, biospeckle and backscattering to evaluate changes in apples subjected to hydrostatic pressures," *Postharvest Biology and Technology*, vol. 96, no. 2014, pp. 88–98, 2014. [Online]. Available: http://dx.doi.org/10.1016/j.postharvbio.2014.05.009

[93] L. S. Magwaza, U. L. Opara, L. A. Terry, S. Landahl, P. J. Cronje, H. Nieuwoudt, A. M. Mouazen, W. Saeys, and B. M. Nicolaï, "Prediction of 'Nules Clementine' mandarin susceptibility to rind breakdown disorder using Vis/NIR spectroscopy," *Postharvest Biology and Technology*, vol. 74, no. 2012, pp. 1–10, 2012. [Online]. Available: http://dx.doi.org/10.1016/j.postharvbio.2012.06.007

[94] K. Yu, Y. Zhao, X. Li, Y. Shao, F. Zhu, and Y. He, "Identification of crack features in fresh jujube using Vis/NIR hyperspectral imaging combined with image processing," *Computers and Electronics in Agriculture*, vol. 103, no. 2014, pp. 1–10, 2014. [Online]. Available: http://dx.doi.org/10.1016/j.compag.2014.01.016

[95] J. C. Tewari, V. Dixit, B. K. Cho, and K. a. Malik, "Determination of origin and sugars of citrus fruits using genetic algorithm, correspondence analysis and partial least square combined with fiber optic NIR spectroscopy," *Spectrochimica Acta - Part A: Molecular and Biomolecular Spectroscopy*, vol. 71, no. 2008, pp. 1119–1127, 2008.

[96] L. S. Magwaza, U. L. Opara, P. J. R. Cronje, S. Landahl, and L. a. Terry, "Canopy position affects rind biochemical profile of 'Nules Clementine' mandarin fruit during postharvest storage," *Postharvest Biology and Technology*, vol. 86, pp. 300–308, 2013. [Online]. Available: http://dx.doi.org/10.1016/j.postharvbio.2013.07.029

[97] B. M. Nicolaï, K. Beullens, E. Bobelyn, A. Peirs, W. Saeys, K. I. Theron, and J. Lammertyn, "Nondestructive measurement of fruit and vegetable quality by means of NIR spectroscopy: A review," *Postharvest Biology and Technology*, vol. 46, pp. 99–118, 2007.

[98] L. S. Magwaza, U. L. Opara, H. Nieuwoudt, P. J. R. Cronje, W. Saeys, and B. Nicolaï, "NIR Spectroscopy Applications for Internal and External Quality Analysis of Citrus Fruit-A Review," *Food and Bioprocess Technology*, vol. 5, no. 2012, pp. 425–444, 2012.

[99] R. Moscetti, R. P. Haff, E. Stella, M. Contini, D. Monarca, M. Cecchini, and R. Massantini, "Feasibility of NIR spectroscopy to detect olive fruit infested by Bactrocera oleae," *Postharvest Biology and Technology*, vol. 99, no. 2015, pp. 58–62, 2015. [Online]. Available: http://linkinghub.elsevier.com/retrieve/pii/S092552141400221X

[100] F. Jiménez-Jiménez, S. Castro-García, G. L. Blanco-Roldán, J. Agüera-Vega, and J. a. Gil-Ribes, "Non-destructive determination of impact bruising on table olives using Vis-NIR spectroscopy," *Biosystems Engineering*, vol. 113, no. 4, pp. 371–378, 2012.

[101] T. Ignat, Z. Schmilovitch, J. Fefoldi, B. Steiner, and S. Alkalai-tuvia, "Postharvest Biology and Technology Non-destructive measurement of ascorbic acid content in bell peppers by VIS-NIR and SWIR spectrometry," *Postharvest Biology and Technology*, vol. 74, pp. 91–99, 2012. [Online]. Available: http://dx.doi.org/10.1016/j.postharvbio.2012.06.010

[102] L. S. Magwaza, U. L. Opara, L. a. Terry, S. Landahl, P. J. R. Cronje, H. H. Nieuwoudt, A. Hanssens, W. Saeys, and B. M. Nicolaï, "Evaluation of Fourier transform-NIR spectroscopy for integrated external and internal quality assessment of Valencia oranges," *Journal of Food Composition and Analysis*, vol. 31, no. 2013, pp. 144–154, 2013.

[103] L. Xue, J. Cai, J. Li, and M. Liu, "Application of particle swarm optimization (PSO) algorithm to determine dichlorvos residue on the surface of navel orange with Vis-NIR spectroscopy," *Procedia Engineering*, vol. 29, pp. 4124–4128, 2012. [Online]. Available: http://dx.doi.org/10.1016/j.proeng.2012.01.631

[104] S. Kawano, "Development of a common calibration model for determining the Brix value of intact apple, pear and persimmon fruits by near infrared spectroscopy," *Journal of Near Infrared Spectroscopy*, vol. 22, no. August, p. 367, 2014. [Online]. Available: http://www.impublications.com/content/abstract?code=J22_0367

[105] A. s. Rinnan, F. V. D. Berg, and S. r. B. Engelsen, "Review of the most common pre-processing techniques for near-infrared spectra," *TrAC Trends in Analytical Chemistry*, vol. 28, no. 10, pp. 1201–1222, 2009. [Online]. Available: http://linkinghub.elsevier.com/retrieve/pii/S0165993609001629

[106] T. Mehmood, K. H. Liland, L. Snipen, and S. Sæbø, "A review of variable selection methods in partial least squares regression," *Chemometrics and Intelligent Laboratory Systems*, vol. 118, pp. 62–69, 2012.

[107] R. Leardi, *Genetic algorithms in feature selection*. Academic Press: London, 1996.

[108] D. A. Coley, *An introduction to genetic algorithms for scientists and engineers*. World scientific Singapore, 1999, vol. 1655.

[109] Y.-L. Wu, C.-Y. Tang, M.-K. Hor, and P.-F. Wu, "Feature selection using genetic algorithm and cluster validation," *Expert Systems with Applications*, vol. 38, no. 3, pp. 2727–2732, 2011. [Online]. Available: http://dx.doi.org/10.1016/j.eswa.2010.08.062

[110] A. Durand, O. Devos, C. Ruckebusch, and J. P. Huvenne, "Genetic algorithm optimisation combined with partial least squares regression and mutual information variable selection procedures in near-infrared quantitative analysis of cotton-viscose textiles," *Analytica Chimica Acta*, vol. 595, pp. 72–79, 2007.

[111] X. Zou, Y. Li, and J. Zhao, "Using genetic algorithm interval partial least squares selection of the optimal near infrared wavelength regions for determination of the soluble solids content of "Fuji" apple," *Journal of Near Infrared Spectroscopy*, vol. 15, no. 3, pp. 153–159, 2007.

[112] L. Cséfalvayová, M. Pelikan, I. Kralj Cigić, J. Kolar, and M. Strli, "Use of genetic algorithms with multivariate regression for determination of gelatine in historic papers based on FT-IR and NIR spectral data," *Talanta*, vol. 82, no. 2010, pp. 1784–1790, 2010.

[113] R. Leardi, "Leardi - Genetic algorithms applied to feature selection in PLS regression how and when to use them - 1998.pdf," *Chemometrics and Intelligent Laboratory Systems*, 1998.

[114] R. Leardi and R. Leardi, "Application of genetic algorithm - PLS for feature selection in spectral data sets," *Journal of Chemometrics*, no. March, pp. 643–655, 2000.

[115] B. Shi, B. Ji, D. Zhu, Z. Tu, and Z. Qing, "Study on genetic algorithms-based NIR wavelength selection for determination of soluble solids content in fuji apples," *Journal of Food Quality*, vol. 31, pp. 232–249, 2008.

[116] X. Zou, Y. Li, and J. Zhao, "Using genetic algorithm interval partial least squares selection of the optimal near infrared wavelength regions for determination of the soluble solids content of "Fuji" apple," *Journal of Near Infrared Spectroscopy*, vol. 15, no. 3, pp. 153–159, 2007.

[117] Y. Ying and Y. Liu, "Nondestructive measurement of internal quality in pear using genetic algorithms and FT-NIR spectroscopy," *Journal of Food Engineering*, vol. 84, no. 2008, pp. 206–213, 2008.

[118] M. Valente, R. Leardi, G. Self, G. Luciano, and J. P. Pain, "Multivariate calibration of mango firmness using vis/NIR spectroscopy and acoustic impulse method," *Journal of Food Engineering*, vol. 94, no. 1, pp. 7–13, 2009. [Online]. Available: http://dx.doi.org/10.1016/j.jfoodeng.2009.02.020

[119] B. K. Lavine, N. Mirjankar, and S. Delwiche, "Classification of the waxy condition of durum wheat by near infrared reflectance spectroscopy using wavelets and a genetic algorithm," *Microchemical Journal*, vol. 117, pp. 178–182, 2014. [Online]. Available: http://dx.doi.org/10.1016/j.microc.2014.06.030

[120] H. Lin, J. Zhao, L. Sun, Q. Chen, and F. Zhou, "Freshness measurement of eggs using near infrared (NIR) spectroscopy and multivariate data analysis," *Innovative Food Science & Emerging Technologies*, vol. 12, no. 2, pp. 182–186, 2011. [Online]. Available: http://dx.doi.org/10.1016/j.ifset.2011.01.008

[121] M. Ghasemi-Varnamkhasti and M. Forina, "NIR spectroscopy coupled with multivariate computational tools for qualitative characterization of the aging of beer," *Computers and Electronics in Agriculture*, vol. 100, no. 2014, pp. 34–40, 2014. [Online]. Available: http://dx.doi.org/10.1016/j.compag.2013.10.001

[122] M. Ferrand, B. Huquet, S. Barbey, F. Barillet, F. Faucon, H. Larroque, O. Leray, J. M. Trommenschlager, and M. Brochard, "Determination of fatty acid profile in cow's milk using mid-infrared spectrometry: Interest of applying a variable selection by genetic algorithms before a PLS regression," *Chemometrics and Intelligent Laboratory Systems*, vol. 106, no. 2, pp. 183–189, 2011. [Online]. Available: http://dx.doi.org/10.1016/j.chemolab.2010.05.004

[123] A. Yalçin, D. Ergün, O. I. Uçar, and D. Özdemir, "Determination of aluminum rolling oil additives and contaminants using infrared spectroscopy coupled with genetic algorithm based multivariate calibration," *Vibrational Spectroscopy*, vol. 54, no. 2010, pp. 10–20, 2010.

[124] R. Leardl and L. Norgaard, "Sequential application of backward interval partial least squares and genetic algorithms for the selection of relevant spectral regions," *Journal of Chemometrics*, vol. 18, pp. 486–497, 2004.

[125] Y. Wang and B. Xiang, "Radial basis function network calibration model for near-infrared spectra in wavelet domain using a genetic algorithm," *Analytica Chimica Acta*, vol. 602, pp. 55–65, 2007.

[126] G. N. Elliott, H. Worgan, D. Broadhurst, J. Draper, and J. Scullion, "Soil differentiation using fingerprint Fourier transform infrared spectroscopy, chemometrics and genetic algorithm-based feature selection," *Soil Biology and Biochemistry*, vol. 39, no. 2007, pp. 2888–2896, 2007.

[127] Q. Fei, M. Li, B. Wang, Y. Huan, G. Feng, and Y. Ren, "Analysis of cefalexin with NIR spectrometry coupled to artificial neural networks with modified genetic algorithm for wavelength selection," *Chemometrics and Intelligent Laboratory Systems*, vol. 97, no. 2, pp. 127–131, 2009. [Online]. Available: http://dx.doi.org/10.1016/j.chemolab.2009.03.003

[128] M. Soltani, R. Alimardani, and M. Omid, "Evaluating banana ripening status from measuring dielectric properties," *Journal of Food Engineering*, vol. 105, no. 4, pp. 625–631, Aug. 2011. [Online]. Available: http://linkinghub.elsevier.com/retrieve/pii/S0260877411001786

[129] S. Yang, K. Lin, J. Chieh, C. Yang, and H. Horng, "Step-Edge High- T_c SQUID Magnetometer for Low-Field NMR Detection," *IEEE Transactions on Applied Superconductivity*, vol. 21, no. 3, pp. 534–537, 2011.

[130] G. C. Borgia, R. J. Brown, and P. Fantazzini, "Uniform-penalty inversion of multiexponential decay data. II. Data spacing, T(2) data, systemic data errors, and diagnostics." *Journal of Magnetic Resonance (San Diego, Calif. : 1997)*, vol. 147, no. 2, pp. 273–85, Dec. 2000. [Online]. Available: http://www.ncbi.nlm.nih.gov/pubmed/11097819

[131] P. B. Pathare, U. L. Opara, and F. A.-J. Al-Said, "Colour Measurement and Analysis in Fresh and Processed Foods: A Review," *Food and Bioprocess Technology*, vol. 6, no. 1, pp. 36–60, May 2012. [Online]. Available: http://link.springer.com/10.1007/s11947-012-0867-9

[132] A. Patras, N. P. Brunton, B. K. Tiwari, and F. Butler, "Stability and Degradation Kinetics of Bioactive Compounds and Colour in Strawberry Jam during Storage," *Food and Bioprocess Technology*, vol. 4, no. 7, pp.

1245–1252, Jul. 2009. [Online]. Available: http://link.springer.com/10.1007/s11947-009-0226-7

[133] J. M. Miller and J. C. Miller, *Statistics and Chemometrics for Analytical Chemistry*. Pearson Education Limited, 2010.

[134] I. T. Jolliffe, *Principal Component Analysis, Second Edition*. Springer Series in Statistics, 2002, vol. 30, no. 3. [Online]. Available: http://onlinelibrary.wiley.com/doi/10.1002/0470013192.bsa501/full

[135] S. Wold, K. Esbensen, and P. Geladi, "Principal component analysis," *Chemometrics and Intelligent Laboratory Systems*, vol. 2, no. 1-3, pp. 37–52, Aug. 1987. [Online]. Available: http://linkinghub.elsevier.com/retrieve/pii/0169743987800849

[136] S. Wold, M. Sjöström, and L. Eriksson, "PLS-regression: A basic tool of chemometrics," *Chemometrics and Intelligent Laboratory Systems*, vol. 58, no. 2, pp. 109–130, 2001.

[137] L. U. Opara, "Bruise susceptibilities of 'Gala' apples as affected by orchard management practices and harvest date," *Postharvest Biology and Technology*, vol. 43, no. 1, pp. 47–54, 2007.

[138] U. L. Opara and P. B. Pathare, "Bruise damage measurement and analysis of fresh horticultural produce-A review," *Postharvest Biology and Technology*, vol. 91, no. 2014, pp. 9–24, 2014. [Online]. Available: http://dx.doi.org/10.1016/j.postharvbio.2013.12.009

[139] N. H. Banks and M. Joseph, "Factors affecting resistance of banana fruit to compression and impact bruising," *Journal of the Science of Food and Agriculture*, vol. 56, no. 3, pp. 315–323, 1991. [Online]. Available: http://doi.wiley.com/10.1002/jsfa.2740560307

[140] X. Luo, T. Takahashi, K. Kyo, and S. Zhang, "Wavelength selection in vis/NIR spectra for detection of bruises on apples by ROC analysis," *Journal of Food Engineering*, vol. 109, no. 3, pp. 457–466, 2012. [Online]. Available: http://dx.doi.org/10.1016/j.jfoodeng.2011.10.035

[141] S. Wold, E. Johansson, and M. Cocchi, "Pls-partial least squares projections to latent structures," *3D QSAR in Drug Design*, vol. 1, pp. 523–550, 1993.

[142] I.-G. Chong and C.-H. Jun, "Performance of some variable selection methods when multicollinearity is present," *Chemometrics and Intelligent Laboratory Systems*, vol. 78, no. 1, pp. 103–112, 2005.

[143] R. Gosselin, D. Rodrigue, and C. Duchesne, "A bootstrap-vip approach for selecting wavelength intervals in spectral imaging applications," *Chemometrics and Intelligent Laboratory Systems*, vol. 100, no. 1, pp. 12–21, 2010.

[144] G. ElMasry, N. Wang, C. Vigneault, J. Qiao, and A. ElSayed, "Early detection of apple bruises on different background colors using hyperspectral imaging," *LWT - Food Science and Technology*, vol. 41, no. 2, pp. 337–345, 2008.

[145] N. Wang and G. ElMasry, "Bruise Detection of Apples using Hyperspectral Imaging," in *Hyperspectral Imaging for Food Quality Analysis and Control*, 2010, pp. 295–320.

[146] J. Ghasemi, A. Niazi, and R. Leardi, "Genetic-algorithm-based wavelength selection in multicomponent spectrophotometric determination by pls: application on copper and zinc mixture," *Talanta*, vol. 59, no. 2, pp. 311–317, 2003.

[147] C. Y. Liew and C. Y. Lau, "Determination of quality parameters in Cavendish banana during ripening by NIR spectroscopy," *International Food Research Journal*, vol. 19, no. 2, pp. 751–758, 2012.

[148] H. W. Von Loesecke, *Bananas: chemistry, physiology and technology*. New York: Interscience Publishers, 1950.

[149] P. S. Belton and B. P. Hills, "The effects of diffusive exchange in heterogeneous systems on {N}.{M}.{R}. line shapes and relaxation processes," *Molecular Physics*, no. 4, pp. 999–1018, 1987.

[150] F. Z. Ribeiro, L. V. Marconcini, I. B. de Toledo, R. B. de Vasconcellos Azeredo, L. L. Barbosa, and L. A. Colnago, "Nuclear magnetic resonance water relaxation time changes in bananas during ripening: a new mechanism." *Journal of the Science of Food and Agriculture*, vol. 90, no. 12, pp. 2052–7, Sep. 2010. [Online]. Available: http://www.ncbi.nlm.nih.gov/pubmed/20586083

[151] A. Bellincontro, I. Nicoletti, M. Valentini, A. Tomas, D. D. Santis, D. Corradini, and F. Mencarelli, "Integration of Nondestructive Techniques with Destructive Analyses to Study Postharvest Water Stress of Winegrapes," *American Journal of Enology and Viticulture*, vol. 1, 2009.

[152] J. S. Wulf, M. Geyer, M. Zude, and B. Nicolaï, "Non-destructive assessment of pigments in apple fruit and carrot by laser-induced fluorescence spectroscopy (LIFS) measured at different time-gate positions," *Acta Horticulturae*, vol. 682, pp. 1387–1394, 2005.

[153] P. E. Zerbini, M. Vanoli, M. Grassi, a. Rizzolo, M. Fibiani, R. Cubeddu, a. Pifferi, L. Spinelli, and a. Torricelli, "A model for the softening of nectarines based on sorting fruit at harvest by time-resolved reflectance spectroscopy," *Postharvest Biology and Technology*, vol. 39, no. 3, pp. 223–232, Mar. 2006. [Online]. Available: http://linkinghub.elsevier.com/retrieve/pii/S092552140500222X

[154] D. Barbon, A. Weber, M. Vescovi, A. Tonini, A. Boschetti, S. Iannotta, L. Fadanelli, and G. Stoppa, "A statistical approach for Proton Transfer Reaction Mass Spectrometry (PTR-MS) data aimed at a qualification of fruits based on VOC emissions," *Acta Horticulturae*, vol. 682, pp. 1497–1504, 2005. [Online]. Available: http://cat.inist.fr/?aModele=afficheN{&}cpsidt=17670876

[155] D. Pérez-Marín, M.-T. Sánchez, P. Paz, M.-A. Soriano, J.-E. Guerrero, and A. Garrido-Varo, "Non-destructive determination of quality parameters in nectarines during on-tree ripening and postharvest storage," *Postharvest Biology and Technology*, vol. 52, no. 2, pp. 180–188, May 2009. [Online]. Available: http://linkinghub.elsevier.com/retrieve/pii/S0925521408002858

[156] S. G. Kulkarni, V. B. Kudachikar, and M. N. Keshava Prakash, "Studies on physico-chemical changes during artificial ripening of banana (musa sp) variety "robusta"," *Journal of Food Science and Technology*, vol. 48, no. 6, pp. 730 – 734, 2011.

[157] P. Jaiswal, S. N. Jha, P. P. Kaur, R. Bhardwaj, A. K. Singh, and V. Wadhawan, "Prediction of textural attributes using color values of banana (Musa sapientum) during ripening," *Journal of Food Science and Technology*, vol. 51, no. 6, pp. 1179–1184, 2014.

[158] M. E. Bailey, "Studies on the Banana - I," *J. Biol. Chem.*, vol. 1, no. 4, 1906.

[159] Y. Geya, T. Kimura, H. Fujisaki, Y. Terada, K. Kose, T. Haishi, H. Gemma, and Y. Sekozawa, "Longitudinal NMR parameter measurements of Japanese pear fruit during the growing process using a mobile magnetic resonance imaging system." *Journal of Magnetic Resonance (San Diego, Calif.:1997)*, vol. 226, pp. 45–51, Jan. 2013.

[160] L. Brizi, G. Castellani, P. Fantazzini, M. Mariani, D. Remondini, and I. Zironi, "Water compartmentalization, cell viability and morphology changes monitored under stress by ^{1}H-NMR relaxometry and phase contrast optical microscopy," *Journal of Physics D: Applied Physics*, vol. 48, no. 41, p. 415401, 2015.

[161] G. C. Borgia, R. J. Brown, and P. Fantazzini, "Uniform-penalty inversion of multiexponential decay data." *Journal of Magnetic Resonance (San Diego, Calif. : 1997)*, vol. 132, no. 1, pp. 65–77, May 1998. [Online]. Available: http://www.ncbi.nlm.nih.gov/pubmed/11097819

[162] V. Bortolotti, R. J. S. Brown, and P. Fantazzini, "UpenWin: a software to invert multi-exponential relaxation decay data," 2010.

[163] P. Barone, A. Ramponi, and G. Sebastiani, "On the numerical inversion of the Laplace transform for nuclear magnetic resonance relaxometry," *Inverse Problems*, vol. 17, no. 1, pp. 77–94, 2001.

[164] P. Fantazzini and R. J. S. Brown, "Units in distributions of relaxation times," *Concepts in Magnetic Resonance Part A: Bridging Education and Research*, vol. 27, no. 2, pp. 122–123, 2005.

[165] T. Fearn, "Standardisation and calibration transfer for near infrared instruments: a review," *J. Near Infrared Spectrosc*, vol. 9, no. 4, pp. 229–244, 2001.

[166] R. N. Feudale, N. A. Woody, H. Tan, A. J. Myles, S. D. Brown, and J. Ferré, "Transfer of multivariate calibration models: a review," *Chemometrics and Intelligent Laboratory Systems*, vol. 64, no. 2, pp. 181–192, 2002.

[167] E.-L. Bergman, H. Brage, M. Josefson, O. Svensson, and A. Sparén, "Transfer of NIR calibrations for pharmaceutical formulations between different instruments," *Journal of Pharmaceutical and Biomedical Analysis*, vol. 41, no. 1, pp. 89–98, 2006.

[168] C. V. Greensill and K. B. Walsh, "Calibration transfer between miniature photodiode array-based spectrometers in the near infrared assessment of mandarin soluble solids content," *Journal of Near Infrared Spectroscopy*, vol. 10, no. 1, pp. 27–36, 2002.

[169] R. N. Feudale, H. Tan, and S. D. Brown, "Piecewise orthogonal signal correction," *Chemometrics and Intelligent Laboratory Systems*, vol. 63, no. 2, pp. 129–138, 2002.

[170] H. Swierenga, P. De Groot, A. De Weijer, M. Derksen, and L. Buydens, "Improvement of pls model transferability by robust wavelength selection," *Chemometrics and Intelligent Laboratory Systems*, vol. 41, no. 2, pp. 237–248, 1998.

[171] P. Tillmann, T.-C. Reinhardt, and C. Paul, "Networking of near infrared spectroscopy instruments for rapeseed analysis: a comparison of different procedures," *Journal of Near Infrared Spectroscopy*, vol. 8, no. 2, pp. 101–108, 2000.

[172] C. Camps, P. Guillermin, J. C. Mauget, and D. Bertrand, "Discrimination of storage duration of apples stored in a cooled room and shelf-life by visible-near infrared spectroscopy," *Journal of Near Infrared Spectroscopy*, vol. 15, no. 3, pp. 169–177, 2007.

[173] E. Bobelyn, A.-S. Serban, M. Nicu, J. Lammertyn, B. M. Nicolai, and W. Saeys, "Postharvest quality of apple predicted by NIR-spectroscopy: Study of the effect of biological variability on spectra and model performance," *Postharvest Biology and Technology*, vol. 55, no. 3, pp. 133–143, Mar. 2010. [Online]. Available: http://linkinghub.elsevier.com/retrieve/pii/S0925521409002154

[174] L. S. Magwaza, "Non-destructive prediction and monitoring of postharvest quality of citrus fruit," Ph.D. dissertation, Stellenbosch University, 2013.

[175] L. S. Magwaza, H. D. Ford, P. J. R. Cronje, U. L. Opara, S. Landahl, R. P. Tatam, and L. a. Terry, "Application of optical coherence tomography to non-destructively characterise rind breakdown disorder of 'Nules Clementine' mandarins," *Postharvest Biology and Technology*, vol. 84, no. 2013, pp. 16–21, 2013. [Online]. Available: http://dx.doi.org/10.1016/j.postharvbio.2013.03.019

[176] J. Xing, C. Bravo, D. Moshou, H. Ramon, and J. De Baerdemaeker, "Bruise detection on 'Golden Delicious' apples by vis/NIR spectroscopy," *Computers and Electronics in Agriculture*, vol. 52, no. 1-2, pp. 11–20, 2006.

[177] S. Zarifneshat, H. R. Ghassemzadeh, M. Sadeghi, M. Abbaspour-Fard, a. E. Hossein, A. Javadi, and M. Shervani-Tabar, "Effect of impact level and fruit properties on 'Golden Delicious' apple bruising," *American Journal of Agricultural and Biological Science*, vol. 5, no. 2, pp. 114–121, 2010.

[178] S. Bosman, "Study of impact of fresh fruit bunch (ffb) of palm fruits on different surfaces," *Jurnaltin*, vol. 21, pp. 91–101, 2012.

[179] V. Van linden, D. N. Sila, T. Duvetter, J. De Baerdemaeker, and M. Hendrickx, "Effect of mechanical impact-bruising on polygalacturonase and pectinmethylesterase activity and pectic cell wall components in tomato fruit," *Postharvest Biology and Technology*, vol. 47, no. 1, pp. 98–106, 2008.

[180] V. Rostampour, A. M. Motlagh, M. H. Komarizadeh, M. Sadeghi, I. Bernousi, and T. Ghanbari, "Using Artificial Neural Network (ANN) technique for prediction of apple bruise damage," *Australian Journal of Crop Sience*, vol. 7, no. 10, pp. 1442–1448, 2013.

[181] S. Zarifneshat, A. Rohani, H. R. Ghassemzadeh, M. Sadeghi, E. Ahmadi, and M. Zarifneshat, "Predictions of apple bruise volume using artificial neural network," *Computers and Electronics in Agriculture*, vol. 82, no. 2012, pp. 75–86, 2012. [Online]. Available: http://dx.doi.org/10.1016/j.compag.2011.12.015

[182] B. Upchurch, H. Affeldt, W. Hruschka, K. Nonis, and J. Throop, "Spectrophotometric study of bruises on whole,'red delicious'apples," *Transactions of the ASAE*, vol. 33, no. 2, pp. 585–0589, 1990.

[183] F. Geoola, F. Geoola, and U. Peiper, "A Spectrophotometric Method for Detecting Surface Bruises on "Golden Delicious" Apples," *Journal of Agricultural Engineering Research*, vol. 58, no. 1, pp. 47–51, 1994.

[184] D. Aneshansley, J. Throop, and B. Upchurch, "Reflectance spectra of surface defects on apples," in *Proceedings of the Sensors for Nondestructive Testing International Conference, Northeast Regional Agricultural Engineering Service*, 1997, pp. 143–160.

[185] M. Keskin, R. Dodd, Y. Han, and A. Khalilian, "Assessing nitrogen content of golf course turfgrass clippings using spectral reflectance," *Applied Engineering in Agriculture*, vol. 20, no. 6, p. 851, 2004.

[186] Y. Liu, W. R. Windham, K. C. Lawrence, and B. Park, "Simple algorithms for the classification of visible/near-infrared and hyperspectral imaging spectra of chicken skins, feces, and fecal contaminated skins," *Applied Spectroscopy*, vol. 57, no. 12, pp. 1609–1612, 2003.

[187] J. Xing, C. Bravo, P. T. Jancsók, H. Ramon, and J. De Baerdemaeker, "Detecting bruises on 'Golden Delicious' apples using hyperspectral imaging with multiple wavebands," *Biosystems Engineering*, vol. 90, no. 1, pp. 27–36, 2005.

[188] W. R. Hruschka, "Data analysis: wavelength selection methods," *Near-infrared technology in the Agricultural and Food Industries*, vol. 2, 1987.

[189] J. Xing, S. Landahl, J. Lammertyn, E. Vrindts, and J. De Baerdemaeker, "Effects of bruise type on discrimination of bruised and non-bruised 'Golden Delicious' apples by VIS/NIR spectroscopy," *Postharvest Biology and Technology*, vol. 30, no. 3, pp. 249–258, 2003.

[190] M. Golic, K. Walsh, and P. Lawson, "Short-wavelength near-infrared spectra of sucrose, glucose, and fructose with respect to sugar concentration and temperature," *Applied Spectroscopy*, vol. 57, no. 2, pp. 139–145, 2003.

[191] M. Van Zeebroeck, V. Van linden, P. Darius, B. De Ketelaere, H. Ramon, and E. Tijskens, "The effect of fruit factors on the bruise susceptibility of apples," *Postharvest Biology and Technology*, vol. 46, no. 1, pp. 10–19, 2007.

[192] Z. Wen and Y. Tao, "Fuzzy-based determination of model and parameters of dual-wavelength vision system for on-line apple sorting," *Optical Engineering*, vol. 37, no. 1, pp. 293–299, 1998.

[193] W. M. Miller, J. A. Throop, and B. L. Upchurch, "Pattern recognition models for spectral reflectance evaluation of apple blemishes," *Postharvest Biology and Technology*, vol. 14, no. 1, pp. 11–20, 1998.

[194] O. Kleynen, "Selection of the most efficient wavelength bands for 'Jonagold' apple sorting," *Postharvest Biology and Technology*, vol. 30, no. 3, pp. 221–232, 2003.

[195] J. Lammertyn, A. Peirs, J. De Baerdemaeker, and B. Nicolaï, "Light penetration properties of NIR radiation in fruit with respect to non-destructive quality assessment," *Postharvest Biology and Technology*, vol. 18, no. 2, pp. 121–132, 2000.

[196] L. Zhang and M. J. McCarthy, "Measurement and evaluation ofo tomato maturity using magnetic resonance imaging," *Postharvest Biology and Technology*, vol. 67, pp. 37–43, 2012.

[197] J. B. Moody and Y. Xia, "Analysis of multi-exponential relaxation data with very short components using linear regularization." *Journal of Magnetic Resonance (San Diego, Calif.:1997)*, vol. 167, no. 1, pp. 36–41, Mar. 2004. [Online]. Available: http://www.ncbi.nlm.nih.gov/pubmed/14987596

[198] Y.-Q. Song, "Recent Progress of Nuclear Magnetic Resonance Applications in Sandstones and Carbonate Rocks," *Vadose Zone Journal*, vol. 9, no. 4, p. 828, 2010. [Online]. Available: https://www.soils.org/publications/vzj/abstracts/9/4/828

[199] L. Zhang and M. J. McCarthy, "Measurement and evaluation of tomato maturity using magnetic resonance imaging," *Postharvest Biology and Technology*, vol. 67, pp. 37–43, May 2012. [Online]. Available: http://linkinghub.elsevier.com/retrieve/pii/S0925521411002912

[200] W. Huang, J. Li, Q. Wang, and L. Chen, "Development of a multispectral imaging system for online detection of bruises on apples," *Journal of Food Engineering*, vol. 146, no. 2015, pp. 62–71, 2015. [Online]. Available: http://dx.doi.org/10.1016/j.jfoodeng.2014.09.002

[201] B. M. Nicolaï, K. Beullens, E. Bobelyn, A. Peirs, W. Saeys, K. I. Theron, and J. Lammertyn, "Nondestructive measurement of fruit and vegetable quality by means of NIR spectroscopy: A review," *Postharvest Biology and Technology*, vol. 46, pp. 99–118, 2007.

[202] L. Samukelo, S. Landahl, P. J. R. Cronje, H. H. Nieuwoudt, A. Mounem, B. M. Nicolaï, L. A. Terry, and U. Linus, "The use of VisNIRS and chemometric analysis to predict fruit defects and postharvest behaviour of 'Nules Clementine' mandarin fruit," *Food Chemistry*, vol. 163, pp. 267–274, 2014.

[203] O. Devos and L. Duponchel, "Parallel genetic algorithm co-optimization of spectral pre-processing and wavelength selection for PLS regression," *Chemometrics and Intelligent Laboratory Systems*, vol. 107, no. 1, pp. 50–58, 2011. [Online]. Available: http://linkinghub.elsevier.com/retrieve/pii/S0169743911000116

[204] Z. Li and C. Thomas, "Quantitative evaluation of mechanical damage to fresh fruits," *Trends in Food Science & Technology*, vol. 35, no. 2, pp. 138–150, 2014.

[205] P. Butz, C. Hofmann, and B. Tauscher, "Recent developments in noninvasive techniques for fresh fruit and vegetable internal quality analysis," *Journal of Food Science*, vol. 70, no. 9, pp. 131–141, 2005.

Appendix A: Additional information

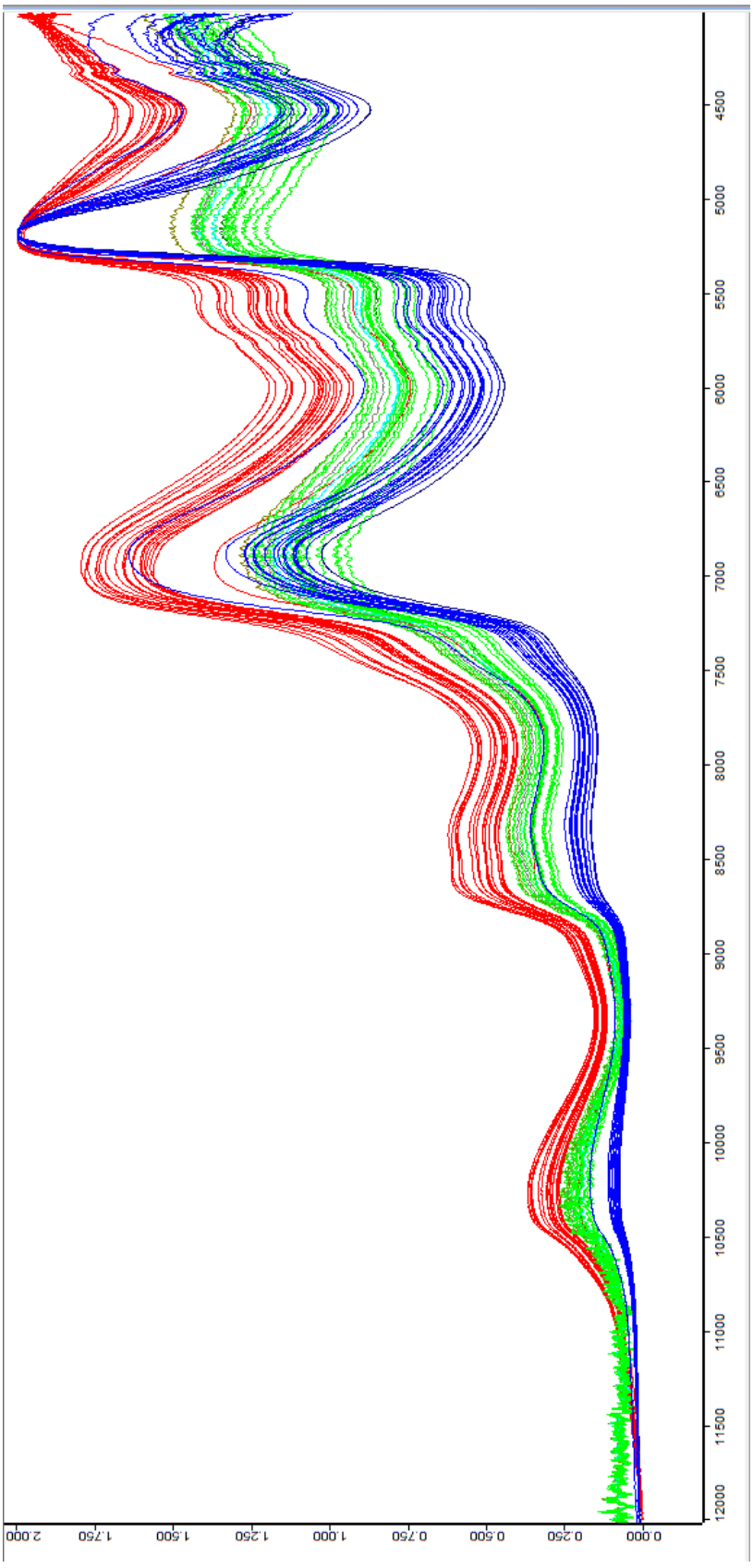

Figure 1: Spectra compared: EH (red), SP (blue) and IS (green). All spectra were normalized.

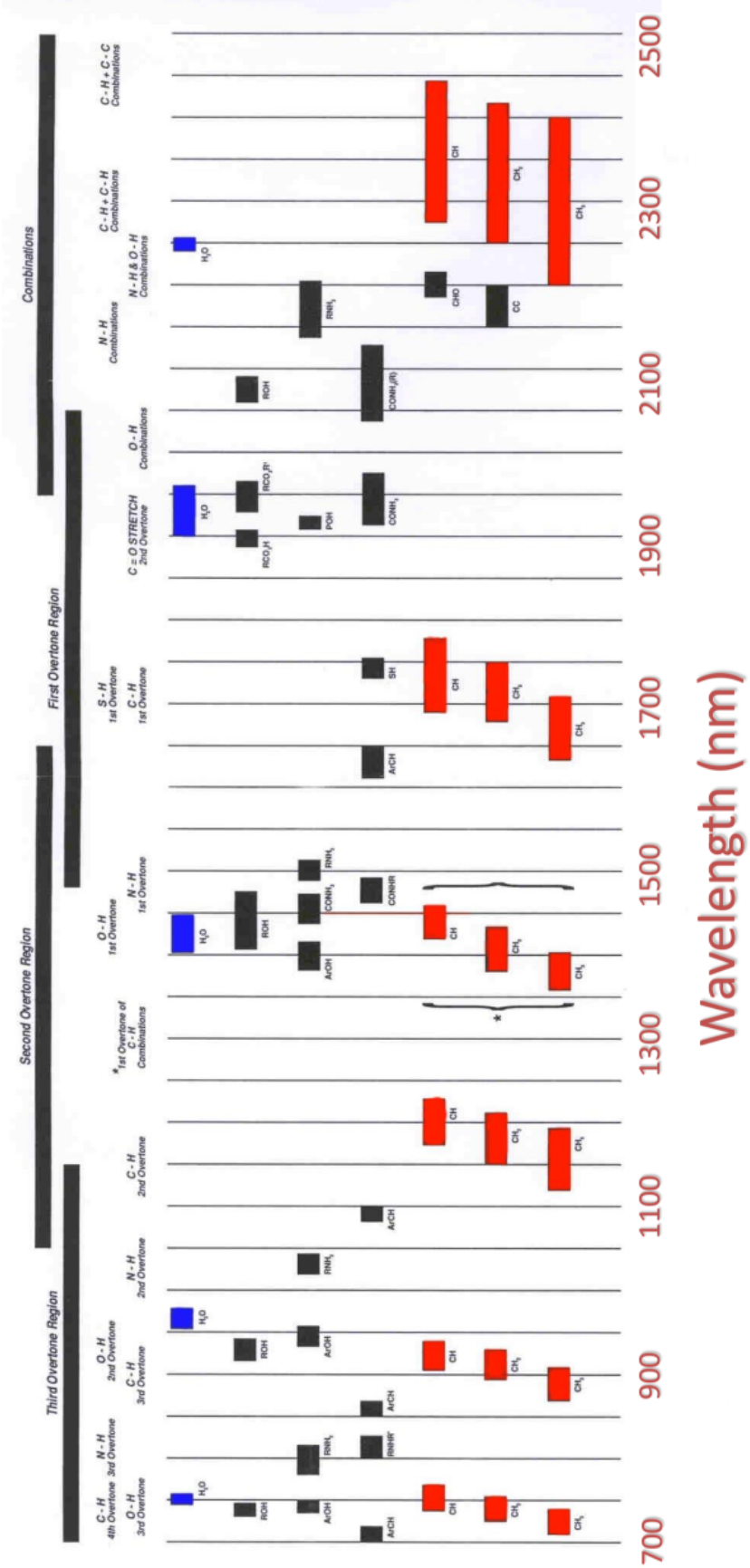

Figure 2: Main vibration bands observed in NIR [84]. Position of the bands → qualitative analysis; intensity of the bands → quantitative analysis.